Gerard Caneba · Yadunandan Dar

Emulsion-based Free-Radical Retrograde-Precipitation Polymerization

Springer

Emulsion-based Free-Radical Retrograde-Precipitation Polymerization

Gerard Caneba • Yadunandan Dar

Emulsion-based Free-Radical Retrograde-Precipitation Polymerization

Springer

Dr. Gerard Caneba
Michigan Technological University
Dept. Chemical Engineering
Townsend Drive 1400
MI 49931-1295 Houghton
USA
caneba@mtu.edu

Dr. Yadunandan Dar
National Starch
10 Finderne Avenue
Bridgewater NJ 08807
USA

ISBN 978-3-642-19871-7 e-ISBN 978-3-642-19872-4
DOI 10.1007/978-3-642-19872-4
Springer Heidelberg Dordrecht London New York

Library of Congress Control Number: 2011932681

Cover design: eStudio Calamar S.L.

Printed on acid-free paper

Springer is part of Springer Science+Business Media (www.springer.com)

Dedicated to my loving wife, Mary Ann; our children, Christine, Richard, Benjamin, and Katherine; and to my parents, Doroteo and Saturnina
Gerard T. Cañeba

Dedicated to my wife Arundhati, my son Vasu, my daughter Jayanti, my parents Rishi and Sadhvi, and my brother Raaghav Dar.
Yadunandan L. Dar

From a little spark may burst a mighty flame
- Dante

Preface

This monograph is a follow-up material to the first FRPPP book by Prof. Gerard T. Caneba in 2010. It includes three parts that are related to one another, i.e., they are applicable to emulsion-based systems and they point to the importance of the consideration of the densification phenomenon that occurs in FRRPP systems. In Part I, additional conceptual results, simulation of dynamic thermal behavior, and conventional emulsion polymerization topics are introduced. Conceptual topics include the application of the quantitative analysis presented in the first FRRPP monograph for the occurrence of the FRRPP process to the polystyrene–styrene–ether (PS–S–Ether) and poly(methacrylic acid)–methacrylic acid–water (PMAA–MAA–Water) systems. Also, the generalization of the quantitative analysis is done to consider molecular weight effects, especially based on changes of the phase envelope to an hourglass type. Part I also includes a substantial analysis of the dynamic thermal behavior of reactive domain FRRPP spherical particles, which is a follow-up from the steady-state analysis of quantitative description of FRRPP behavior introduced in Chap. 2 of the first FRRPP monograph. It will be shown that overall composition-based parameters used for steady-state analysis of the PS–S–Ether and PMAA–MAA–Water systems apparently pertain to unstable dynamic behavior in these formulations. This actually agrees with the formation of hot spots in FRRPP systems as introduced in the two cases in Sect. 2.2 of the first FRRPP monograph. However, it has also been established from the first FRRPP monograph that FRRPP reactive sites eventually attain low mobility and possibly vitrified states, which would have to involve much lower monomer concentrations and higher polymer concentrations, due to the inherent tendency of reactive sites toward polymer chain propagation reactions. When lower monomer concentrations are introduced in the analysis of the dynamic thermal behavior of both PS–S–Ether and PMAA–MAA–Water systems, the expected stable FRRPP behavior was obtained from the simulation results.

Part II of this monograph involves implementation of the FRRPP process in emulsion and other dispersed media to produce various polymer products. Topics in implementation of the FRRPP process from pre-emulsions of monomers and the

solvent/precipitant are highlighted, predominantly based on the collaborative efforts with Dr. Yadunandan Dar of Corporate Research, National Starch and Chemical Co. including experimental evidence of the densification phenomenon for the formation of both PS and poly(methyl methacrylate) (PMMA) polymers from emulsion FRRPP. The level of densification has been found to increase as the chain length increases, going through a crossover point compared to densities predicted from polymer physics principles. Quantitatively, the crossover degree of polymerization is found to scale to the particle size and number of chains per particle to the power of 2. Also, the so-called Confinement Index (*CI*) is found to scale with the degree of polymerization (*DP*) by 0.5 and with the particle diameter by 1.5. These results are relatively new, and their polymer physics implications are not yet known.

In Part III of this monograph, additional FRRPP topics are included that pertain to more recent efforts of G. Caneba, such as oil spill control, oil dispersant systems, and caustic sludge remediation from emulsion-based FRRPP materials, hydrolysis of vinyl acetate–acrylic acid-based copolymers, and other polymer modification studies from FRRPP-based emulsions.

One of the authors (GC) would like to thank the following individuals who have assisted him in the effort that culminated in his portion of this monograph: Mathkar Alharthi, Shubham Borole, Walt Kurnik, Jerry Lutz, Zach Tanghetti-Abrams, Dr. Rajesh Tiwari, and Dr. Paul Zeimer. He is also grateful to the Center for Environmentally Benign Materials (CEBFM) of Michigan Tech for its support in the continuing effort on the FRRPP research, especially its current membership (Dr. Gordon Parker the associate director, Dr. David Shonnard, Dr. Gregory Odegard, and Dr. Spandan Maiti). Moreover, he is grateful for the financial support of industrial sponsors, such as National Starch LLC, for facilitating the research on emulsion-based systems. Finally, acknowledgment is given to Michigan Tech and its support personnel for providing the atmosphere that resulted in this monograph.

YD would like to thank his colleagues (when working for National Starch and Chemical Company), especially Dr. Peter Schlom and Dr. Chaodong Xiao, for helpful discussions. YD would also like to thank Michigan Technological University and ICI plc for partly supporting his work at Michigan Tech and for the collaborative project between Michigan Tech and National Starch and Chemical Co.

Houghton, MI — Gerard T. Caneba
Bridgewater, NJ — Yadunandan L. Dar
May 2011

Contents

Part II Emulsion FRRPP (EFRRPP)

Part I
The FRRPP Theory

No army can withstand the strength
of an idea whose time has come
Victor Hugo

Chapter 1
Calculations to Probe FRRPP Behavior of the PMAA–MAA–Water System

1.1 Quantitative Expressions for FRRPP Behavior

In a groundbreaking monograph (Caneba 2010), the FRRPP concept was introduced as a free-radical-based polymerization process that occurs when the polymer-containing reactive solution undergoes phase separation above the lower critical solution temperature (LCST) (Caneba 1992a, b). The temperature–composition phase diagram for the polymer–monomer–solvent/precipitant system representing FRRPP components (Fig. 1.1) indicates a cascade of localized temperature increases within the polymer-rich domains that also involve the spinodal curve, wherein it was shown that the mutual diffusivity of the system approaches zero (Caneba 2010).

In Fig. 1.1, the basal triangular diagram corresponds to the reactor fluid temperature. Before the polymer is formed, the system is at Point O, wherein it contains only the monomer and solvent. When the reaction is started with the addition of the initiator, polymer material is formed and the system traverses the OA trajectory, based on the amount of primary radicals that are formed from the initiator and monomer as a function of time and temperature. Even while the polymer solution is in the dilute regime, it already has the capability of preventing radical sites from reacting with other polymer radicals, based on the coil-globule transition picture that was introduced in the first FRRPP monograph (Caneba 2010). Isolated polymer Gaussian coils that were formed during propagation reactions can agglomerate into globules with other isolated coils. At Point A, when the polymer-rich domains start to phase separate, collapsed globules are formed and spinodal decomposition structures evolve from them. Such structures are of the network cocontinuous type, which comprise both polymer-rich and polymer-lean domains. As it has been demonstrated theoretically and experimentally, once a structure is formed, various coarsening mechanisms start to occur (Feke and Prins 1974; Siggia 1979; Voight-Martin et al. 1986). The earliest form of coarsening was shown to occur even during spinodal decomposition, which can result in disappearance of polymer-rich domains under the so-called asymmetric domain growth process (Caneba and

G. Caneba and Y. Dar, *Emulsion-based Free-Radical Retrograde-Precipitation Polymerization*, DOI 10.1007/978-3-642-19872-4_1,

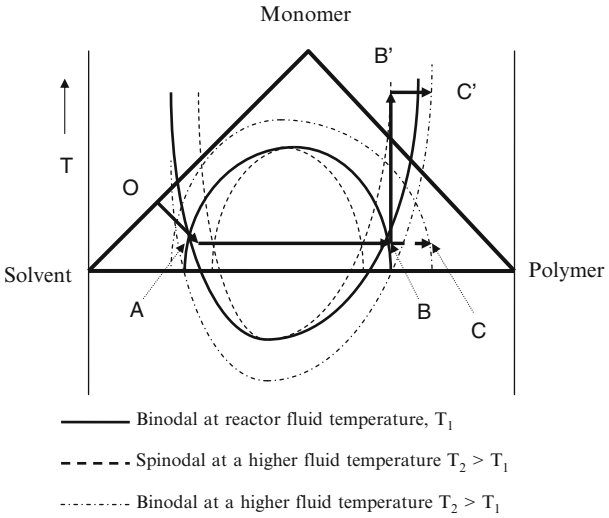

Fig. 1.1 Temperature-ternary composition diagram showing the proposed reaction pathway OABB′C′ for an FRRPP system, in which the BB′ segment occurs due to local heating. Segment ABC is the tie line. The segment OACB is in the basal ternary composition triangular diagram plane. Vertically oriented phase envelopes at T_1 and T_2 intersect with the tie line

Saxena 1995). Agglomeration of polymer-rich domains has also been hypothesized, along with Ostwald ripening (Shewmon 1969), hydrodynamic flow (Siggia 1979), and gravity flow (Siggia 1979). These latter coarsening mechanisms have been proposed to occur due to the free energy change associated with the decrease in interfacial area of the system.

While phase separation is going on, the reaction exotherm is causing local temperatures to increase, resulting in deeper quench levels of the phase separating polymer-rich domains. Based on the phase diagram shown in Fig. 1.1, higher local temperatures in the polymer-rich domains correspond to higher polymer concentrations leading to vanishing mutual diffusivities (Trajectory BB′). The population of reactive sites and polymer-rich domains corresponds to an overall system behavior that straddles the region between the binodal and spinodal curves of the polymer-rich phase in the temperature–composition space (Fig. 1.1). The resulting overall trajectory of the reactive polymer-rich phase has been used in a mathematical modeling effort that yielded a flat temperature profile for the FRRPP process, and the quantitative criterion of the occurrence of this profile was determined with validating data from the polystyrene–styrene–ether system (Caneba 2010). In the foregoing, the proposed quantitative criterion for the FRRPP process is clarified with data from the polystyrene–styrene–ether and poly(methacrylic acid)–methacrylic acid–water systems. Mathematical modeling analysis is also done to incorporate the effect of changes in molecular weight of the polymer, which is more applicable to emulsion-based FRRPP systems.

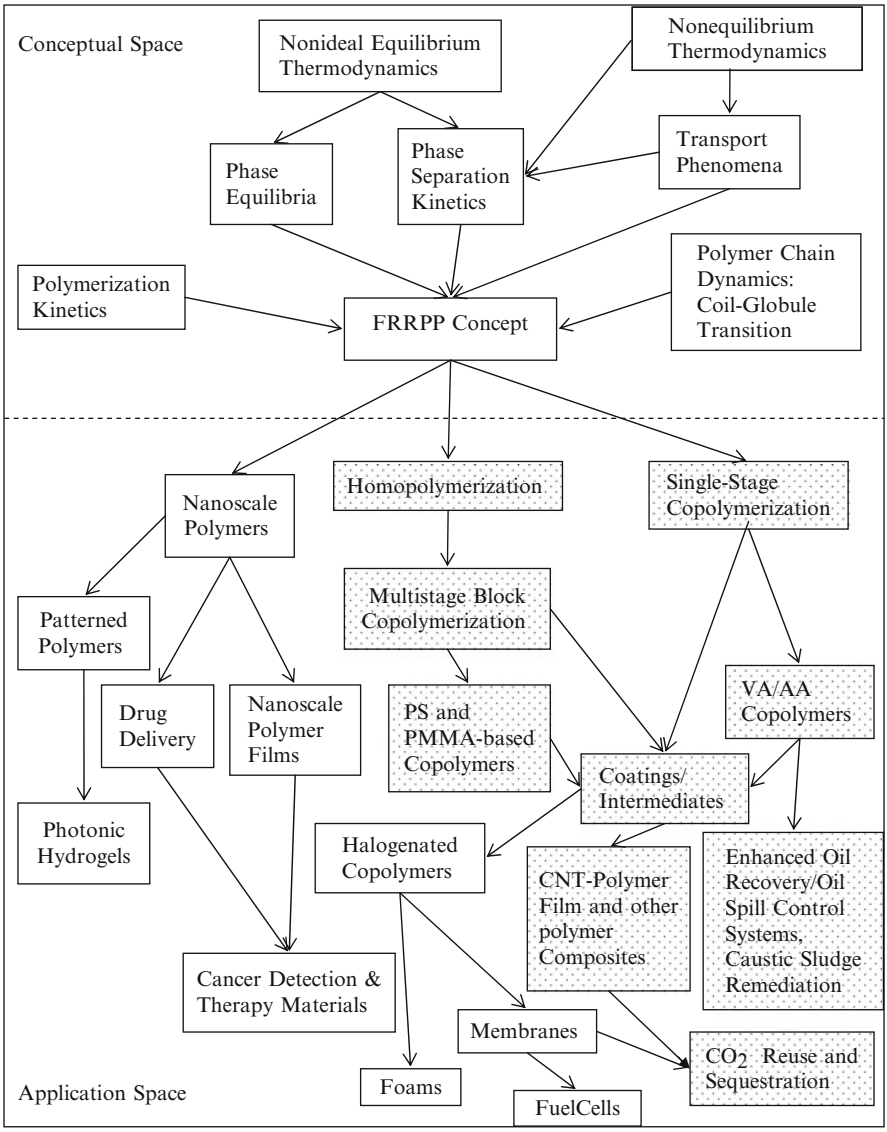

Fig. 1.2 Concepts and applications pertaining to the FRRPP process, showing textured application areas that at least partially fall under emulsion-based systems

Figure 1.2 shows the range of concepts and application areas covered by the FRRPP process, thus far; most of them are explained in the first FRRPP monograph (Caneba 2010). The figure is subdivided into conceptual and application spaces. In the conceptual space, various fundamental areas used to theoretically characterize the FRRPP process are presented, along with their relationships to one another.

A similar presentation of topic areas is done in the application space. As more application areas are discovered and developed, they can be added to this growing list. Textured application boxes are shown, which fall under emulsion-based systems. Under this categorization, it is suffice that at some point during processing, the system is in the form of an emulsion. Processing in emulsion has been found to improve the progress of the propagation reaction in FRRPP systems while suppressing chain termination.

Emulsion products have been found to preserve reactive polymer radicals for subsequent formation of block multipolymers, and for applications that are normally advantageous to be in emulsion or latex form. It is worth noting that applications of emulsion FRRPP include a variety of sustainability materials/systems, such as low VOC coatings, surfactants, interfacial materials, surface modifiers, nanocomposites, thermoplastic elastomers, etc.

In the first part of this monograph, additional conceptual discussions will be presented that lead to emulsion-domain applications. It starts with the attempted validation of the quantitative criterion presented in the first FRRPP monograph to the poly(methacrylic acid)–methacrylic acid–water (PMAA–MAA–Water) system, which has been implemented in emulsion fluid system. Then, a summary of fundamental concepts of emulsion polymerization is presented. Subsequently, the analysis is made to involve the effect of molecular weight of the polymer in situations where an hourglass-shaped phase envelope is obtained (Siow et al. 1972). The result is the possibility of obtaining FRRPP behavior even when the reactive system apparently starts out under conventional precipitation polymerization conditions.

The occurrence of the LCST has been established as a necessary condition for the FRRPP phenomenon in free-radical polymerization systems. Based on the energy balance for a quasi-steady-state approximation of the FRRPP system, the dimensionless energy source term was obtained to result in the following mathematical expression (Caneba 2010)

$$\Phi = (\alpha\theta + \beta)\exp\left(-\frac{\gamma}{\theta}\right), \tag{1.1}$$

where the dimensionless parameters are related to the following dimensional quantities in the energy balance and phase equilibria equations[1]:

$$\alpha = r_0^2 A/k = r_0^2\left(-\Delta H_p\right)k_0' a/k, \tag{1.2}$$

$$\beta = r_0^2 B/kT_s = r_0^2\left(-\Delta H_p\right)k_0' b/kT_s, \tag{1.3}$$

$$\gamma = E_a/RT_s, \tag{1.4}$$

[1]The quantity for r_0 used in expressing α in (2.2.7) is erroneously listed as γ_0 in the first FRRPP monograph (Caneba 2010).

$$\theta = T/T_s, \tag{1.5}$$

$$\eta = r/r_0, \tag{1.6}$$

$$A = \left(-\Delta H_p\right)k_0' a, \tag{1.7}$$

$$B = \left(-\Delta H_p\right)k_0' b. \tag{1.8}$$

The phase behavior for the polymer-rich phase was approximated by the linear representation

$$X_P = aT + b, \tag{1.9}$$

where X_P is the product of the weight fractions of the monomer and polymer (or just the weight fraction of the polymer if the monomer concentration is the same for both polymer-rich and polymer-lean phases at equilibrium, as the case for the PS–S–Ether system), while a and b were proposed to be obtained from experimental data points referred in Fig. 1.1; thus,

$$a = \frac{X_{P,C} - X_{P,B}}{T_2 - T_1}, \tag{1.10}$$

$$b = X_{P,C} - aT_2 = X_{P,B} - aT_1. \tag{1.11}$$

For the expectation of a flat temperature profile, $\theta = 1$ for $\eta = 0$; thus, the dimensionless source term was symbolized as Φ_0 and Eq. (1.1) became

$$\Phi_0 = (\alpha + \beta)\exp(-\gamma). \tag{1.12}$$

Then, a combined dimensionless quantity was introduced to quantitatively characterize strict FRRPP behavior, wherein the reactive polymer-rich domains attained flat temperature profiles. The dimensionless quantity was symbolized by $C\tilde{n}$ (pronounced see-enye), and defined as

$$C\tilde{n} = \frac{\alpha\beta}{\Phi_0} = \left[\frac{1}{\alpha} + \frac{1}{\beta}\right]^{-1} \exp(\gamma). \tag{1.13}$$

Values of $C\tilde{n}$ from computational efforts indicated that for the FRRPP process, it should be below around −1,000. This cut-off number was validated by experimental data from the PS–S–Ether system (Dar 1999) for a particular experimental run at 80°C (Caneba 2010). Based on Fig. 1.1, equilibrium weight fraction values (binodal curves, also representing collapsed globules for polymer-rich phase) at 80°C used in the calculations for a and b (Caneba, 2010).

If X in Eqs. (1.9)–(1.11) is the product of the weight fractions of PS and S, then values in Table 1.1 result in $a = 0.00018\ \mathrm{K}^{-1}$ and $b = -0.041895$ [Equation (2.5.7)

Table 1.1 Thermodynamic values for weight fractions of polymer (PS) and monomer (S) in the solvent/precipitant (Ether) used in the calculations of a and b in Eqs. (1.9)–(1.11)

	Binodal weight fraction			
	Polymer-lean phase		Polymer-rich phase	
Component	$T = 80°C$	$T = 90°C$	$T = 80°C$	$T = 90°C$
Monomer (S)	0.09	0.09	0.09	0.09
Polymer (PS)	0.01	<0.01	0.2405	0.2605

Values at 80°C are at equilibrium with one another (binodal curves), while values at 90°C are extrapolated from equilibrium data at 50°C and 80°C (Caneba 2010). Starting monomer composition is 10 wt%

in Caneba 2010]. To relate k_0' in Eqs. (1.2)–(1.3) to the propagation rate coefficient, k_P, the conversion factor is used because the rate expression for the consumption of the monomer via chain propagation is actually based on the concentrations of monomer and polymer, while the calculations of a and b are based on weight fractions. Thus,

$$k_0' = \frac{\rho_{\text{Soln}}^2}{(\text{MW}_P)} k_{Po} \tag{1.14}$$

and

$$k_P = k_{Po} \exp\left(-\frac{E_a}{RT}\right). \tag{1.15}$$

When k_{Po} is considered the intrinsic propagation rate coefficient, the resulting calculation for $C\tilde{n}$ [Eq. (1.13)] pertains to that of collapsed globules or the polymer-rich phase. A cut-off value of $C\tilde{n}$ to be less than −1,000 includes particle radii of more than 20 μm for collapsed globules in the polymer-rich phase (Fig. 2.5.2 of Caneba 2010). These are relatively small numbers, which are consistent with the polymer radical preservation capabilities of this system (Fig. 2.3.15 of Caneba 2010).

1.2 Experimental Data for PMAA–MAA–Water System

For the PMAA–MAA–Water system, phase equilibria data was obtained by Shi (1997). Corresponding kinetic data was obtained by Aggarwal (1993) and Wang (1997). Finally, gel effect modeling was done with the kinetic data by Aggarwal (1993) and Dar (1999).

For this calculation, we will use the kinetic data gathered by Aggarwal (1993) for this system at 60°C and 80°C, and atmospheric pressure. The initiator used was V-50, a water-soluble azo-based initiator obtained from Wako Chemicals (1987). Starting system compositions were 7.2, 12 g MAA, 120 g Water, and 0.03, 0.06 g V-50. The reaction system was dispersed in n-Heptane using a Span®20 surfactant.

The half-life of the initiator is 350 and 28 min at 60°C and 80°C, respectively (Wako chemicals 1987). The reaction was carried out in a 2-l jacketed atmospheric autoclave (Fig. 1.3). At 60°C, the asymptotic conversion for this system was close to 100%; at 80°C, the asymptotic conversion for this system was at 60–80%.

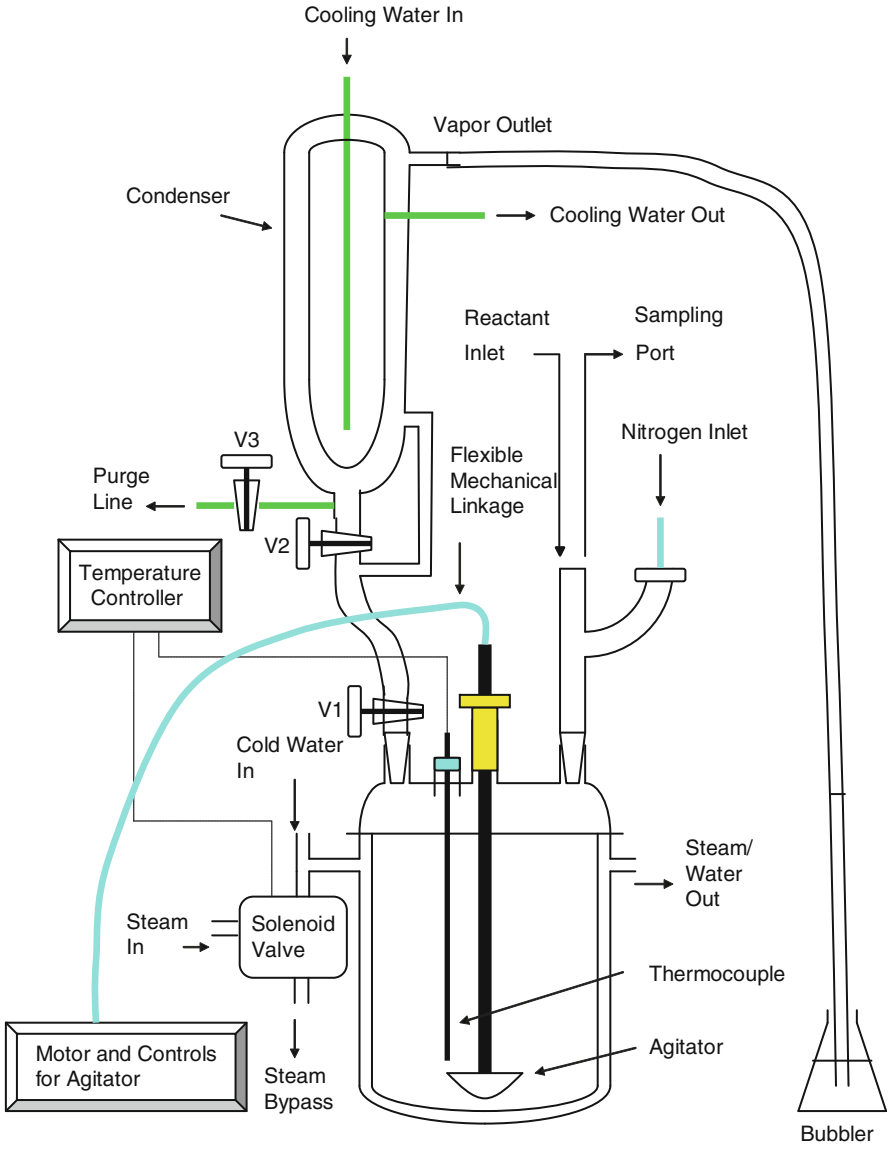

Fig. 1.3 Apparatus used in the polymerization of MAA via FRRPP process. The reactor is a 2-l steam/water jacketed atmospheric glass autoclave that is run under Nitrogen gas blanket

Number-average molecular weights at asymptotic conversions were at around 105,000 and 30,000–70,000 Da at 60°C and 80°C, respectively. For all the FRRPP-based samples, polydispersity indices at asymptotic conversions were in the 1.2–1.8 range. These conversion and molecular weight values are used for subsequent calculations, since they pertain to the maintenance of FRRPP control in the system.

Another set of kinetic data for the PMAA–MAA–Water system initiated by V-50 at 90°C was presented in Figs. 2.3.17, 2.3.20, and 2.3.21 of the first FRRPP monograph (Caneba 2010), wherein asymptotic values of conversion, number-average molecular weight, and polydispersity index were at 70%, 120,000 Da, and 1.4, respectively.

Scanning electron micrographs of instantaneously frozen and cryogenically dried samples show particle sizes ranging from 50 to several hundred μm in the initial stages of polymerization (just after phase separation was observed). For samples taken at later times (much after phase separation in the system was observed), the particle and pore morphologies had agglomerated and coarsened to particle sizes ranging from hundreds of μm to the mm range. The particles in the initial stages still displayed the cocontinuous structure typical of spinodal decomposition (Strobl 1996). The latter stage showed a coarsened structure with no apparent porosity. The particles seemed to be solid chunks of polymer.

1.3 Determination of Model Parameters

In order to obtain the values of α and β, the following experimental values are used (Dar 1999):

$$\begin{aligned}
&\text{Molecular weight of MAA monomer} = 102\,\text{g/mol}\\
&\text{Molecular weight of PMAA polymer} = 105,000\,\text{g/mol}\\
&\text{Temperature of the reactor fluid} = 80^{\circ}\text{C and } 90^{\circ}\text{C}\\
&\text{Starting monomer composition} = 9.09\,\text{wt.}\%\\
&\text{Solvent/precipitant (Water) composition} = 90.91\,\text{wt.}\%\\
&\text{Thermal conductivity of MAA monomer} = 0.0003\,\text{cal/(cm s }^{\circ}\text{C)}\\
&\text{Thermal conductivity of PMAA polymer} = 0.0003\,\text{cal/(cm s }^{\circ}\text{C)}\\
&\text{Thermal conductivity of Water} = 0.0014\,\text{cal/(cm s }^{\circ}\text{C)}\\
&\text{Thermal conductivity of collapsed globule or polymer-rich phase is calculated}\\
&\qquad\text{based on weighted mean at component compositions}\\
&\text{Heat of polymerization} = 118.1\,\text{cal/g}\\
&\text{Density of MAA} = 1.015\text{g/cm}^3\\
&\text{Density of PMAA} = 1.275\,\text{g/cm}^3
\end{aligned} \tag{1.16}$$

Based on the work of Shi (1999), binodal compositions for tie lines and polymer-rich phase curves are available at temperatures of 80°C and 90°C and molecular weight of 180,000 Da (Sect. 1.1 of Caneba 2010). In order to match these thermodynamic data with the kinetic data of Aggarwal (1993), an extrapolation of the thermodynamic data is made. The key assumption made in this extrapolation involves the placement of tie lines that are invariant with respect to the number-average molecular weight and the temperature, since the tie lines are most dependent on the chemical nature of the components in the system. As shown in Fig. 1.4, tie line L–L would have been obtained if the monomer distributes itself equally in the solvent/precipitant-rich and the polymer-rich phases. On the other hand, tie line M–M would have been obtained if the polymer distributes itself in the solvent/precipitant-rich and the monomer-rich phases. For relative levels of interactions between these two extremes, tie line N–N would be obtained. Even if the phase curves widen due to an increase in molecular weight and/or temperature, one of

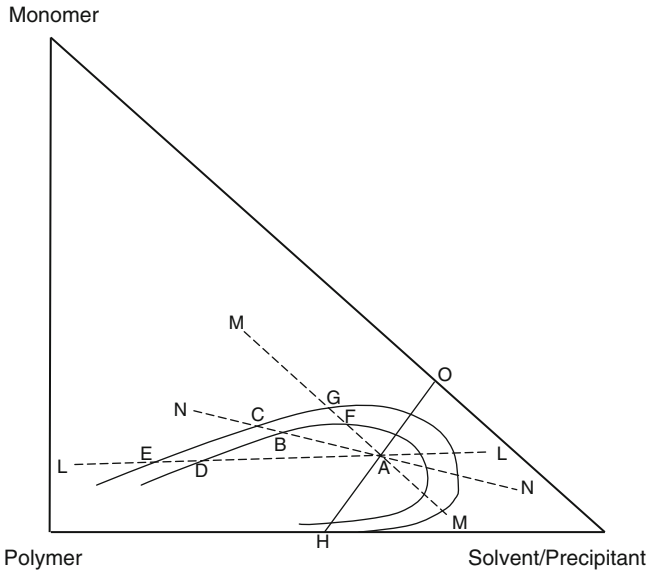

Fig. 1.4 Illustration of the invariance of tie lines for a particular polymer–monomer–solvent/precipitant system from a common overall composition A. Tie line L–L corresponds to a system in which the monomer distributes itself equally in the polymer-rich and solvent/precipitant-rich phases, and L–L intersects with the polymer-rich phase curves at D and E. Tie line M–M corresponds to a system in which the polymer distributes itself in the solvent/precipitant-rich and the monomer-rich phases, and M–M intersects with the monomer-rich phase curves at F and G. Tie line N–N corresponds to the system between these two extremes that occurs in the PMAA–MAA–Water system, and N–N intersects with the polymer-rich and solvent-rich phase curves at B and C. In accordance with the symbolism in Fig. 1.1, OA is the first stage of the reaction trajectory. Conversion is obtained based on the fraction of the trajectory distance of OA compared to OH. Note that OH corresponds to the line of constant overall composition of nonreactive solvent/precipitant

Table 1.2 Thermodynamic values for weight fractions of polymer (PMAA) and monomer (MAA) used in the calculations of a and b in Eqs. (1.9)–(1.11)

	Polymer-rich binodal weight fraction for PMAA MW = 180 kDa	
Component	$T = 80°C$	$T = 90°C$
Monomer (MAA)	0.05	0.067
Polymer (PMAA)	0.158	0.17

Starting monomer composition is 9.09 wt% and conversion is 60% where molecular weight is 105,000 g/mol

these tie lines would be valid, as long as the binodal composition is obtained from the intersection of the tie line with the phase curve. These intersections are points E, D for two polymer-rich phase curves corresponding to tie line L–L; F, G for two polymer-rich phase curves corresponding to tie line M–M; and B, C for two polymer-rich (and also monomer-rich) phase curves corresponding to tie line N–N. If N–N is the actual tie line for the system, the conversion is obtained from the fraction of the portion of the reaction trajectory OA compared to OH. Note that line segment OH corresponds to the line of constant solvent/precipitant composition, which is a nonreactive component.

Based on the above-mentioned considerations, extrapolated and experimental values of the polymer-rich binodal points are shown in Table 1.2 at 60% conversion.

It has been shown that only 3% of radicals produced from the initiator become live polymer radicals in the PMAA–MAA–Water system (Fig. 2.3.22 of Caneba 2010). This is consistent with the relatively high molecular weights obtained, compared to the PS–S–Ether system. The root cause is the relatively high critical conversion required for the PMAA–MAA–Water system at around 60%, which is much higher than critical conversions obtained for the PS–S–Ether system at 23–30% (Sect. 2.4.3 of Caneba 2010). In order to account for this inefficiency in radical maintenance, a polymer radical efficiency factor has to be used for the product of the monomer and polymer concentrations. As a result, the PMAA–MAA–Water system will spend a big part of its initial reaction time in the solution regime, where it will result in higher levels of termination reactions.

In order to quantitatively characterize the relatively lower inefficiency of radical maintenance in the PMAA–MAA–Water system, the expression for X_P in Eq. (1.9) can be modified to include a polymer radical efficiency factor f_P; thus,

$$X_P = f_P X_M^P X_P^P, \tag{1.17}$$

where the superscript "P" corresponds to polymer-rich phase composition. It should be noted that for the PS–S–Ether system at 80°C using AIBN as initiator, f_P was measured to be in the order of 0.80–0.85 (Wang 1997). Thus, for all practical purposes, f_P is assumed to be in the order of 1.0 for the PS–S–Ether system. Note that f_P is the same as the quantity X in Fig. 2.3.15 of Caneba (2010). For the PMAA–MAA–Water system at 80°C using V-50 initiator, it is believed to be in the order of 0.01 (Fig. 1.4).

Since both α and β are both proportional to the square of the particle radius, r_0, constant values of α_0 and β_0 are obtained based on

$$\alpha = f_P \alpha_0 r_0^2, \tag{1.18}$$

$$\beta = f_P \beta_0 r_0^2. \tag{1.19}$$

The last piece of information needed for the calculation of values of $C\tilde{n}$ pertains to propagation rate coefficient data. Fortunately, this is available in the literature for propagation of PMAA radicals in water, and the result is $k_{po} = 9.41 \times 10^3$ l/(mol s) and activation energy $E_a = 17.7$ kJ/mol (Kucha et al. 2000). At 80°C or 353 K, this gives a value of $\gamma = 5.21$ [Eq. (1.4)].

1.4 Results and Discussion

Based on Eqs. (1.2)–(1.11), Eqs. (1.14)–(1.16), and values of binodal polymer-rich phases in Table 1.2, numerical values of $\alpha_0 = 3.445 \times 10^3$ cm^{-2} and $\beta_0 = -3.571 \times 10^2$ cm^{-2} are obtained for conversion of 60% and number-average molecular weight of 105,000 g/mol.

Figure 1.5 shows the plot of $C\tilde{n}$ for different values of f_P and particle radii during the FRRPP of MAA in water at 80°C for collapsed globules and agglomerated globules (from polymer-rich binodal points) at 60% conversion. The plot indicates that for $f_P = 0.01$, particles smaller than around 1.2 cm would not follow strict FRRPP behavior, based on the cutoff for $C\tilde{n} < -1{,}000$. For $f_P = 0.1$, particles smaller than around 0.4 cm would not follow strict FRRPP behavior. Thus, for $f_P = 0.03$, particles smaller than around 0.4–1.2 cm would not follow strict FRRPP behavior.

Since molecular weights are relatively high for this system, the cut-off value of $C\tilde{n}$ could be relaxed, because the polydispersity index does not seem to be heavily dependent on operating temperature, as evidenced by only a factor of 2 in number-average molecular weights between operating temperatures of 60°C and 80°C in the PMAA–MAA–Water system (Aggarwal 1993).

Looking back at Table 2.5.1 of Caneba (2010), a relaxed cut-off value of less than -1.0 for $C\tilde{n}$ indicates a 5% difference in absolute temperature between the middle and surface of the reactive particulate. For an operating temperature of 60°C or 333 K, this translates to an interior particle temperature of only 77°C. Going from 80°C to 60°C, the number-average molecular weight for 12 g MAA charge went from 60,000 to 105,000 Da or an increase of 75% (Aggarwal 1993). On the other hand, for the PS–S–Ether system, Fig. 2.3.9a of Caneba (2010) shows that going from 80°C to 60°C involves a change in number-average molecular weight from 2,000 to 10,000 Da or an increase by 5,000%. Thus, from Fig. 1.5 at a cut-off value of $C\tilde{n}$ less than -1.0, the system would still have a relatively narrow MWD if they are confined to particulates greater than 120–300 μm. This is not the case for

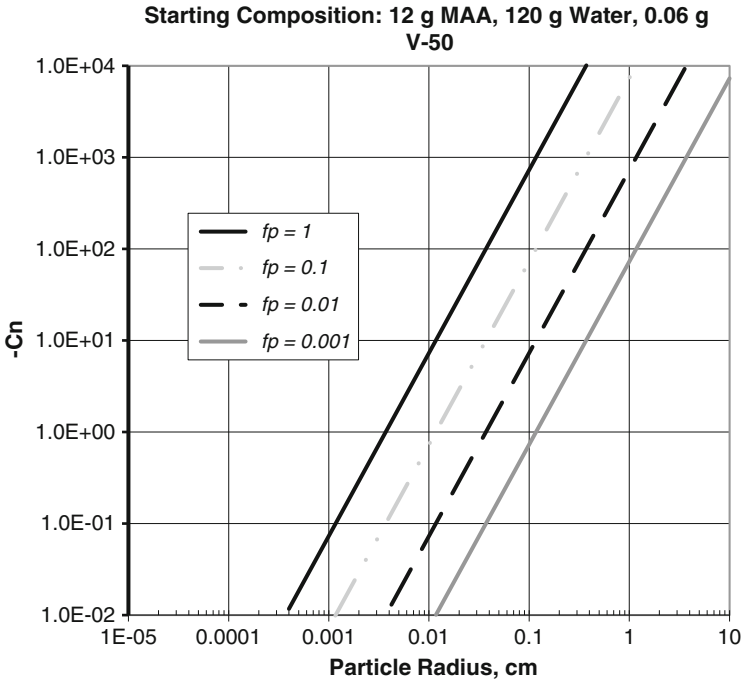

Fig. 1.5 Predicted values of $C\tilde{n}$ at different particle radii and polymer radical fractions (f_P) for FRRPP of MAA in water at 80°C, 60% conversion, number-average molecular weight of 105,000 g/mol. The actual system should correspond most closely to $f_P = 0.01 - 0.1$, which results in strict FRRPP behavior (flat temperature profile) for polymer domain sizes in the 1.2–0.4 cm range

the PS–S–Ether system, due to its relatively large proportional change in molecular weight with reaction temperature.

The cut-off particle size range of 0.4–1.2 μm for strict FRRPP behavior is in the slightly smaller polymer size range for the nonreactive PMAA–MAA–Water phase separating system at 80°C (Table 1.4.36 of Caneba 2010). As for comparison with the reactive stirred-tank fluid system, this size range is also observed (Figs. 2.1.3 and 2.1.4 of Caneba 2010).

Based on the above analysis of thermodynamic, transport, and quasi-steady-state polymerization behavior of the PMAA–MAA–Water system, it is no surprise that narrow molecular weight distributions are obtained at relatively high molecular weights. The primary reason why the PS–S–Ether system that resulted in relatively low molecular weights is its relatively lower critical conversion for the onset of FRRPP behavior as reflected in its phase diagram (Fig. 2.3.1 of Caneba 2010). Based on Fig. 1.1, the OA line segment is longer for the PMAA–MAA–Water system than that of the PS–S–Ether system at the same temperature of 80°C.

It should be noted that the above analysis is based on the attainment of quasi-steady-state temperature profiles within the reactive particulates. Later on, we

will show unsteady-state temperature profiles for the PS–S–Ether and PMAA–MAA–Water systems, and make comparisons with the above-mentioned quasi-steady-state-based analysis.

Differences in PDI values can also be explained by the closeness of binodal curves at higher molecular weights. This can be seen from the phase diagrams for both the PS–S–Ether and PMAA–MAA–Water systems (Caneba 2010), and from various other types of phase equilibria data of polymer solutions. The case of the PMAA–MAA–Water system illustrates that flatness of temperature profiles within reacting particles does not necessarily result in less broad MWDs, if molecular weights are relatively large.

1.5 Nomenclature

1.5.1 Alphabets

1.5.1.1 Upper Case

A	Defined in Eq. (1.7)
B	Defined in Eq. (1.8)
E	Activation energy for reaction, J/mol
MW	Polymer molecular weight, g/mol or Daltons
R	Universal gas constant, J/(mol K)
T	Absolute temperature, K
X	Defined in Eqs. (1.9)–(1.11) and Eq. (1.17)

1.5.1.2 Lower Case

a	Defined in Eq. (1.10)
b	Defined in Eq. (1.11)
k	Thermal conductivity of the reaction fluid
r	Radial distance, m or cm

1.5.2 Subscripts

a	Pertains to activation energy [Eq. (1.4)]
B	Point in Fig. 1.1
C	Point in Fig. 1.1

M Pertains to monomer in Eq. (1.17)
P Pertains to polymer-rich phase in Eqs. (1.9)–(1.11) or polymer in Eq. (1.17)
Soln Pertains to overall solution
0 Pertains to Preexponential rate coefficient [Eq. (1.15)] or Dimensionless Energy Source Term [Eq. (1.13)]
1, 2 Temperature points

1.5.3 Superscripts

P Pertains to polymer-rich phase in Eq. (1.17)

1.5.4 Greek Symbols

α Dimensionless version of a from Eq. (1.2)
β Dimensionless version of b from Eq. (1.3)
γ Dimensionless activation energy, defined in Eq. (1.4)
η Dimensionless radius, defined in Eq. (1.6)
ρ Density, g/cm^3 or kg/m^3
θ Dimensionless temperature, defined in Eq. (1.5)
Φ Dimensionless heat of polymerization, defined in Eq. (1.12)

1.5.5 Other Symbols

α_0 Defined in Eq. (1.18), cm^{-2} or m^{-2}
β_0 Defined in Eq. (1.19), cm^{-2} or m^{-2}
$C\tilde{n}$ Defined in Eq. (1.13), dimensionless
f_P Polymer radical fraction
ΔH_P Heat of polymerization, J/mol
k_0' Defined in Eq. (1.14)
k_P Propagation rate coefficient, l/(mol s)
Φ_0 Dimensionless energy source term at the center of the particle, defined in Eq. (1.12)
r_0 Particle radius, cm or m
X_P Defined in Eq. (1.17)
$X_{P,B}$ Defined in Eq. (1.10)
$X_{P,C}$ Defined in Eq. (1.10)

References

Aggarwal A (1993) M.S. Thesis, Michigan Technological University, Houghton, MI
Caneba GT (1992a) Adv Polym Technol 11:277
Caneba GT (1992b) U.S. Patent No. 5,173,551, 22 Dec 1992
Caneba GT (2010) Free-radical retrograde-precipitation polymerization (FRRPP): novel concept, processes, materials, and energy aspects. Springer, Heidelberg. ISBN 978-3-642-03024-6
Caneba GT, Saxena R (1995) Polym Eng Sci 55:753
Dar Y (1999) Ph.D. Dissertation, Michigan Technological University, Houghton, MI
Feke GT, Prins W (1974) Macromolecules 7:527
http://www.wako-chem.co.jp/specialty/waterazo/V-50.htm
Kucha FD, Van Herk AM, German AL (2000) Macromolecules 33:3641
Shewmon PG (1969) Transformations in metals. McGraw-Hill, New York
Shi L (1997) M.S. Thesis, Michigan Technological University
Siggia ED (1979) Phys Rev A20:595
Siow KS, Delmas G, Patterson D (1972) Macromolecules 5:29
Strobl G (1996) The physics of polymers. Springer, Berlin
Voight-Martin IG, Leister KH, Rosenau R, Koningsveld R (1986) J PolymSci B Polym Phys 24:723
Wang B (1997) Ph.D. Dissertation, Michigan Technological University, Houghton, MI

Chapter 2
Closed-Form Estimation of Minimum Reactive Polymer Domain Size for FRRPP Control

This chapter pertains to the derivation of the analytical expression for estimation of the minimum reactive polymer-rich domain size for the occurrence of a flat temperature profile in FRRPP systems, under quasi-steady-state conditions. The method assumes a cut-off value of $-1{,}000$ for $C\tilde{n}$, and it is based on temperature dependency of the product of the monomer and polymer composition in the polymer-rich domains. With the derived approximate equation, the resulting minimum polymer-rich domain sizes for FRRPP control are obtained for the PS–S–Ether and PMAA–MAA–Water systems. Finally, the resulting analytical expressions explain why asymptotic conversions in FRRPP systems can be relatively low if good radical trapping is realized in the system.

2.1 Derivation of Equations

Local monomer concentration $[M]$ and the polymer radical concentration $[P\cdot]$ can be compared to their base values ($[M]_0$ and $[P\cdot]_0$) through

$$[M] = [M]_0 + \Delta[M], \tag{2.1}$$

$$[P\cdot] = [P\cdot]_0 + \Delta[P\cdot]. \tag{2.2}$$

If x is the average degree of polymerization, then it should also be noted from a reactive component balance that

$$\Delta[M] = -x\Delta[P\cdot]. \tag{2.3}$$

For the propagation reaction rate, $R_P = k_P[M][P\cdot]$, that is to be used in the expression for $C\tilde{n}$, we obtain the expression for $[M][P\cdot]$ as

G. Caneba and Y. Dar, *Emulsion-based Free-Radical Retrograde-Precipitation Polymerization*, DOI 10.1007/978-3-642-19872-4_2,

$$[M][P\cdot] = ([M]_0[P\cdot]_0 + \Delta[M])([P\cdot]_0 + \Delta[P\cdot]) = ([M]_0 - x\Delta[P\cdot])([P\cdot]_0 + \Delta[P\cdot])$$
$$= [P\cdot]_0[M]_0 + [M]_0\Delta[P\cdot] - x[P\cdot]_0\Delta[P\cdot] - x(\Delta[P\cdot])^2. \tag{2.4}$$

The last term of the right-hand side of eq. (2.4) could be neglected compared to the other terms because $\Delta[P\cdot] \ll [P\cdot]_0$; thus,

$$[M][P\cdot] = [P]_0[M]_0 + \Delta[P\cdot]([M]_0 - x[P\cdot]_0). \tag{2.5}$$

If $[P\cdot]$ is considered to vary only with the temperature and a linear dependence with temperature is invoked,

$$\Delta[P\cdot] \cong \left(\frac{\mathrm{d}[P\cdot]}{\mathrm{d}T}\right)(T - T_0). \tag{2.6}$$

Substituting the $\Delta[P\cdot]$ approximation from eq. (2.1.6) into eq. (2.1.5), we obtain

$$[M][P\cdot] = [P]_0[M]_0 + ([M]_0 - x[P\cdot]_0)\left(\frac{\mathrm{d}[P\cdot]}{\mathrm{d}T}\right)(T - T_0)$$
$$= \left(\frac{\mathrm{d}[P\cdot]}{\mathrm{d}T}\right)\{[M]_0 - x[P\cdot]_0\}T - \left\{[P\cdot]_0[M]_0 + \left(\frac{\mathrm{d}[P\cdot]}{\mathrm{d}T}\right)([M]_0 - x[P\cdot]_0)T_0\right\}. \tag{2.7}$$

If $[M][P\cdot] = a'T + b'$, then comparing with eq. (2.7),

$$a' = \left(\frac{\mathrm{d}[P\cdot]}{\mathrm{d}T}\right)\{[M]_0 - x[P\cdot]\}, \tag{2.8}$$

$$b' = [P\cdot]_0[M]_0 - a'T_0. \tag{2.9}$$

From the derivation in Sect. 1.1, the quantity $C\tilde{n}$ can be obtained as

$$C\tilde{n} = \Gamma\frac{a'b'T_0}{a'T_0 + b'}, \tag{2.10}$$

where

$$\Gamma = \frac{k_\mathrm{P}(-\Delta H_\mathrm{P})r_0^2}{k} = \frac{k_{\mathrm{P}0}\exp\left(-\frac{E_{\mathrm{Pa}}}{RT_0}\right)r_0^2}{k}. \tag{2.11}$$

Simplification of eq. (2.10) leads to

$$C\tilde{n} = \frac{\Psi}{1 + \left(\frac{1}{\Omega - 1}\right)}, \tag{2.12}$$

where

$$\Psi = a'\Gamma T_0 \tag{2.13}$$

and

$$\Omega = \frac{[P\cdot]_0[M]_0}{a'T_0} < 1. \tag{2.14}$$

From dimensional analysis,

$$[P\cdot]_0 = \left(\frac{\rho_{\text{Soln}}}{\text{MW}_{\text{Polymer}}}\right) f_{\text{P}} X_{\text{P}}, \quad [M]_0 = \left(\frac{\rho_{\text{Soln}}}{\text{MW}_{\text{Monomer}}}\right) X_{\text{M}}, \tag{2.15}$$

where ρ_{Soln} is the density of the reactive solution environment; $\text{MW}_{\text{Polymer}}$ and $\text{MW}_{\text{Monomer}}$ are the molecular weights of the polymer and monomer, respectively; and f_{P} is the fraction polymer radical from all polymer species (live and dead polymer molecules). Thus,

$$\Omega = \left(\frac{\rho_{\text{Soln}}^2}{\text{MW}_{\text{Monomer}}\text{MW}_{\text{Polymer}}a'T_0}\right) f_{\text{P}} X_{\text{M}} X_{\text{P}}. \tag{2.16}$$

From Eqs. (1.10) and (1.11), the polymer-rich domain size can be obtained as

$$r_0 = \sqrt{\frac{C\tilde{n}}{T_0\alpha_0}\left(1 + \frac{1}{\Omega - 1}\right)}, \tag{2.17}$$

where the quantity α_0 is defined in Eq. (1.18). If the cutoff $C\tilde{n} \leq -1{,}000$ for flat temperature profile FRRPP behavior applied to quasi-steady-state conditions, then this corresponds to the cutoff r_0 as

$$r_0 \geq \sqrt{\frac{1{,}000}{T_0\alpha_0}\left(\frac{1}{1 - \Omega} - 1\right)}. \tag{2.18}$$

2.2 Results and Discussion

Applying the values of T_0, α_0, and Ω for the PS–S–Ether and PMAA–MAA–Water system, the cut-off values of r_0 are obtained for flat temperature profile FRRPP behavior (Table 2.1).

Table 2.1 Approximate predictions of the cut-off values of r_0 for the PS–S–Ether and PMAA–MAA–Water systems, based on the derivation in eqs. (2.1)–(2.16)

System	T_0, K	α_0, cm^{-2}	Ω	r_0, cm
PS–S–Ether	353	1.700×10^8	0.00261–0.00278 ($f_p = 0.8$–0.85)	0.000124–0.000128 ($f_p = 0.8$–0.85)
PMAA–MAA–Water	353	3.44×10^3	6.287×10^{-6}–6.287×10^{-5} ($f_p = 0.01$–0.1)	0.00135–0.00427 ($f_p = 0.01$–0.1)

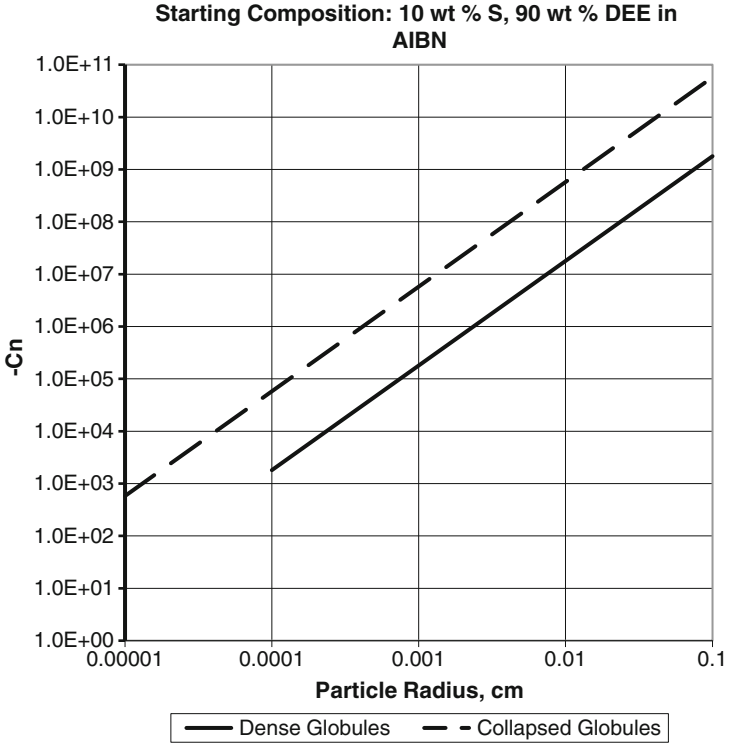

Fig. 2.1 Cutoff off reactive domain size for the PS–S–Ether FRRPP system at 80°C, based on $C\bar{n} < -1{,}000$ (Discrepancy between this plot and Fig. 2.5.2 of Caneba (2010) is also due to an arithmetic error. Corrected values of α_0 and β_0 are 1.700×10^8 and -1.121×10^8 cm^{-2} for collapsed globules, respectively; also respective values are 8.10×10^4 and -5.34×10^4 cm^{-2} for dense globules). The value of $f_P = 0.80$. Note that *lines* for $f_P = 0.85$ has been found to be almost the same for *corresponding lines* at $f_P = 0.80$

It is evident that the predictions of eq. (2.18) provide conservative values for the cutoff r_0 based on results in Sect. 2.5 of Caneba (2010) for PS–S–Ether system (which has been modified to Fig. 2.1). For the PMAA–MAA–Water system, Chap. 1 of this monograph indicates that the results in Table 2.1 are approximate.

The reason why only approximate values were obtained is the use of approximations in the above-mentioned derivations of Ω [eq. (2.16)] and r_0 [eq. (2.18)]. Still, these expressions are very useful in estimation of values of r_0 for FRRPP behavior.

Equation (2.8) can be further developed to yield a result that explains some of the critical experimental observation in FRRPP systems. An assumption is made here in which the polymer radical fraction, f_P, is a constant, as it was observed in both PS–S–Ether system (Figs. 2.3.14 and 2.3.15 of Caneba 2010) and also in the PMAA–MAA–Water system (Fig. 2.3.22 of Caneba 2010). With the use of eq. (2.15) and the fact that $x = MW_{Polymer}/MW_{Monomer}$,

$$a' = \frac{f_P \rho_{Soln}^2}{MW_{Polymer} MW_{Monomer}} (X_M - f_P X_P) \frac{dX_P}{dT} > 0. \tag{2.19}$$

Based on initial phase equilibrium conditions, $a' > 0$, or

$$X_M - f_P X_P > 0. \tag{2.20}$$

The implication of eq. (2.20) for FRRPP behavior is that it happens when the monomer concentration is relatively large compared to the polymer concentration. For example, if the system converts all polymer species into radicals ($f_P = 1$), then the asymptotic conversion of polymerization may not be more than 50%. This explains the relatively low asymptotic conversions for some FRRPP systems, such as the PS–S–Ether system at 80°C (23–30%). Note that the relatively high value of f_P (0.80–0.85) for this system forces the asymptotic conversion to be relatively low for FRRPP behavior, based on eq. (2.20). In this case, the cut-off reactive domain size is obtained and shown in Fig. 2.1 for $f_P = 0.80$, based on $C\tilde{n} < -1{,}000$.

Based on Fig. 2.1, reactive domains of the PS–S–Ether system at 350 μm in the reactor are definitely going to fall into the strict FRRPP category, if it is under quasi-steady-state conditions. However, if emulsification of these domains is done to reduce domain sizes to 0.1–1 μm, then these domains could start to exhibit less flat temperature profiles.

If a relatively high asymptotic conversion is obtained, such as the PMAA–MAA–Water system at 80°C or 90°C (80–90%), a relatively low polymer radical fraction value (f_P) would have to happen, as it actually occurs to be in the order of 0.03 for such a system (Sect. 1.1).

The above-mentioned analysis is based on local temperature variations that occur in FRRPP systems that do not employ a dispersing agent for the polymer-rich domains. If an emulsifier is used to force the polymer-rich domains into micron or even submicron scales, domain temperatures may not be flat and they approach those of the dispersing fluid. The implication of this kind of situation will be discussed in the next chapters.

2.3 Nomenclature

2.3.1 Alphabets

2.3.1.1 Upper Case

MW	Molecular weight, g/mol or Daltons
R	Universal gas constant, J/(mol K)
T	Absolute temperature, K
X	Weight fraction, dimensionless

2.3.1.2 Lower Case

a'	Defined in eq. (2.8)
b'	Defined in eq. (2.9)
k	Thermal conductivity of the reaction fluid
r	Radial distance, m or cm
x	Average degree of polymerization of the polymer

2.3.2 Subscripts

a	Pertains to activation energy [eq. (2.11)]
M	Pertains to monomer in eqs. (2.15), (2.16), (2.19), and (2.20)
Monomer	Pertains to monomer
P	Pertains to polymer-rich phase in eqs. (2.15), (2.16), (2.19), and (2.20)
Polymer	Pertains to polymer
Soln	Pertains to overall solution

2.3.3 Superscripts

None

2.3.4 Greek Symbols

Γ	Defined in eq. (2.11), dimensionless
Ψ	Defined in eq. (2.13), dimensionless
Ω	Defined in eq. (2.14), dimensionless

2.3.5 Other Symbols

a'	Defined in Eq. (2.8)
b'	Defined in Eq. (2.9)
α_0	Defined in Eq. (1.18), cm^{-2} or m^{-2}
β_0	Defined in Eq. (1.19), cm^{-2} or m^{-2}
$C\tilde{n}$	Defined in Eq. (1.13), dimensionless
Δ	Change operator (Final minus Initial)
E_P	Activation energy for propagation reaction, used in Eq. (2.11), J/(mol K)
f_P	Polymer radical fraction, dimensionless
ΔH_P	Heat of polymerization, J/mol
k'_0	Defined in Eq. (1.14)
k_P	Propagation rate coefficient, l/(mol s)
MW	Molecular weight, Daltons or g/mol
$[M]$	Monomer concentration, mol/l
$[M]_0$	Initial monomer concentration, mol/l
ρ	Density, g/cm^3 or kg/m^3
r_0	Particle radius, cm or m
$[P\cdot]$	Polymer radical concentration, mol/l
$[P\cdot]_0$	Initial polymer radical concentration, mol/l
T_0	Initial temperature, K

Reference

Caneba GT (2010) Free-radical retrograde-precipitation polymerization (FRRPP): novel concept, processes, materials, and energy aspects. Springer, Heidelberg. ISBN 978-3-642-03024-6

Chapter 3
Molecular Weight Considerations in FRRPP Behavior

Changes in molecular weight in the system can have a profound effect on the progress of FRRPP behavior, especially under conditions where the temperature is easily distributed within the reactive polymer-rich domains. This can occur when domain sizes have been forced to be relatively small through the addition of an emulsifier or a fine dispersing agent. In our experimental efforts, we discovered that a viable first stage of FRRPP behavior for PS–S–Ether system could end at relatively low conversions with relatively large polymer-rich domain sizes (hundreds of microns) that are relatively hot compared to the average reaction fluid of 80°C. Dropping the reactor temperature or adding a good solvent could result in some increase in conversion, but at the expense of terminating the polymer radicals. However, if a fine dispersing agent and its dispersing medium were admixed into the reactor, the reactor polymer-rich domain sizes could be reduced dramatically, and this allows the increase in molecular weight and fractional conversion in the system without terminating a significant portion of the polymer radicals.

Consider a binary polymer-solvent phase diagram with hourglass phase envelopes at higher molecular weights (Figure 1.1.1b in Caneba 2010; Siow et al. 1972). A depiction of the phase diagram that includes hourglass polymer-rich curves is shown in Fig. 3.1. The figure also includes the reaction trajectory in temperature–composition space. After the initial polymer-rich domains are formed at Point B where the polymer has a molecular weight of MW_1, the local temperature will increase to the point that the system reaches a molecular weight MW_2 and a higher temperature T_2. Continued chain extension at T_2 will result in a higher molecular weight MW_3.

What is shown in Fig. 3.1 is the obvious situation in which the value of $C\tilde{n} > 0$. The leap to FRRPP behavior from negative low values of $C\tilde{n}$ is also possible through the hourglass phase envelope by emulsification of an FRRPP-based Polymer–Monomer–Solvent/precipitant system (such as PS–S–Ether). The emulsification will bring such a system to low values of $C\tilde{n}$, which will continue to propagate in a controlled fashion at a higher temperature, and then could reach above LCST temperatures again by itself or through slow removal of the solvent precipitant. The other approach is to carry out the FRRPP polymerization using

G. Caneba and Y. Dar, *Emulsion-based Free-Radical Retrograde-Precipitation Polymerization*, DOI 10.1007/978-3-642-19872-4_3,

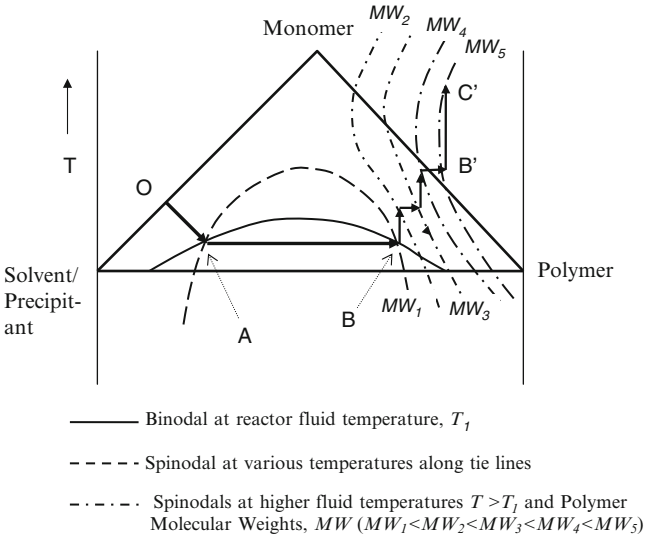

Fig. 3.1 Proposed reaction trajectory for the transition of chain polymerization from the upper critical solution temperature (UCST) to LSCT phase separation via an increase in polymer molecular weight

an emulsion polymerization methodology, with the nonemulsion FRRPP system starting from a conventional precipitation polymerization system and going through an hourglass phase envelope once the high molecular weight polymer is formed (PMMA–MMA–Pentane system).

As it can be noted, this transition through high molecular weight polymer formed in the system depends heavily on the dramatic rise in reactive domain temperatures, which will be shown in the subsequent unsteady state analysis of the thermal effects of the FRRPP system in Chap. 5.

3.1 Nomenclature

$C\tilde{n}$	Cutoff dimensionless number for FRRPP behavior.
MW_1, MW_2	Polymer molecular weights at T_1 and T_2, respectively.
T_1, T_2	Binodal temperature in Fig. 3.1.

References

Caneba GT (2010) Free-radical retrograde-precipitation polymerization (FRRPP): novel concept, processes, materials, and energy aspects. Springer, Heidelberg. ISBN 978-3-642-03024-6

Siow KS, Delmas G, Patterson D (1972) Macromolecules 5:29

Chapter 4
LCST–UCST-Based Copolymerizations

It was shown in Chap. 3 that a polymerization system can start as a conventional precipitation system and end as an FRRPP system, especially if the phase diagram exhibits an hourglass-shaped phase envelope at relatively high polymer molecular weight. This sets up the arguments for other types of shifts from UCST- and LCST-based chain polymerizations, especially in cases wherein multiple monomers are involved. The analysis here will be made for two monomers (copolymerizations), but can be easily extended to multiple monomers. Operationally, it should be emphasized that this is basically a one-pot polymerization methodology, which can be extended to semibatch reactant introduction into the reactor.

There are two known examples of this type of behavior wherein one of the monomers (Monomer 1) form a polymer that precipitates via conventional polymerization while the other monomer (Monomer 2) forms a homopolymer that has an LCST below or a little above the operating temperature. In both cases, reactivity ratios should be that Monomer 1 would tend to react with any polymer radical first, and initial proportion of Monomer 1 is much smaller than that of Monomer 2. Symbolically,

$$f_{1O} = \frac{[M_1]_O}{[M_1]_O + [M_2]_O} < f_{2O} = \frac{[M_2]_O}{[M_1]_O + [M_2]_O}. \tag{4.1}$$

The two cases are going to be discussed in more detail below. In both cases, Monomer 1 was acrylic acid (AA), which produces a homopolymer that exhibits conventional precipitation with a wide variety of small-molecule fluids. Products formed from copolymers of this kind are either water-soluble or self-surfactants in water. It is the former set of products that are of more interest commercially.

G. Caneba and Y. Dar, *Emulsion-based Free-Radical Retrograde-Precipitation Polymerization*, DOI 10.1007/978-3-642-19872-4_4,

4.1 Case 1: Monomer 2 Produces Homopolymer at an Operating Temperature Above the LCST

This case is typified by the use of S as Monomer 2, and the one-pot copolymerization is done in ether at 80°C. Product properties from the S-AA copolymers made from this methodology are presented in Chaps. 3 and 4 of Caneba (2010). Monomer 1 is AA, wherein it was established that its polymer forms below-UCST behavior at the operating temperature. The progression of the reaction trajectory in the temperature–composition phase diagram plots is shown in Fig. 4.1.

The reaction trajectory starting at Point O and the operating temperature enters the phase diagram, where it finds a point in the envelope between the binodals of Homopolymers 1 and 2. When the polymer-rich phase is formed at a copolymer composition CP_1, domain temperatures increase in the system and finds the spinodal at the copolymer composition CP_2. This goes on until Monomer 1 is used up and the system finds the spinodal at a relatively high temperature at the composition P_2 (Point B). The net result is at least a tapered block copolymer of Monomer 1 on one end and Monomer 2 on the other end of the copolymer chain.

It should be noted that the copolymer spinodals are depicted as hourglass shaped in Fig. 4.1, although they do not have to be so.

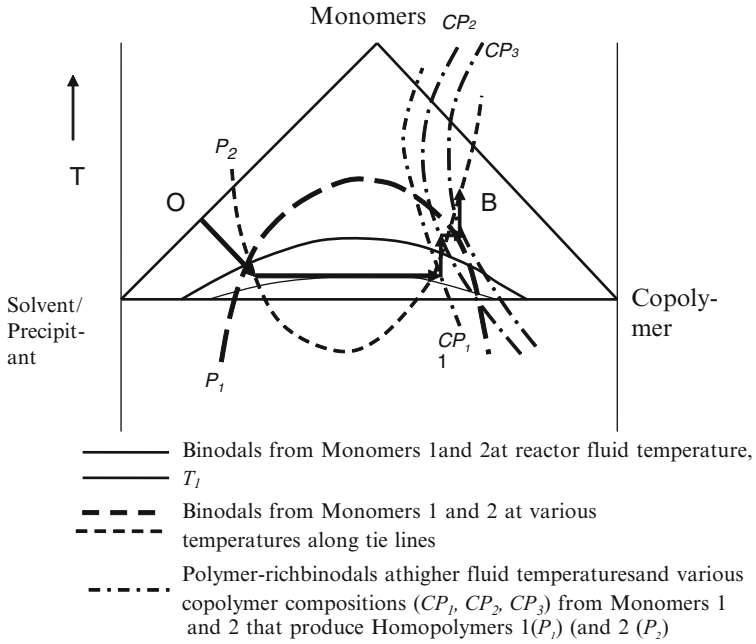

Fig. 4.1 Depicted progress of the reaction trajectory in phase space for one-pot Case 1 FRRPP copolymerization, starting from Point O. Experimentally, the diagram is represented with Monomer 1 as acrylic acid and Monomer 2 as styrene that were copolymerized in ether at 80°C (Caneba 2010)

4.2 Case 2: Monomer 2 Produces Homopolymer at an Operating Temperature Below the LCST

This case is typified by the use of VA as Monomer 2, and the one-pot copolymerization is done in azeotropic *t*-butanol/water at 65°C. Monomer 1 is AA, wherein it was established that its polymer forms below-UCST behavior at the operating temperature. The progression of the reaction trajectory in the temperature–composition phase diagram plots is shown in Fig. 4.2.

The reaction trajectory starting at Point O and the operating temperature enters the phase diagram, where it finds a point in the envelope between the binodals of Homopolymers 1 and 2. When the polymer-rich phase is formed at a point in the binodal phase curve of copolymer composition CP_1, domain temperatures increase in the system and finds the spinodal at the point in the spinodal phase curve of copolymer composition CP_2. This goes on until Monomer 1 is used up and the system finds the spinodal (Point B) at a relatively high temperature at the spinodal phase curve P_2 of copolymer 2.

One important difference between Case 2 from Case 1 is that the high-temperature reaction trajectory can drop to the reactor operating temperature (Point C), without attaining the phase curve (P_2) for Homopolymer 2. This is believed to possibly happen with the VA–AA copolymers made from this method. Again, it should be noted that the copolymer spinodals are depicted as hourglass shaped in

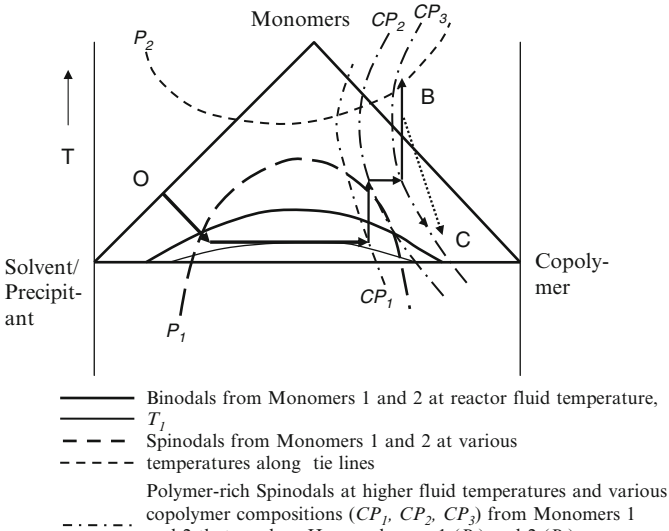

Fig. 4.2 Depicted progress of the reaction trajectory in phase space for one-pot Case 2 FRRPP copolymerization, starting from Point O. Experimentally, the diagram is represented with Monomer 1 as acrylic acid and Monomer 2 as vinyl acetate that were copolymerized in azeotropic *t*-butanol/water at 65°C (Caneba 2010)

Fig. 4.1, although they do not have to be so. It is also possible for a certain fraction of reacting copolymer to end up in Point B, while other fractions are ending up in Point C. Furthermore, Point C can exhibit architectural product variation due to termination of some chains via recombination while the other may not have terminated at all. This explains the possibility of the formation of tapered triblock products. Finally, chain transfer to the polymer should be factored into the analysis of the product distribution, if applicable.

Reference

Caneba GT (2010) Free-radical retrograde-precipitation polymerization (FRRPP): novel concept, processes, materials, and energy aspects. Springer, Heidelberg. ISBN 978-3-642-03024-6

Chapter 5
Unsteady-State Mathematical Modeling/Computer Simulation of FRRPP Behavior

In terms of fluid flow patterns around reactive polymer-rich domains, there were two kinds of experiments that have been done in the past: quiescent fluid FRRPP and mixed-fluid FRRPP reaction systems. The former mode of experimentation was done by Tirumala, both for the formation of polymer nanoparticles (Tirumala 2003; Tirumala et al. 2003) and for the formation of patterned hydrogels (Tirumala et al. 2003c, 2004a, b, c, 2005a, b, 2006). The latter mode of experimentation is the type that occurs in stirred-tank vessels, which is an experimental system that pertains to larger-scale production of bulk homopolymers, copolymers, and multipolymers (Caneba 2010).

In this section, we show results of mathematical modeling/computer simulation work on the reactive spherical FRRPP particle that is immersed in the nonreactive fluid. This model is most applicable to the propagation reaction of emulsion FRRPP systems. Choices of model parameters in the numerical work are determined by analytical efforts, since the nonlinearity of the resulting set of differential equations has been found to complicate the interpretation of numerical results.

5.1 Mathematical Modeling/Computer Simulation of Mixed-Fluid Systems

Two mathematical models will be introduced to simulate FRRPP behavior applicable to emulsion systems: the stagnant boundary-layer-fluid model and the convective-fluid model. The former model involves a layer of stagnant fluid film adjacent to the reactive polymerization spherical domain; the fluid outside the stagnant film is well-mixed with uniform properties and operating conditions. The latter model is not really that much different in picture with the boundary-layer-fluid model, except that its model equations use a convective heat transfer coefficient to characterize fluid behavior outside the reacting polymerization spherical domain. Note that the steady-state model representation in the first FRRPP monograph

G. Caneba and Y. Dar, *Emulsion-based Free-Radical Retrograde-Precipitation Polymerization*, DOI 10.1007/978-3-642-19872-4_5,

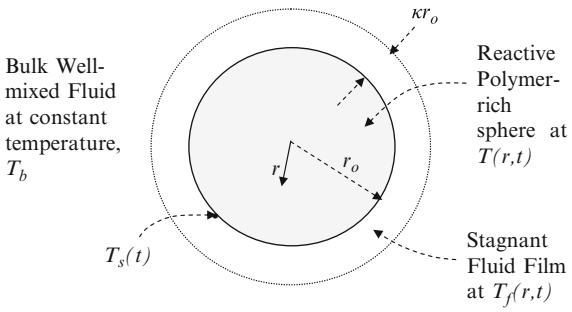

Fig. 5.1 Model representation for the stagnant-fluid reactive polymer-rich domain system. The spherical reactive polymer-rich domain of radius r_0 is assumed to be noninteracting with other polymer-rich domains, and it is bounded by a stagnant fluid film of thickness κr_0

(Chap. 2 of Caneba 2010) is closest to this latter model representation. Both model approaches have their own advantages and disadvantages, and it was hoped that their predictions converge to the same set of results.

5.1.1 Stagnant Boundary-Layer-Fluid Model

5.1.1.1 Model Representation

Figure 5.1 shows a schematic diagram of the model for the reactive polymer-rich domains in a well-mixed solvent/precipitant-rich fluid. The reactive domain is represented by a spherical particle with radius, r_0. Within it, the temperature, $T(r,t)$, varies with time t and radial distance r. Its surface temperature, $T_s(t)$, is also time-dependent. The reactive polymer-rich sphere is covered by a stagnant fluid film with thickness, κr_0, at a temperature $T_f(r,t)$ that varies with time and radial distance. Outside the stagnant film is the well-mixed solvent/precipitant-rich fluid with a constant bulk temperature, T_b. The reacting particle model is noninteracting, i.e., each of the spherical domains is independent of the others.

At the start of reaction ($t = 0$), the reactive spherical polymer-rich domain, its outer surface, and adjacent stagnant fluid film are at a uniform temperature of the bulk fluid. As the reaction progresses ($t > 0$), temperature profiles will be established in the reactive polymer-rich sphere and adjacent stagnant fluid film.

5.1.1.2 Model Equations

If the reactive solid is nonconvecting, a differential energy balance results in (Bird et al. 2007)

$$\frac{\partial T}{\partial t} = \alpha_s \frac{1}{r^2}\frac{\partial}{\partial r}\left(r^2 \frac{\partial T}{\partial r}\right) + \frac{\dot{q}}{\rho_s \hat{C}_{ps}}, \tag{5.1}$$

where α_s is the thermal diffusivity of the reacting spherical polymer-rich domain ($= k_s/\rho_s \hat{C}_{ps}$), k_s is its thermal conductivity, ρ_s is its mass density, and $\hat{C}_{ps}$ is its mass heat capacity. Note that Eq. (5.1) is the unsteady-state version of the quasi-steady-state energy balance equation in the first FRRPP monograph (Equation 2.1.1 of Caneba 2010). Nondimensionalization of Eq. (5.1) results in

$$\frac{\partial \Theta}{\partial \tau} = \frac{1}{\eta^2}\frac{\partial}{\partial \eta}\left(\eta^2 \frac{\partial \Theta}{\partial \eta}\right) + \Phi = \left(\frac{\partial^2 \Theta}{\partial \eta^2}\right) + \frac{2}{\eta}\left(\frac{\partial \Theta}{\partial \eta}\right) + (\alpha\Theta + \beta')e^{-\frac{\gamma'}{\Theta}}. \tag{5.2}$$

Definitions of the dimensionless quantities are obtained in Eqs. (1.1)–(1.15), except that the dimensionless temperature is defined as

$$\Theta = \frac{T}{T_b}, \tag{5.3}$$

and the dimensionless time is

$$\tau = \frac{\alpha_s t}{r_0^2}. \tag{5.4}$$

The implication of Eq. (5.3) is that T_s is substituted with T_b in the definition of all the dimensionless quantities used from Eqs. (1.1) to (1.15), because T_s is varying with time. This means

$$\Theta = \theta\left(\frac{T_s}{T_b}\right), \tag{5.5}$$

$$\beta' = \beta\left(\frac{T_s}{T_b}\right), \tag{5.6}$$

$$\gamma' = \gamma\left(\frac{T_s}{T_b}\right). \tag{5.7}$$

As for the stagnant fluid film, a nonreacting version of Eq. (5.2) is applicable; thus,

$$\frac{\partial T_f}{\partial t} = \alpha_f \frac{1}{r^2}\frac{\partial}{\partial r}\left(r^2 \frac{\partial T_f}{\partial r}\right). \tag{5.8}$$

For a seamless numerical analysis of dimensionless versions of Eqs. (5.1) and (5.8), it should be recognized that the stagnant fluid film can attain thicknesses that are very small (extreme turbulence) or relatively large even compared to the reactive polymer-rich domain size. When the ratio of the film thickness with the reactive particulate domain approaches infinity, the system reverts to a semi-infinite stagnant fluid film. A convenient nondimensionalization of the fluid film is done wherein the dimensionless radial distance in the fluid film is defined as

$$\eta_f = 1 + \frac{r - r_0}{\kappa r_0}. \tag{5.9}$$

This allows η_f to have a range of 1 to 2, while the dimensionless radial distance in the reactive polymer-rich domain η has a range of 0 to 1. With this approach, the dimensionless form of Eq. (5.5) becomes

$$\frac{\partial \Theta_f}{\partial \tau} = \frac{\varepsilon}{[1+(\eta_f-1)\kappa]^2\kappa^2}\frac{\partial}{\partial \eta_f}\left([1+(\eta_f-1)\kappa]^2\frac{\partial \Theta_f}{\partial \eta_f}\right) \tag{5.10}$$

where

$$\Theta_f = \frac{T_f}{T_b}, \tag{5.11}$$

$$\varepsilon = \text{Thermal Diffusivity Ratio} = \frac{\alpha_f}{\alpha_s}. \tag{5.12}$$

It should be noted that Eq. (5.10) is numerically seamless with Eq. (5.2), because their dimensionless times are the same at τ and their respective temperatures are scaled with T_b.

Initial conditions for Eqs. (5.2) and (5.10) are:

$$\Theta(\eta, \tau = 0) = \Theta_f(\eta_f, \tau = 0) = 1. \tag{5.13}$$

Boundary conditions are:

$$\left.\frac{\partial \Theta}{\partial \eta}\right|_{\eta=0} = 0 \quad \text{for all } \tau, \tag{5.14}$$

$$\Theta_f(\eta_f = 2, \tau) = 1. \tag{5.15}$$

For the interface between the reactive polymer-rich domain and stagnant film,

$$\Theta(\eta = 1, \tau) = \Theta_f(\eta_f = 1, \tau) = \frac{T_s}{T_b}, \tag{5.16}$$

$$\left.\frac{\partial \Theta}{\partial \eta}\right|_{\eta=1} = \left.\frac{\partial \Theta_f}{\partial \eta_f}\right|_{\eta_f=1} \quad \text{for all } \tau, \tag{5.17}$$

where

$$\delta = \text{Thermal Conductivity Ratio} = \frac{k_f}{k_s}. \tag{5.18}$$

It should be noted that Eq. (5.16) means that the temperature at the interface is the same T_s on both the reactive polymer-rich domain side and the stagnant fluid film side. Also, Eq. (5.17) means that the heat flux entering the interface from the reactive

polymer-rich domain is balanced by the heat flux leaving the interface into the stagnant fluid film, because energy is neither accumulated nor produced in the interface.

5.1.1.3 Computer Simulation

The computer simulation of the model equation based on Eqs. (5.2) and (5.7) is done using finite difference spatial grid definition with the method-of-lines approach for the solution of the set of initial-value problems (Riggs 1994) of temperature at equal-interval points in the radial distance. A total of 60 intervals in the radial distance is used; 20 on the reactive polymer-rich domain and 40 in the stagnant fluid film.

Reactive Solid Numerical Equations

For interior points, central difference approximations were used to represent spatial derivatives at order of Δx^2. Thus, for $i = 2$–19,

$$\frac{\mathrm{d}\Theta_i}{\mathrm{d}\tau} = \left[\frac{\Theta_{i+1} - 2\Theta_i + \Theta_{i-1}}{(\Delta\eta)^2}\right] + \frac{2}{\eta_i}\left(\frac{\Theta_{i+1} - \Theta_{i-1}}{2\,\Delta\eta}\right) + (\alpha\Theta_i + \beta')\mathrm{e}^{-\frac{\gamma'}{\Theta_i}}. \quad (5.19)$$

At $\eta = 0$, forward-difference of order Δx^2 was used for the spatial derivative equal to zero, in order to obtain the differential equation for Θ_0 based on Eq. (5.2). Note that at $\eta = 0$, the second term of the righthandside of Eq. (5.2) is indeterminate. Applying L'Hospital's rule, this term becomes

$$\lim_{\eta=0}\left[\frac{1}{\eta}\left(\frac{\partial\Theta}{\partial\eta}\right)\right] = \frac{\partial^2\Theta}{\partial\eta^2}. \quad (5.20)$$

Thus, the differential equation at $\eta = 0$ becomes

$$\frac{\mathrm{d}\Theta_1}{\mathrm{d}\tau} = 3\left[\frac{2\Theta_1 - 5\Theta_2 + 4\Theta_3 - \Theta_4}{(\Delta\eta)^2}\right] + (\alpha\Theta_1 + \beta')\mathrm{e}^{-\frac{\gamma'}{\Theta_1}}. \quad (5.21)$$

Stagnant Fluid Numerical Equations

For the interior points ($i = 21$–60), Eq. (5.10) reduces to

$$\frac{d\Theta_{f,i}}{d\tau} = \varepsilon\left[\frac{\Theta_{f,i+1} - 2\Theta_{f,i} + \Theta_{f,i-1}}{\left(\kappa\,\Delta\eta_f\right)^2}\right] + \frac{2\varepsilon}{\kappa\left[1 + \left(\eta_f - 1\right)\kappa\right]}\left(\frac{\Theta_{f,i+1} - \Theta_{f,i-1}}{2\,\Delta\eta_f}\right). \quad (5.22)$$

At the outer boundary of the stagnant fluid ($\eta_f = 2$, $i = 61$), the dimensionless temperature, Θ_f, is equal to 1.0 (or $\Theta_{f,61} = 1.0$). This means that for $i = 60$,

$$\frac{d\Theta_{f,60}}{d\tau} = \varepsilon\left[\frac{1 - 2\Theta_{f,60} + \Theta_{f,59}}{(\kappa\Delta\eta_f)^2}\right] + \frac{2\varepsilon}{[1 + (\eta_f - 1)\kappa]^2\kappa^2}\left(\frac{1 - \Theta_{f,59}}{2\,\Delta\eta_f}\right). \tag{5.23}$$

Solid–Fluid Interface Numerical Equations

At the interface between the reactive polymer-rich domain and the stagnant fluid film, forward difference of order Δx^2 is used to represent the first spatial derivative on the reactive polymer-rich domain side, while backward difference is used for the first spatial derivative of the same order on the stagnant fluid film side. Thus, Eq. (5.17) reduces to

$$\frac{3\Theta_{20} - 4\Theta_{19} + \Theta_{18}}{2\Delta\eta} = \delta\left[\frac{-3\Theta_{f,20} + 4\Theta_{f,21} - \Theta_{f,22}}{2\Delta\eta_f}\right]. \tag{5.24}$$

Equation (5.24) was used to determine $\Theta_{f,20} = \Theta_{20}$, which was substituted into Eq. (5.22) for $i = 21$.

Method of Lines Implementation

For the method-of-lines integration with time, the predictor–corrector method was used through the MATLAB software. Values of 10^{-6} absolute and 10^{-4} relative errors were used in the calculations.

The initial condition used in the simulation corresponds the situation wherein the reactive solid temperature is the same as that of the bulk fluid. In a conventional large-scale reactor operation, it can be obtained in emulsion polymerization systems with a purely redox-based initiation mechanism or approximately for thermal-based initiation in conventional emulsion polymerization. Another viable initial condition is when the reactive solid material and its adjacent fluid film are at a lower temperature than the bulk fluid. This would correspond to an emulsion-based FRRPP system wherein a pre-emulsion monomer/precipitant/thermal initiator material is suddenly mixed with the fluid medium at a higher temperature than the pre-emulsion.

The initial selection for the set of data for the simulation effort is shown in Table 5.1. It is a systematic design-of-experiment listing of the parameter values for α, β', γ', κ, ε, and δ. We note obvious physico-chemical restrictions, such as $(\alpha + \beta)$, γ, κ, ε, $\delta > 0$; the first one used as a rough guide to ensure that the system is exothermic at the start of reaction. From a practical qualitative standpoint, the quantities ε and δ could have similar magnitudes, especially at the low end when they are both equal to zero for an insulating reactive system.

Table 5.1 Parameter set of values for the simulation of model representation from FRRPP and related systems, based on Eqs. (5.1)–(5.18)

Set #	α	β'	γ'	κ	ε	δ	Solid profile	Profile stability	T_s/T_b	β	γ	$C\tilde{n}$
1	−0.1	0.5	0.5	0.1	0	0	Flat	Stable	5.0	0.1	0.10	$-\infty$
2	−0.1	0.5	0.5	0.1	0.001	0.001	Flat	Stable	4.6	0.11	0.11	−1.2
3	−0.1	0.5	0.5	0.1	10	10	Parabolic	Stable	1.01	0.5	0.50	−0.2
4	−0.1	0.5	0.5	1	1	1	Parabolic	Stable	1.06	0.5	0.1	−0.1
5	−0.1	0.5	0.5	1	10	10	Parabolic	Stable	1.04	0.5	0.48	−0.2
6	−0.1	0.5	10	0.1	0	0	Flat	Stable	5.0	0.1	2.0	$-\infty$
7	−0.1	0.5	1	0.1	0	0	Flat	Stable	5.0	0.1	0.2	$-\infty$
8	−0.1	0.5	1	0.1	1	1	Parabolic	Stable	1.02	0.5	1.0	−0.3
9	−0.1	0.5	10	1	0	0	Flat	Stable	5.0	0.1	2	$-\infty$
10	−0.1	0.5	1	1	1	1	Parabolic	Stable	1.01	0.5	1.0	−0.3
11	−2.0	5	0.5	0.1	0	0	Flat	Stable	2.5	2.0	0.2	$-\infty$
12	−2.0	5	0.5	0.1	0.001	0.001	Flat	Stable	2.5	2.0	0.2	$-\infty$
13	−2.0	5	0.5	0.1	10	10	Parabolic	Stable	1.03	4.9	0.1	−3.7
14	−2.0	5	0.5	1	1	1	Parabolic	Stable	1.1	4.5	0.45	−5.6
15	−2.0	5	0.5	1	10	10	Parabolic	Stable	1.01	5.0	1.0	−9.1
16	−2.0	5	10	0.1	0	0	Flat	Stable	2.5	2.0	4.0	$-\infty$
17	−2.0	5	10	0.1	1	1	Flat	Stable	1.0	5.0	10.0	-8×10^6
18	−2.0	5	10	0.1	0.1	0.1	Flat	Stable	1.0	5.0	10.0	-7.3×10^4
19	4.0	−2.5	0.5	0.1	0	0	Flat	Unstable	0.625	−4.0	0.8	$-\infty$
20	4.0	−2.5	0.5	0.1	0.1	0.1	Slightly parabolic	Unstable	N/A	N/A	N/A	N/A
21	4.0	−2.5	0.5	0.1	1	1	Parabolic	Stable	1.3	−1.9	0.4	−5.4
22	4.0	−2.5	0.5	1	10	10	Parabolic	Stable	1.01	−2.5	0.5	−11
23	4.0	−2.5	1	0.1	0	0	Flat	Unstable	0.625	−4.0	1.6	$-\infty$
24	4.0	−2.5	1	1	0	0	Flat	Unstable	0.625	−4.0	1.6	$-\infty$
25	4.0	−2.5	1	0.1	0.1	0.1	Slightly parabolic	Unstable	N/A	N/A	N/A	N/A
26	4.0	−2.5	1	1	10	10	Parabolic	Stable	1.01	−2.5	1.0	−18
27	0.1	5	0.5	0.1	0	0	Flat	Unstable	−50	−0.1	−0.01	N/A
28	0.1	5	0.5	0.1	1	1	Parabolic	Stable	1.5	3.3	0.33	0.11

For low activation energies of monomer-consumption-reactions ($\gamma' = 0.5$) involving Parameter Sets 1–5 (Figs. 5.2–5.6), relatively insulating reactive domains were shown to exhibit flat temperature profiles even at relatively low exotherm levels ($\alpha = -0.1$ and $\beta' = 0.5$ in Parameter Sets 1 and 2 in Figs. 5.2 and 5.3). However, for noninsulating dispersing fluids shown in Parameter Sets 3–5 (Figs. 5.4–5.6), profiles assume the more conventional parabolic type, because surface temperatures have been dragged down by the fluid that is acting as a heat sink. In short, the low levels of exotherms and reaction activation energies cannot keep up with the more efficient heat removal rate from the dispersing fluid. One should also note that as the heat sink capacity of the fluid increases due to higher values of ε and δ (going from Fig. 5.5 to Fig. 5.4), the temperature profile is dragged down with it.

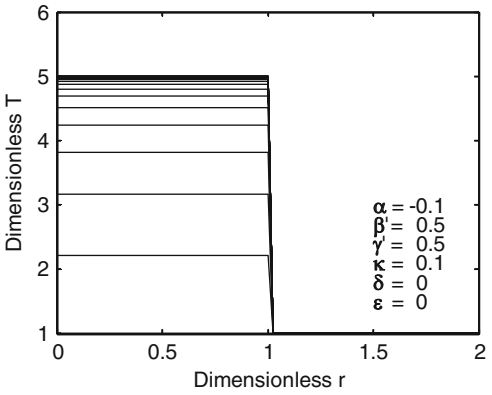

Fig. 5.2 Temperature profile evolution (Dimensionless temperature, Θ vs. Dimensionless Radial distance, η or η_f) for Parameter Set 1. Starting dimensionless time, τ, is 0 at dimensionless temperature of 1.0. Final dimensionless time is 200, with profile dimensionless time step of 10

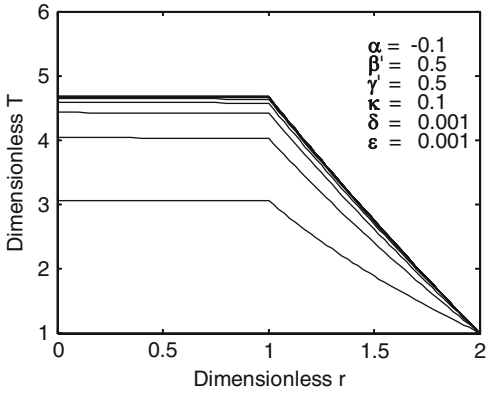

Fig. 5.3 Temperature profile evolution (Dimensionless temperature, Θ vs. dimensionless radial distance, η or η_f) for Parameter Set 2. Starting dimensionless time, τ, is 0 at dimensionless temperature of 1.0. Final dimensionless time is 200, with profile dimensionless time step of 10

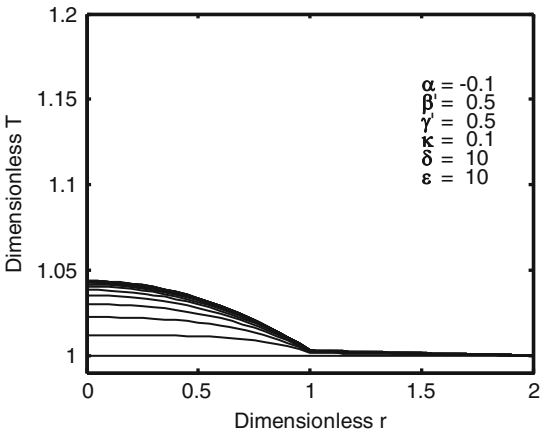

Fig. 5.4 Temperature profile evolution (Dimensionless temperature, Θ vs. dimensionless radial distance, η or η_f) for parameter set 3. Starting dimensionless time, τ, is 0 at dimensionless temperature of 1.0. Final dimensionless time is 0.8, with profile dimensionless time step of 0.05

For higher activation energies of monomer-consumption-reactions ($\gamma' = 1.0, 10$) involving Parameter Sets 6–10 (Figs. 5.7–5.11), relatively insulating reactive domains were also shown to exhibit flat temperature profiles as long as the exotherm

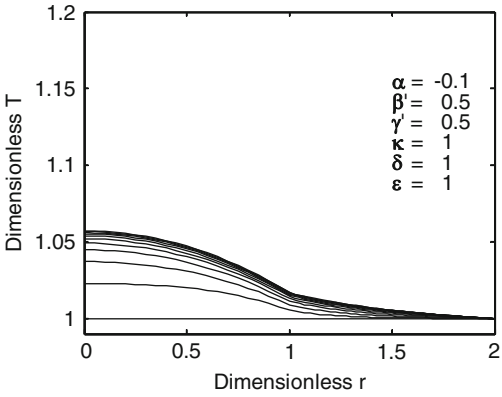

Fig. 5.5 Temperature profile evolution (Dimensionless temperature, Θ vs. dimensionless radial distance, η or η_f) for parameter set 4. Starting dimensionless time, τ, is 0 at dimensionless temperature of 1.0. Final dimensionless time is 1.0, with profile dimensionless time step of 0.1

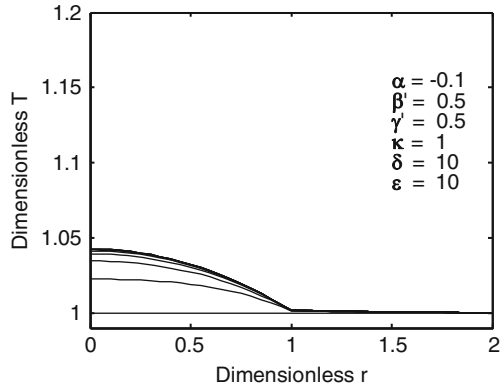

Fig. 5.6 Temperature profile evolution (Dimensionless temperature, Θ vs. dimensionless radial distance, η or η_f) for parameter set 5. Starting dimensionless time, τ, is 0 at dimensionless temperature of 1.0. Final dimensionless time is 1.0, with profile dimensionless time step of 0.1

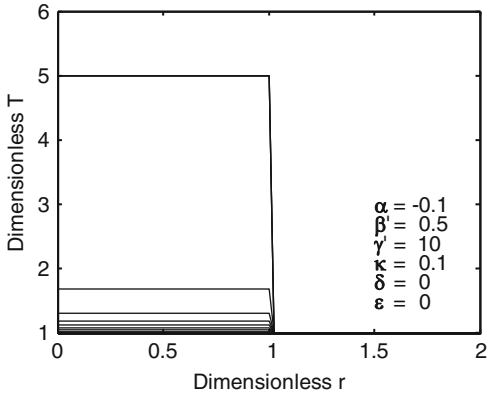

Fig. 5.7 Temperature profile evolution (Dimensionless temperature, Θ vs. dimensionless radial distance, η or η_f) for parameter set 6. Starting dimensionless time, τ, is 0 at dimensionless temperature of 1.0. Final dimensionless time is 10,000, with profile dimensionless time step of 1,000

levels are still relatively low ($\alpha = -0.1$ and $\beta' = 0.5$ in Parameter Sets 6–7 and 9 in Figs. 5.7, 5.8, and 5.10). With a more efficient heat removal fluid (Parameter Sets 8 and 10 in Figs. 5.9 and 5.11), the flat profiles also became parabolic at lower dimensionless temperature levels.

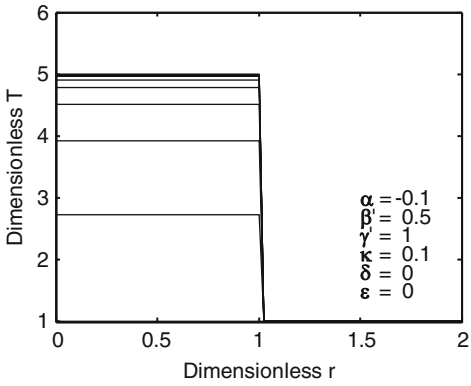

Fig. 5.8 Temperature profile evolution (Dimensionless temperature, Θ vs. dimensionless radial distance, η or η_f) for parameter set 7. Starting dimensionless time, τ, is 0 at dimensionless temperature of 1.0. Final dimensionless time is 100, with profile dimensionless time step of 10

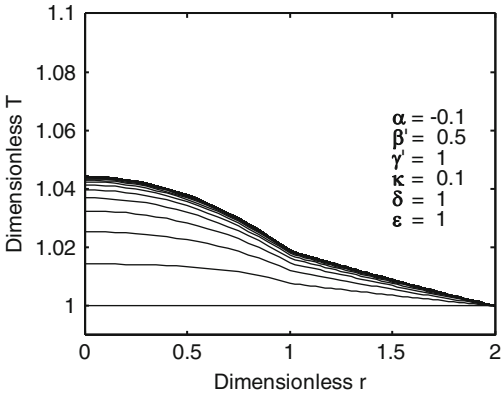

Fig. 5.9 Temperature profile evolution (dimensionless temperature, Θ vs. dimensionless radial distance, η or η_f) for parameter set 8. Starting dimensionless time, τ, is 0 at dimensionless temperature of 1.0. Final dimensionless time is 10, with profile dimensionless time step of 0.1

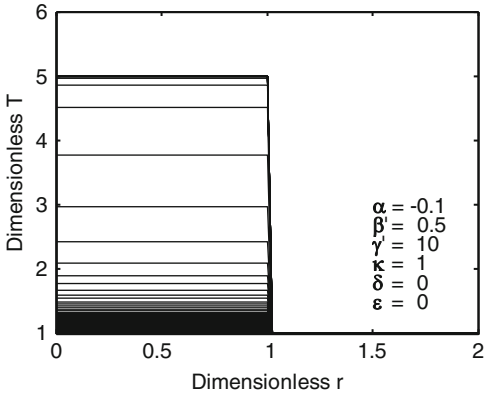

Fig. 5.10 Temperature profile evolution (dimensionless temperature, Θ vs. dimensionless radial distance, η or η_f) for parameter set 9. Starting dimensionless time, τ, is 0 at dimensionless temperature of 1.0. Final dimensionless time is 10,000, with profile dimensionless time step of 100

At higher exotherm levels ($\alpha = -2$ and $\beta' = 5$) and relatively low activation energies of monomer-consumption-reactions ($\gamma' = 0.5$), flat temperature profiles can be maintained with noninsulating dispersion fluids, as seen in the comparison

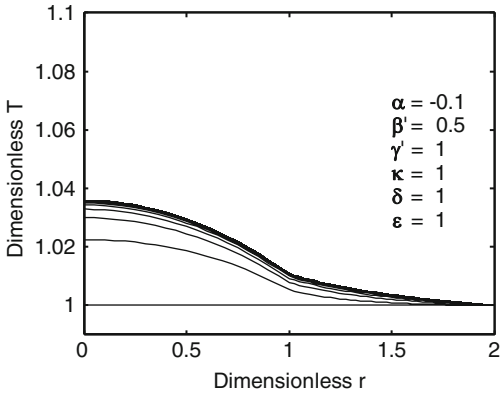

Fig. 5.11 Temperature profile evolution (dimensionless temperature, Θ vs. dimensionless radial distance, η or η_f) for parameter set 10. Starting dimensionless time, τ, is 0 at dimensionless temperature of 1.0. Final dimensionless time is 50, with profile dimensionless time step of 0.2

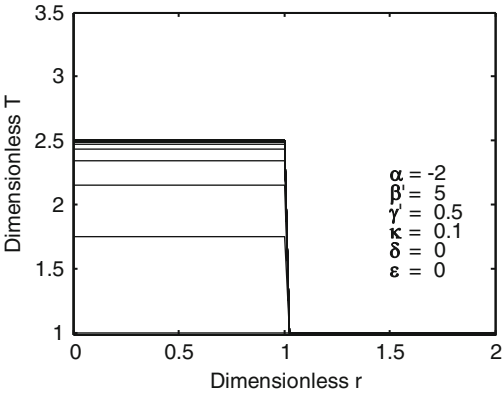

Fig. 5.12 Temperature profile evolution (dimensionless temperature, Θ vs. dimensionless radial distance, η or η_f) for parameter set 11. Starting dimensionless time, τ, is 0 at dimensionless temperature of 1.0. Final dimensionless time is 20, with profile dimensionless time step of 0.5

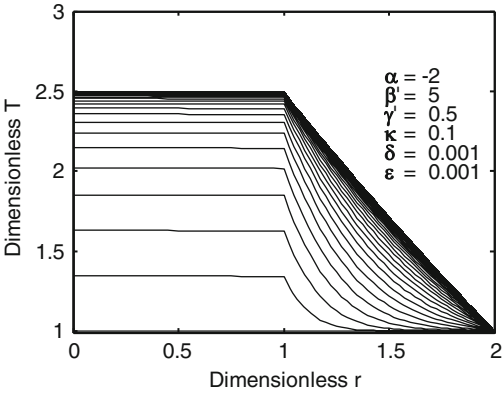

Fig. 5.13 Temperature profile evolution (dimensionless temperature, Θ vs. dimensionless radial distance, η or η_f) for parameter set 12. Starting Dimensionless time, τ, is 0 at dimensionless temperature of 1.0. Final dimensionless time is 100, with profile dimensionless time step of 0.2

between Figs. 5.12 and 5.13. However, with more efficient heat removal fluid system (Figs. 5.14–5.16), the profiles are again changed to parabolic type and dragged down to lower temperatures. When the activation energy of the

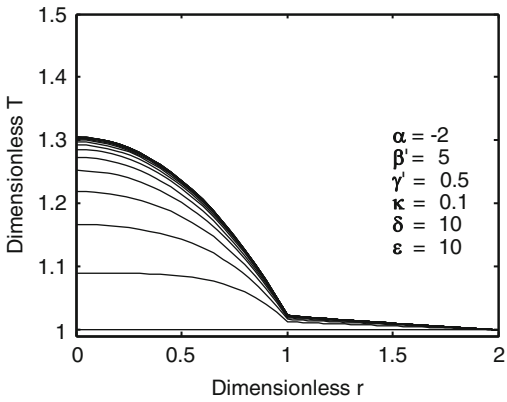

Fig. 5.14 Temperature profile evolution (dimensionless temperature, Θ vs. dimensionless radial distance, η or η_f) for parameter set 13. Starting dimensionless time, τ, is 0 at dimensionless temperature of 1.0. Final dimensionless time is 1.0, with profile dimensionless time step of 0.05

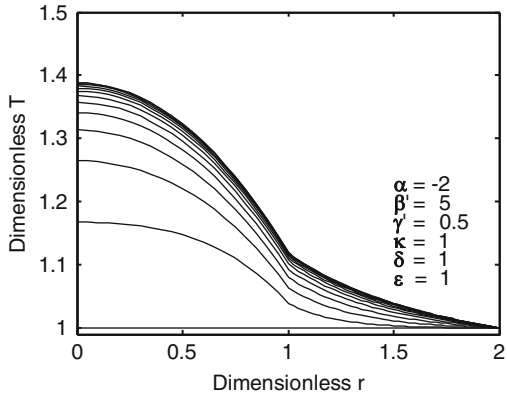

Fig. 5.15 Temperature profile evolution (Dimensionless Temperature, Θ vs. Dimensionless Radial distance, η or η_f) for Parameter Set 14. Starting Dimensionless time, τ, is 0 at Dimensionless Temperature of 1.0. Final Dimensionless Time is 1.2, with profile Dimensionless Time step of 0.1

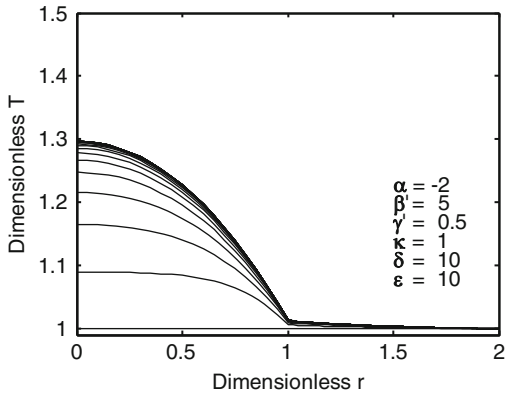

Fig. 5.16 Temperature profile evolution (Dimensionless Temperature, Θ vs. Dimensionless Radial distance, η or η_f) for Parameter Set 15. Starting Dimensionless time, τ, is 0 at Dimensionless Temperature of 1.0. Final Dimensionless Time is 1.5, with profile Dimensionless Time step of 0.05

monomer-consumption-reaction ($\gamma' = 10$) is relatively high at relatively high exotherm levels (Figs. 5.17–5.19), efficient heat removal resulted in the maintenance of the flat temperature profile at levels down to the bulk fluid temperature.

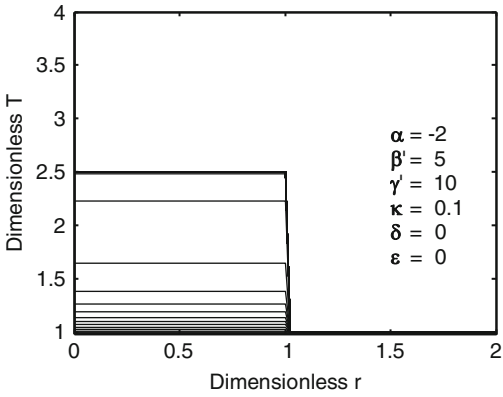

Fig. 5.17 Temperature profile evolution (Dimensionless Temperature, Θ vs. Dimensionless Radial distance, η or η_f) for Parameter Set 16. Starting Dimensionless time, τ, is 0 at Dimensionless Temperature of 1.0. Final Dimensionless Time is 10,000, with profile Dimensionless Time step of 100

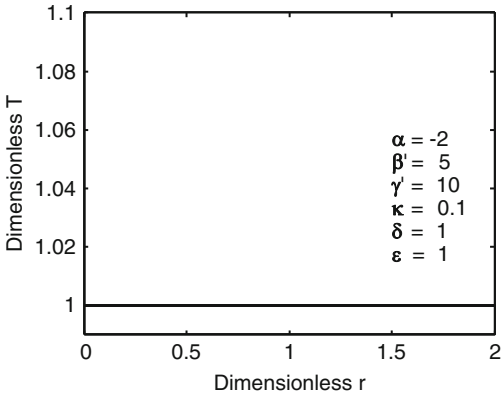

Fig. 5.18 Temperature profile evolution (Dimensionless Temperature, Θ vs. Dimensionless Radial distance, η or η_f) for Parameter Set 17. Starting Dimensionless time, τ, is 0 at Dimensionless Temperature of 1.0. Final Dimensionless Time is 10,000, with profile Dimensionless Time step of 100

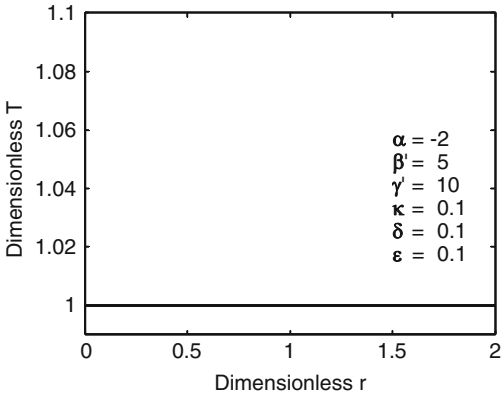

Fig. 5.19 Temperature profile evolution (Dimensionless Temperature, Θ vs. Dimensionless Radial distance, η or η_f) for Parameter Set 18. Starting Dimensionless time, τ, is 0 at Dimensionless Temperature of 1.0. Final Dimensionless Time is 10,000, with profile Dimensionless Time step of 100

In all the above-mentioned Parameter Sets (Parameter Sets 1–18 in Figs. 5.2–5.19), temperature profiles are approaching stable steady-state values versus time. This is seen based on the density of the profiles when steady-state is approached from the starting flat profile of Dimensionless Temperature, $\Theta = 1.0$.

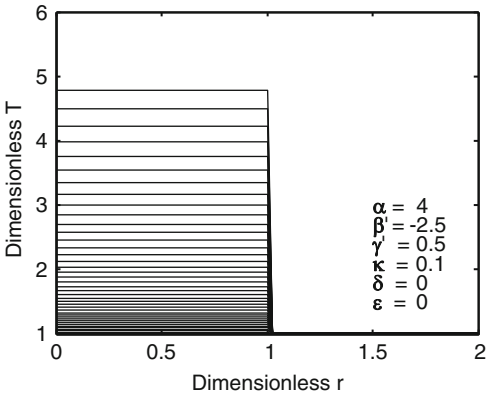

Fig. 5.20 Temperature profile evolution (Dimensionless Temperature, Θ vs. Dimensionless Radial distance, η or η_f) for Parameter Set 19. Starting Dimensionless time, τ, is 0 at Dimensionless Temperature of 1.0. Final Dimensionless Time is 8.0, with profile Dimensionless Time step of 0.02

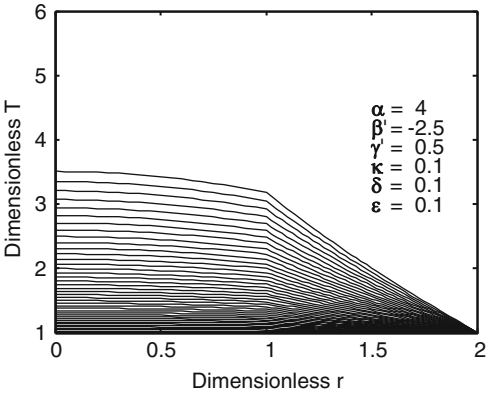

Fig. 5.21 Temperature profile evolution (Dimensionless Temperature, Θ vs. Dimensionless Radial distance, η or η_f) for Parameter Set 20. Starting Dimensionless time, τ, is 0 at Dimensionless Temperature of 1.0. Final Dimensionless Time is 0.80, with profile Dimensionless Time step of 0.02

This is contrasted with the unstable evolution of flat temperature profiles in Fig. 5.20 through Parameter Sets 19, which involves an insulating fluid layer around the reactive solid. The instability is seen from the observation that the temperature profile starts at $\Theta = 1.0$, and it keeps on deviating from that value with time. Simulation was stopped when the dimensionless temperature neared 5.0, but the pattern has become obvious at that point in time. A more efficient heat removal fluid layer results in a slightly flat solid temperature profiles at lower temperature values (Fig. 5.21), although the system is still unstable. As the efficiency of the heat removal is increased in Fig. 5.22, the profile became more parabolic but the system also approaches a stable steady-state pattern. When the activation energy of monomer-consumption-reaction is increased to $\gamma' = 10$, the same qualitative pattern was observed (Figs. 5.23–5.27) in more intense ways. Finally, having positive signs of α and β' did not change the pattern qualitatively (Figs. 5.28 and 5.29).

Table 5.1 also shows results of calculation of the quantity $C\tilde{n}$ for the purpose of validating its use to characterize FRRPP behavior, as proposed in Chap. 2 of Caneba (2010). It should be noted that the value of $C\tilde{n}$ should be less than $-1{,}000$

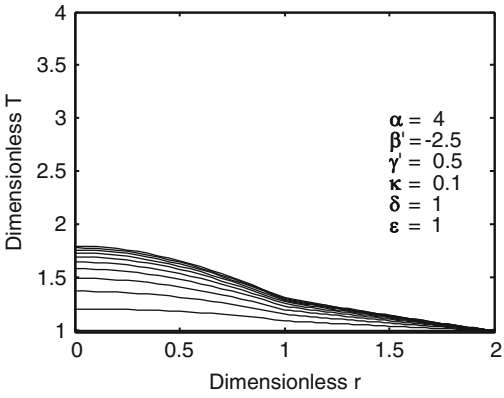

Fig. 5.22 Temperature profile evolution (Dimensionless Temperature, Θ vs. Dimensionless Radial distance, η or η_f) for Parameter Set 21. Starting Dimensionless time, τ, is 0 at Dimensionless Temperature of 1.0. Final Dimensionless Time is 2.0, with profile Dimensionless Time step of 0.2

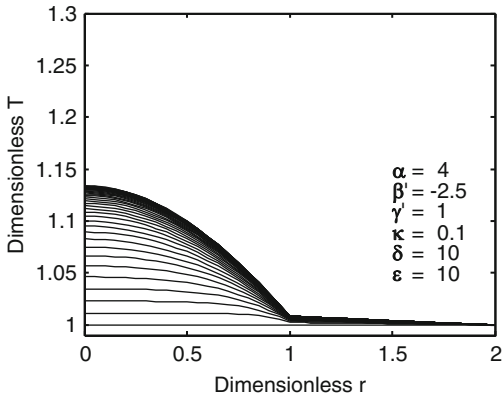

Fig. 5.23 Temperature profile evolution (Dimensionless Temperature, Θ vs. Dimensionless Radial distance, η or η_f) for Parameter Set 22. Starting Dimensionless time, τ, is 0 at Dimensionless Temperature of 1.0. Final Dimensionless Time is 8.0, with profile Dimensionless Time step of 0.02

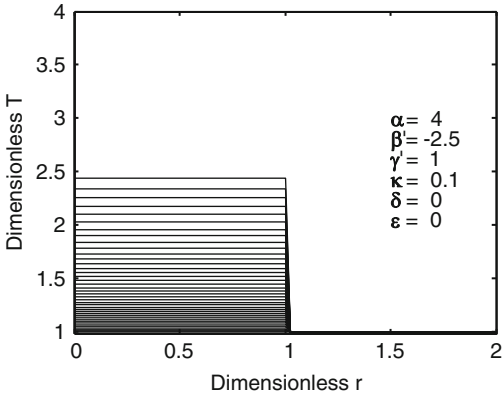

Fig. 5.24 Temperature profile evolution (Dimensionless Temperature, Θ vs. Dimensionless Radial distance, η or η_f) for Parameter Set 23. Starting Dimensionless time, τ, is 0 at Dimensionless Temperature of 1.0. Final Dimensionless Time is 2.0, with profile Dimensionless Time step of 0.2

for a strict adherence to FRRPP behavior, as manifested in achieving a flat steady-state temperature profile. This is confirmed in the results of Table 5.1, specifically in Parameter Sets #1, 6–7, 9, 11–12, 16–18, and 22–23. Even for unstable systems

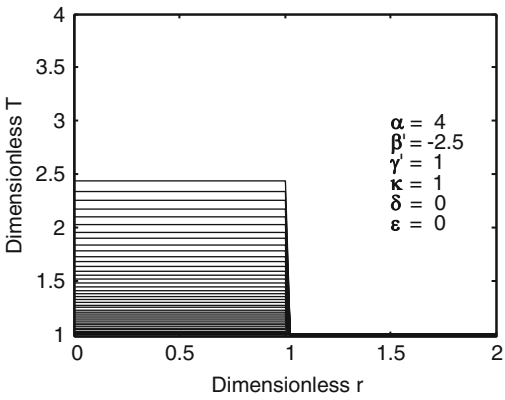

Fig. 5.25 Temperature profile evolution (Dimensionless Temperature, Θ vs. Dimensionless Radial distance, η or η_f) for Parameter Set 24. Starting Dimensionless time, τ, is 0 at Dimensionless Temperature of 1.0. Final Dimensionless Time is 0.8, with profile Dimensionless Time step of 0.02

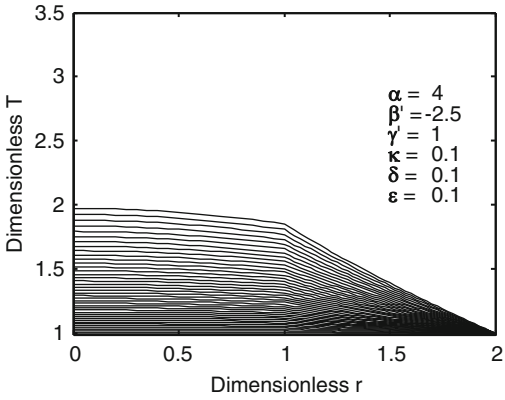

Fig. 5.26 Temperature profile evolution (Dimensionless Temperature, Θ vs. Dimensionless Radial distance, η or η_f) for Parameter Set 25. Starting Dimensionless time, τ, is 0 at Dimensionless Temperature of 1.0. Final Dimensionless Time is 0.8, with profile Dimensionless Time step of 0.02

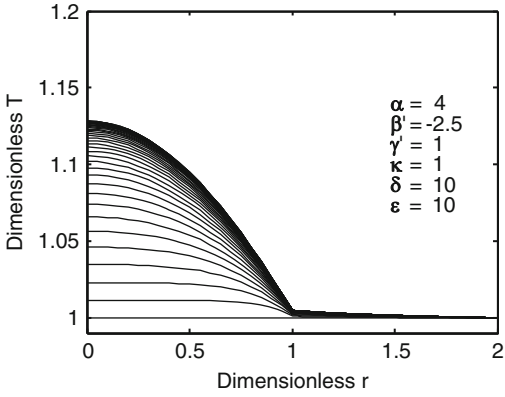

Fig. 5.27 Temperature profile evolution (Dimensionless Temperature, Θ vs. Dimensionless Radial distance, η or η_f) for Parameter Set 26. Starting Dimensionless time, τ, is 0 at Dimensionless Temperature of 1.0. Final Dimensionless Time is 0.8, with profile Dimensionless Time step of 0.02

with Parameter Sets #19 and 22–23, flat temperature profiles are obtained for large negative values of $C\tilde{n}$ even though realistically the system will not attain their steady-state conditions. Furthermore, flat temperature profiles seem to be possible

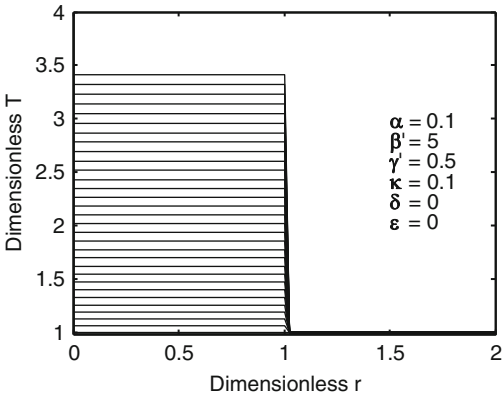

Fig. 5.28 Temperature profile evolution (Dimensionless Temperature, Θ vs. Dimensionless Radial distance, η or η_f) for Parameter Set 27. Starting Dimensionless time, τ, is 0 at Dimensionless Temperature of 1.0. Final Dimensionless Time is 0.6, with profile Dimensionless Time step of 0.02

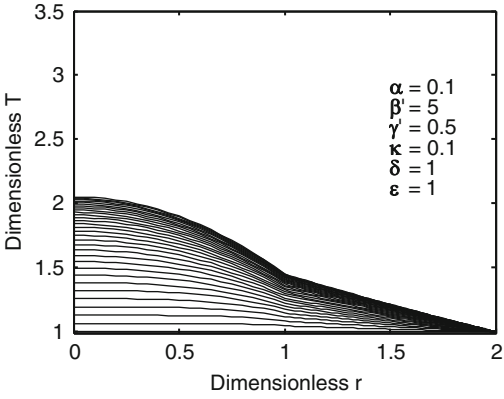

Fig. 5.29 Temperature profile evolution (Dimensionless Temperature, Θ vs. Dimensionless Radial distance, η or η_f) for Parameter Set 28. Starting Dimensionless time, τ, is 0 at Dimensionless Temperature of 1.0. Final Dimensionless Time is 0.6, with profile Dimensionless Time step of 0.02

for systems with $C\tilde{n}$ between zero and −1,000, if they involve almost insulating fluid layers, as seen in Parameter Set #2. This explains why 1–2 nm PS nanoparticles were obtained in quiescent FRRPP systems by Tirumala (Tirumala 2003; Tirumala et al. 2003).

A more perceptive analysis of parameters sets exhibiting unstable behavior is shown in Sect. 5.2. Finally, MATLAB codes for the above-mentioned unsteady-state analysis can be found in Alharthi (2010).

5.1.2 Convective-Fluid Model

This model representation is illustrated in Fig. 5.30. The symbolism on the reactive polymer-rich sphere is the same as that of the stagnant-boundary-layer model (Fig. 5.1). Outside the reactive particle, the fluid is convecting with a convective heat transfer coefficient, h.

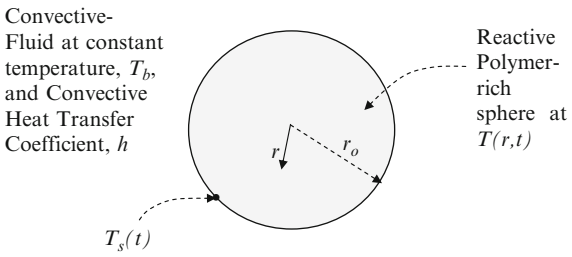

Fig. 5.30 Model representation for the convective-fluid reactive polymer-rich domain system. The spherical reactive polymer-rich domain of radius r_0 is assumed to be noninteracting with other polymer-rich domains, and it is bounded by the convective-fluid film medium with the convective heat transfer coefficient, h

The numerical equations are the same for the reactive domain sphere [Eqs. (5.19)–(5.21)]. At the solid–fluid interface, the boundary condition involves the equality of the conductive heat transfer rate at the surface and the convective heat transfer rate on the adjacent fluid.

$$-k_{\mathrm{s}}\frac{\partial T}{\partial r} = hA(T_{\mathrm{s}} - T_{\mathrm{f}}), \tag{5.25}$$

where A is the surface area of the reactive sphere. Numerically, this translates to the following equation

$$\frac{3\Theta_{10} - 4\Theta_9 + \Theta_8}{2\ \Delta\eta} = \mathrm{Nu}\left[\frac{\Theta_{10} - 1}{2}\right], \tag{5.26}$$

where Nu is the Nusselt Number that is expressed as

$$\mathrm{Nu} = \frac{h(2r_0)}{k_{\mathrm{s}}}. \tag{5.27}$$

Based on the work by Alharthi (2010), we have shown the direct equivalence of this model with the above-mentioned Boundary-Layer Model, through calculation of values of Nusselt Numbers from the temperature profiles.

5.2 Flat Temperature Profile Analysis

If it is known that the temperature profile is flat, then the first term on the righthandside of Eq. (5.28) can be neglected and the dimensionless temperature is solely a function of the dimensionless time; thus,

$$\frac{\mathrm{d}\Theta}{\mathrm{d}\tau} = \Phi = (\alpha\Theta + \beta')\mathrm{e}^{-\gamma'/\Theta}. \tag{5.28}$$

Integrating at $\tau = 0$ to τ and $\Theta = 1$ to Θ, the following is obtained

$$\tau = \int_1^{\Theta} \frac{e^{\gamma'/\Theta}}{(\alpha\Theta + \beta')} d\Theta. \tag{5.29}$$

An analytical result for Eq. (5.29) can be obtained through the software Mathematica®, resulting in the so-called Exponential Integral Function, Ei:

$$\tau = \left[\frac{e^{-\alpha\gamma'/\beta'} \mathrm{Ei}\left(\gamma'\left(\frac{\alpha}{\beta'} + \frac{1}{\Theta}\right)\right) - \mathrm{Ei}\left(\frac{\gamma'}{\Theta}\right)}{\alpha} \right]. \tag{5.30}$$

The function, Ei, is a special transcendental function which has been found to occur in only a few experimental systems, and can be evaluated through the following infinite series expansion for real positive arguments ($x \to 0$):

$$\mathrm{Ei}(x) = (\text{Euler} - \text{Mascheroni Constant}) + \ln(x) + \sum_{k=1}^{\infty} \frac{x^k}{k(k!)}. \tag{5.31}$$

The Euler–Mascheroni constant (also called Euler's constant) has been cited to be equal to 0.5772156649 (Spanier and Oldham 1987).

In general, the argument within the Ei function can be a complex number, which can result in periodic behavior. However, in FRRPP, Ei can only take real number arguments resulting in nonperiodic behavior. Quantitative complications for Ei are that it exhibits a discontinuity at argument value of zero and an inflection point at the argument value of 1.0 (Spanier and Oldham 1987).

5.2.1 *Stability Analysis of Unsteady-State Thermal History from Flat Temperature Profiles*

In order to further narrow down the range of parameters in Eq. (5.28), a stability analysis is done. It starts with the determination of the steady-state condition or fixed point, which is obtained by equating the righthandside of Eq. (5.28) to zero. Thus,

$$\Theta_{ss} = -\frac{\beta'}{\alpha}, \tag{5.32}$$

where Θ_{ss} is the steady-state or fixed point value of Θ. Stability characteristics of this fixed point is obtained by evaluating the velocity vector of Eq. (5.28), i.e.,

$$\frac{\partial\Phi}{\partial\Theta} = \Phi' = \left[\alpha + \frac{\alpha\gamma'}{\Theta} + \frac{\beta'\gamma'}{\Theta^2}\right] e^{-\frac{\gamma'}{\Theta}}. \tag{5.33}$$

Applying the fixed-point condition of $\Theta = \Theta_{ss}$ to Eq. (5.33) results in

$$\Phi' = \alpha e^{\alpha\gamma'/\beta'}. \tag{5.34}$$

Equation (5.34) reveals that the stability characteristic of Eq. (5.28) is based on the sign of α, i.e.,

$$\alpha < 0 \quad \text{for a stable fixed point or steady-state behavior.} \tag{5.35}$$

It should be noted that the arguments in the exponential integral functions in Eqs. (5.30) and (5.31) are both positive numbers. The $\gamma'\left(\frac{\alpha}{\beta'} + \frac{1}{\Theta}\right)$ argument is positive because γ' is positive and $\left(\frac{\alpha}{\beta'} + \frac{1}{\Theta}\right)$ should be positive for an exothermic reaction, as noted in Eqs. (5.1) and (5.2). The argument in the other exponential integral is positive because γ'/Θ is also positive. Conditions specifying positive values in arguments within the Exponential Integral Functions in Eqs. (5.30) and (5.31) are convenient for interpretation of short-cut numerical results for evolution of temperature within the FRRPP reactive spherical particulate system.

5.2.2 *Approximate Analytical Solutions to Unsteady-State Thermal History from Flat Temperature Profiles*

It should be noted that since Eq. (5.28) does not involve any boundary conditions, its results would be approximate at best. However, these results are still applicable in certain situations and are good ways of checking the validity of the method used for the full numerical solution of the unsteady-state FRRPP problem.

The following mathematical conditions summarize various features of the FRRPP behavior:

1. The quantity $\alpha < 0$ for an asymptotically stable approach to steady-state condition.
2. The quantity $\beta' > 0$ for an asymptotically stable approach to steady-state condition. Since $\beta' = (T_s/T_b)\beta$, then $\beta > 0$ as well for an asymptotically stable approach to steady-state condition.
3. The quantities γ' and γ are always positive real numbers.
4. In order to satisfy an exothermic polymerization reaction kinetics, the quantities $(\alpha\Theta + \beta')$ and $(\alpha\theta + \beta)$ have to assume positive values. This is not a trivial condition, because even if the above Conditions 1 and 2 are not satisfied at the start of the unsteady-state behavior, this exothermicity condition should always be satisfied.
5. For an isolated reactive domain with thermally insulating boundaries, $\varepsilon = \delta = 0$. This is believed to be the condition for the applicability of a flat temperature profile that results in Eq. (5.28) in FRRPP systems, as it will be shown below.

6. Based on steady-state analysis, for a strict FRRPP behavior of a flat temperature profile, the quantity $C\tilde{n}$ [see Eq. (1.13)] has been proposed to be less than $-1{,}000$ (Caneba 2010).

Accordingly, the following results are obtained for the evolution of flat temperature profiles in stable FRRPP parameter shown in Table 5.1 (Figs. 5.31–5.38).

It is evident from Fig. 5.31 that the dimensionless temperature Θ is approaching the value of 5.0 at steady-state ($\tau \rightarrow \infty$), in accordance with the prediction of Eq. (5.32). Stable steady-state is also obtained, because the parameter $\alpha < 0$, in accordance with the prediction of Eq. (5.34).

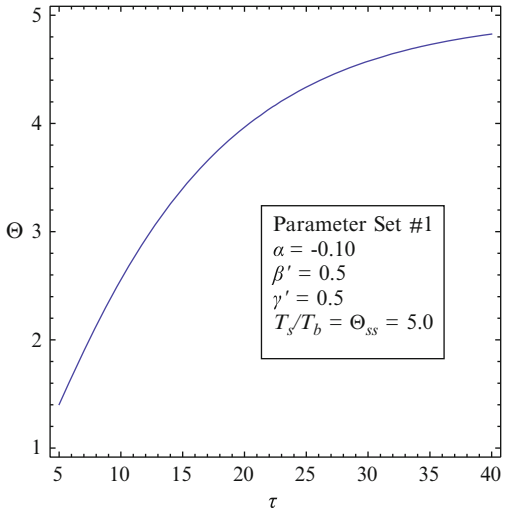

Fig. 5.31 Evolution of flat temperature profile for a simulated FRRPP system with stable steady-state behavior, using Parameter Set #1

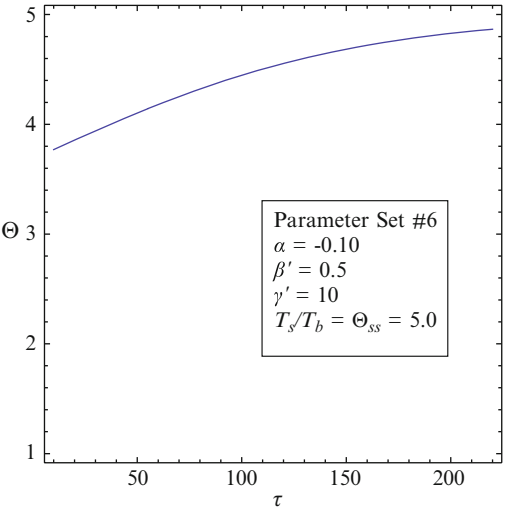

Fig. 5.32 Evolution of flat temperature profile for a simulated FRRPP system with stable steady-state behavior, using Parameter Set #6

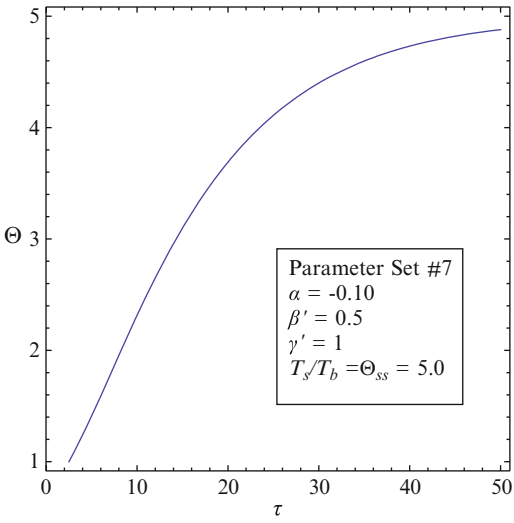

Fig. 5.33 Evolution of flat temperature profile for a simulated FRRPP system with stable steady-state behavior, using Parameter Set #7

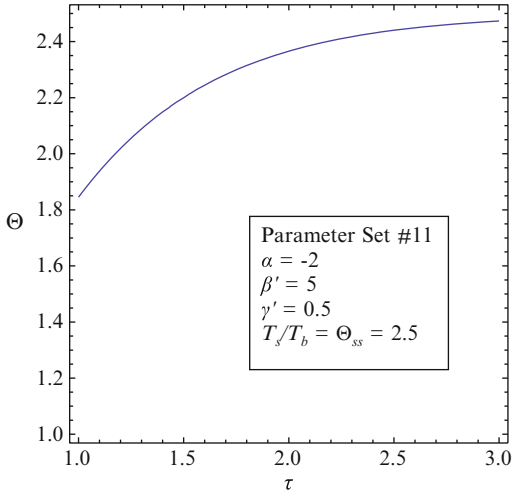

Fig. 5.34 Evolution of flat temperature profile for a simulated FRRPP system with stable steady-state behavior, using Parameter Set #11

A similar pattern was observed for the profile in Figs. 5.32 and 5.33, in which the dimensionless temperature Θ is approaching the value of 5.0 at steady-state ($\tau \rightarrow \infty$), in accordance with the prediction of Eq. (5.32).

In Figs. 5.34 and 5.35, a similar evolution profile is observed, except that the steady-state value of the dimensionless temperature Θ is at 2.5, in accordance with the prediction of Eq. (5.32). Stable steady-state is also obtained, because the parameter $\alpha < 0$, in accordance with the prediction of Eq. (5.34).

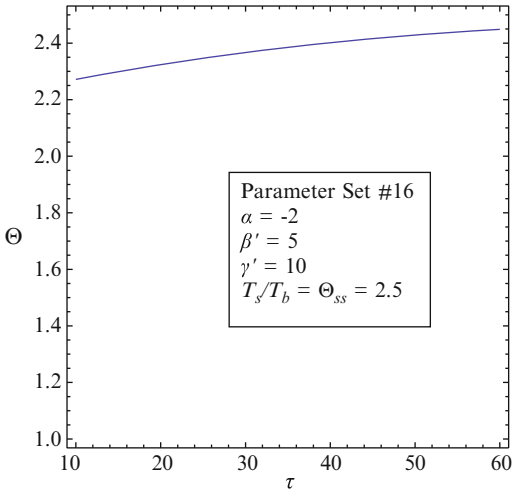

Fig. 5.35 Evolution of flat temperature profile for a simulated FRRPP system with stable steady-state behavior, using Parameter Set #16

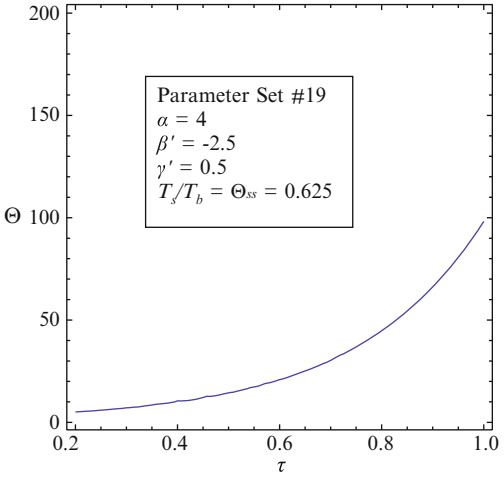

Fig. 5.36 Evolution of flat temperature profile for a simulated FRRPP system with an unstable steady-state behavior, using Parameter Set #19

In the next set of figures (Figs. 5.36–5.38), evolution of unsteady-state profiles are plotted, because values of α are greater than zero. Unstable steady-state values of the dimensionless temperature indicated in the legends (Θ_{ss}) are values of Θ that the system would be approaching if simulations of Eq. (5.28) were ran backwards in dimensionless time.

It should again be noted that these evolution profiles calculated from the exponential integral functions at $\tau \rightarrow 0$ would exhibit some errors, due to the discontinuity at argument limits of zero. Such errors are reflected in the left side

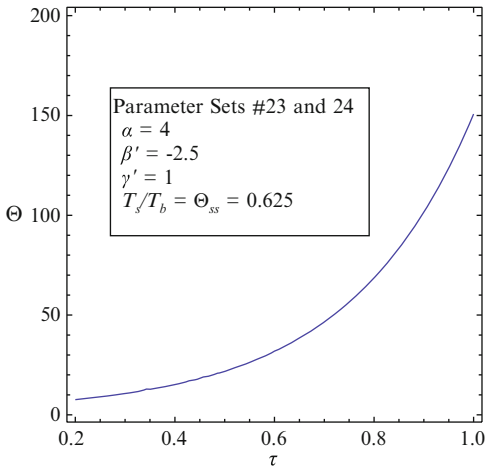

Fig. 5.37 Evolution of flat temperature profile for a simulated FRRPP system with an unstable steady-state behavior, using Parameter Sets #23 and 24

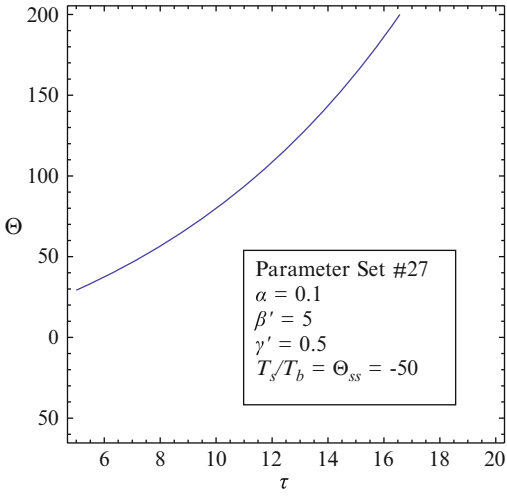

Fig. 5.38 Evolution of flat temperature profile for a simulated FRRPP system with an unstable steady-state behavior, using Parameter Set #27

of the curves of Figs. 5.31–5.38. Nevertheless, patterns in these curves agree with the full simulation results of the Boundary Fluid Model, especially towards larger values of dimensionless time, τ.

5.2.3 Physical Interpretation of Eq. (5.28)

The use of Eq. (5.28) does not take into account the relative thickness of the boundary layer fluid (κ), and the results correspond to a perfectly insulated reactive

spherical material ($\varepsilon = \delta = 0$). This makes perfect sense, since thermal gradients are not supposed to exist at insulating boundary conditions. Simulation results of the full set of partial differential equations and their numerical expressions [Eqs. (5.1)–(5.18)] have been shown to match with predictions of the short-cut method of determining the evolution of the dimensionless temperature in flat temperature profile systems.

5.3 Comparison of Model Predictions with Behavior of Experimental Systems

5.3.1 PS–S–Ether System

For the reaction system that corresponds to the PS–S–Ether recipe at 80°C bulk fluid temperature, the following parameters are used for collapsed globules:

$\alpha_0 = 1.700 \times 10^8\ \text{cm}^{-2}$
$\beta_0 = -1.121 \times 10^8\ \text{cm}^{-2}$
Reactive Polymer-rich Domain radius, $r_0 = 0.00001$–$0.001, 0.05$ cm
$\alpha = 0.017$–$170, 42{,}500$
$\beta = -0.01121$ to $112.1, -28{,}025$
$\gamma = 10$
Thermal Diffusivity Ratio, $\varepsilon = 0.01$–10
Thermal Conductivity Ratio, $\delta = 0.01$–10
Fluid Film Thickness relative to Reactive Polymer-rich domain radius, $\kappa = 0.001$–10
$C\tilde{n} = -725 - -7.25 \times 10^6, -1.81 \times 10^9$ (at $r_0 = 0.00001$–$0.001, 0.05$ cm)
Starting Dimensionless Time $= 0$
Relative Tolerance $= 10^{-4}$
Absolute Tolerance $= 10^{-6}$

For the range of parameters pertaining to the 0.00001–0.001 cm particle radii, dimensionless temperature profiles have been found to be stable and almost parabolic between 1.00 and 1.01 only. An extreme case of a profile that reached the Dimensionless Temperature of 1.01 is shown in Fig. 5.39. Since it was suggested in the first FRRPP monograph (Caneba 2010) that particle diameters are in the 350-μm range, its dynamic behavior was investigated, and the result shown in Fig. 5.40. In this case, the unstable steady-state behavior of the system started to show up with more of a parabolic temperature profile. In a practical sense, this means that the reactive domain could become relatively hot. The cooling off of these hot relatively large domains can occur if and when the thermodynamic phase distribution could result in crossover of the signs of α and β, which would then bring the dynamic system into a stable quasi-steady-state behavior.

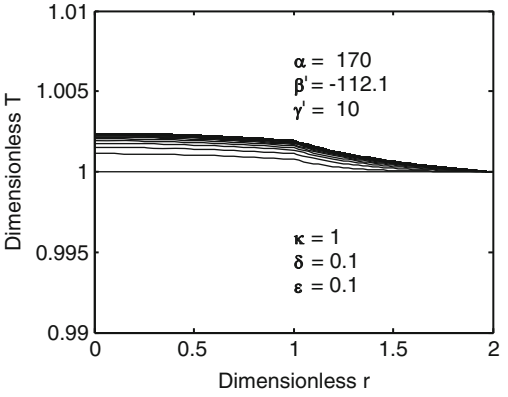

Fig. 5.39 Temperature profile evolution (Dimensionless Temperature, Θ vs. Dimensionless Radial distance, η or η_f) for the PS–S–Ether system at 80°C. The reactive spherical particulate has a radius of 0.001 cm. Starting Dimensionless time, τ, is 0 at Dimensionless Temperature of 1.0. Final Dimensionless Time is 100, with profile Dimensionless Time step of 1

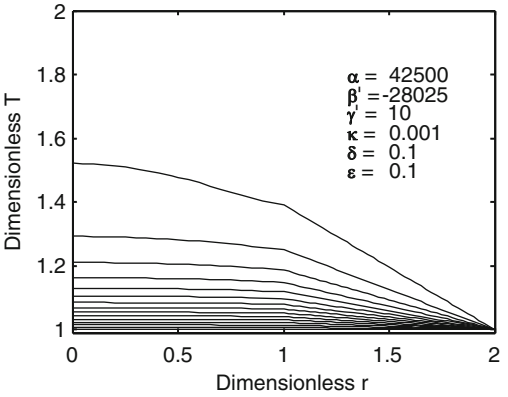

Fig. 5.40 Temperature profile evolution (Dimensionless Temperature, Θ vs. Dimensionless Radial distance, η or η_f) for the PS–S–Ether system at 80°C. The reactive spherical particulate has a radius of 0.05 cm. Starting Dimensionless time, τ, is 0 at Dimensionless Temperature of 1.0. Final Dimensionless Time is 1, with profile Dimensionless Time step of 0.01

5.3.2 PMAA–MAA–Water System

For the reaction system that corresponds to the PMAA–MAA–Water reacting system, the following parameters are used:

$\alpha_0 = 3{,}445\ \text{cm}^{-2}$

$\beta_0 = -357.1\ \text{cm}^{-2}$

Reactive Polymer-rich Domain radius, $r_0 = 0.001$–0.1 cm

$\alpha = 3.445 \times 10^{-3} - 34.45$

$\beta = -3.571 \times 10^{-4}$ to -3.571

$\gamma = 5.21$
Thermal Diffusivity Ratio, $\varepsilon = 0.01$–10
Thermal Conductivity Ratio, $\delta = 0.01$–10
Fluid Film Thickness relative to Reactive Polymer-rich domain radius, $\kappa = 0.001$–10
$C\tilde{n} = -0.073$ to -730
Relative Tolerance $= 10^{-4}$
Absolute Tolerance $= 10^{-6}$

Profiles for the PMAA–MAA–Water system at the low end of reactive particulate size of 0.001 cm have been shown to be flat close to Dimensionless Temperature of 1.0. Figures 5.41 and 5.42 show results of evolution of temperature profiles at the high end of the size scale at 0.1 cm reactive particulate radius. In Fig. 5.41, heat removal capability of the fluid is not efficient due to relatively small values of ε and δ. Since the system is inherently unstable (due to the positive value of α), an almost insulating fluid layer would not be able to arrest the uncontrolled rise in profile temperature, as seen in the figure. When a more efficient heat removal fluid layer is employed, as seen in Fig. 5.42, the rise in profile temperature has been brought under control. With an aqueous solvent/precipitant, this would be the more likely scenario, although a mass transfer-based mechanism has been shown in the first FRRPP monograph (Caneba 2010) as a crucial factor for reaction control in the system.

It should be noted that the above quantitative analysis thus far used overall compositions of the polymer-rich phase domains of reactive systems. The next level of analysis will have to involve reactive site compositions, which should involve decreased monomer and increased polymer concentrations as the temperature increases. An investigation of this idea is done using some of deviated values of compositions of polymer and monomer at 90°C, from base values at 80°C in Tables 1.1 and 1.2 (Table 5.2).

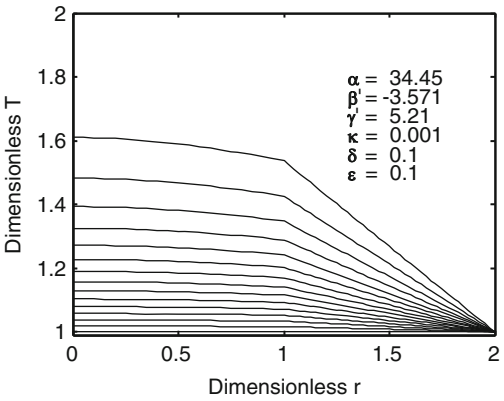

Fig. 5.41 Temperature profile evolution (Dimensionless Temperature, Θ vs. Dimensionless Radial distance, η or η_f) for the PMAA–MAA–Water system at 80°C. The reactive spherical particulate has a radius of 0.1 cm. Starting Dimensionless time, τ, is 0 at Dimensionless Temperature of 1.0. Final Dimensionless Time is 100, with profile Dimensionless Time step of 1

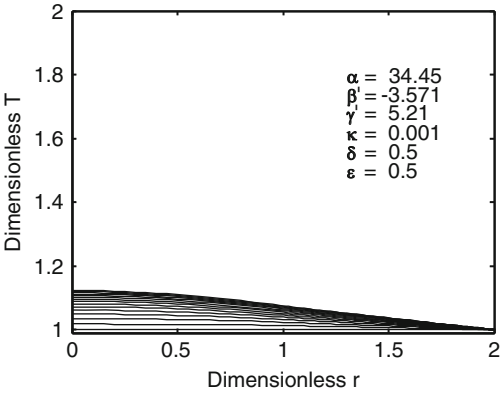

Fig. 5.42 Temperature profile evolution (Dimensionless Temperature, Θ vs. Dimensionless Radial distance, η or η_f) for the PMAA–MAA–Water system at 80°C. The reactive spherical particulate has a radius of 0.1 cm, and heat removal capability through the fluid is better than that in Fig. 5.41. Starting Dimensionless time, τ, is 0 at Dimensionless Temperature of 1.0. Final Dimensionless Time is 1.4, with profile Dimensionless Time step of 0.1

Table 5.2 Effects of deviated values of reactive domain compositions for PS–S–Ether and PMAA–MAA–Water systems at 90°C, from base values at 80°C in Tables 1.1 and 1.2

Reactive polymer domains system and compositional weight fractions						
X_M	X_P	r_0, cm	α (f_p)	$\beta = \beta'$ (f_p)	$\gamma = \gamma'$	$C\tilde{n}$ (f_p)
PS–S–Ether						
0.01	0.2605	0.035	-1.929×10^6 (0.80)	1.990×10^6 (0.80)	10.0	-1.375×10^{12} (0.80)
0.01	0.6	0.035	-1.448×10^6 (0.80)	1.505×10^6 (0.80)	10.0	-8.456×10^{11} (0.80)
0.01	0.2605	1.0×10^{-6}	−0.00197 (0.80)	0.002031 (0.80)	10.0	−1,123 (0.8)
0.01	0.6	1.0×10^{-6}	−0.00148 (0.80)	0.001535 (0.80)	10.0	−690 (0.8)
PMAA–MAA–Water						
0.001	0.17	0.1	−0.7620 (0.01)	0.7841 (0.01)	5.21	−4,959 (0.01)
0.001	0.80	0.1	−1.0440 (0.01)	1.0758 (0.01)	5.21	−6,465 (0.01)
0.001	0.17	0.01	−0.00762 (0.01)	0.007841 (0.01)	5.21	−49.6 (0.01)
0.001	0.80	0.01	−0.01044 (0.01)	0.01076 (0.01)	5.21	−64.6 (0.01)

One can see from the table the shift in the signs of α and β, indicating stable steady-state systems when the monomer concentration is dropped due to reactive domain densification. In the PS–S–Ether system, a drop of the monomer weight fraction from 0.067 to 0.01 results in $C\tilde{n} < -1{,}000$ for particle radius as small as

10 nm for the same reactive domain polymer weight fraction of 0.2605 and $f_p = 0.80$. As for the PMAA–MAA–Water system, the shifting of the signs also occur when the monomer weight fraction in the reactive domains are decreased. A strict FRRPP behavior based on the steady-state analysis done in Chap. 2 of the first FRRPP monograph (Caneba 2010) is apparently shown to occur when the particle radius is larger than 1 mm, even when the initiator efficiency was reduced to 0.01.

When the unsteady-state analysis is done in both PS–S–Ether and PMAA–MAA–Water systems at 80°C reactor temperature, the cases in Table 5.2 all resulted in a stable flat temperature profile as the one shown in Figs. 5.18 (Parameter Set #17) and 5.19 (Parameter Set #18) for reasonable values of relative stagnant film thickness, κ, thermal diffusivity ratio, ε, and thermal conductivity ratio, δ. In these instances, the reactive domain temperature ends up to be the same as the reactor operating temperature; thus $\beta = \beta'$ and $\gamma = \gamma'$. Only when the stagnant film is insulating at $\varepsilon = \delta = 0$ did the flat temperature profile show a slight higher value as predicted in Eq. (5.32), with actual profiles shown in Figs. 5.43 and 5.44. This is quite surprising, but can be explained by the fact that the fluid is removing heat from the reactive polymer-rich domain. How much lower in reactive domain particle size can the PMAA–MAA–Water system can this effect be observed? Based on the computer simulation of the system, it can go down to 10 nm domain size.

An aspect of the discussion of the implications of these unsteady-state results pertains to the difference in system behavior between interacting or noninteracting domain systems. All of the results being discussed so far can be ascribed to noninteracting domain cases as base scenario. When reaction domains interact with one another, the bulk fluid temperature tends to increase if there is no control system that brings it down to a setpoint temperature. The absence or lack of a temperature control scheme is also found in reactor fluid systems that have less intense mixing capabilities, such as the case of large-scale reactor vessels or

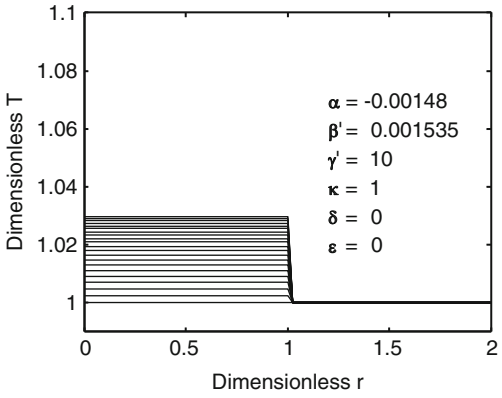

Fig. 5.43 Temperature profile evolution (Dimensionless Temperature, Θ vs. Dimensionless Radial distance, η or η_f) for the PS–S–Ether system at 80°C. The reactive spherical particulate has a radius of 0.000001 cm. Starting Dimensionless time, τ, is 0 at Dimensionless Temperature of 1.0. Final Dimensionless Time is 20,000,000, with profile Dimensionless Time step of 1,000,000

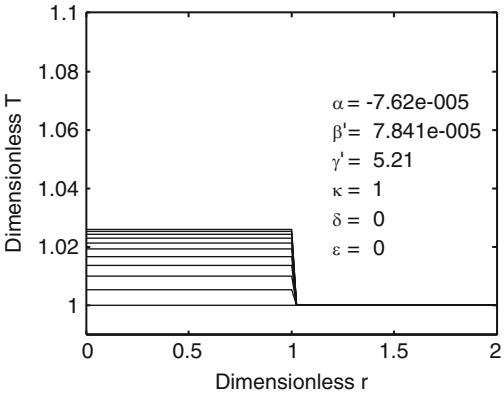

Fig. 5.44 Temperature profile evolution (Dimensionless Temperature, Θ vs. Dimensionless Radial distance, η or η_f) for the PMAA–MAA–Water system at 80°C. The reactive spherical particulate has a radius of 0.001 cm. Starting Dimensionless time, τ, is 0 at Dimensionless Temperature of 1.0. Final Dimensionless Time is 5,000,000, with profile Dimensionless Time step of 500,000

quiescent reaction systems. The result is an increase in reactive domain temperature, which can lower the polymerization rate of an FRRPP system. In contrast, with a good temperature control system, reactive domain temperatures tend to be lower resulting in higher polymerization rates in FRRPP systems. A final point can be made that for a reactor system with good temperature control, higher reactive domain temperatures are expected for noninteracting domains found in extremely dilute reaction systems. This is the situation in Sect. 2.2 of the first FRRPP monograph (Caneba 2010), which have been shown to exhibit carbon formation and possibly catastrophic reactor material failure.

5.4 Summary of Simulation Results

The unsteady-state model employed in this section is able to shed some light on the occurrence of FRRPP behavior in polymerization systems. Prior analysis did not provide the condition required for an inherently stable system, which has been obtained here to correspond to the value of $\alpha < 0$. Simulation results summarized in Table 5.1 shows that this condition should be included with $C\tilde{n} < -1{,}000$, for strict adherence to FRRPP behavior, which should be qualified to involve the attainment of a stable flat temperature profile in the reacting polymer-rich domains.

Even when the set of system parameters correspond to an inherently unstable dynamic behavior, flat temperature profiles can still be obtained with the use of an aggressive heat sink around the reactive material. In this case, the profile ends up to be at the same temperature level as the nonreactive boundary fluid layer, or the profile does not deviate too much from the unstable quasi-steady-state condition in cases where $C\tilde{n}$ is less than $-1{,}000$. The exception could occur in situations when reactive

agglomerates are formed to result in a more parabolic temperature profile. Thus, more dynamic control might be occurring in the two experimental systems being analyzed (PS–S–Ether and PMAA–MAA–Water systems) here, and these calculations show that emulsification of the reacting system would tend to stabilize the polymerization process. This has in fact been shown in foregoing experimental results, which has become a basis for controlled propagation after the initial stages of the FRRPP runs.

The differential overall mass balance has been totally ignored here, because we assumed that phase separation kinetics is faster than the reaction rate of the system. In this case, the resulting differential equation for the monomer transport is similar to the differential energy equation used in this section [Eq. (5.1)]. Both the differential mass and energy balance equations can be decoupled as a first approximation, and could have been solved separately (Alharthi 2010).

Since the thermal-based dynamic analysis of the evolution of temperature profiles seem to be unable to completely explain reaction control in the two experimental systems of interest in this monograph, it is believed that the use of the mass transport-based mechanism is needed. This is a subject of our continuing efforts in the study of the FRRPP theory, although a reduction in the monomer weight fraction that represents reactive domain densification shows the shift of both the PS–S–Ether and PMAA–MAA–Water systems to stable flat temperature profiles with equal temperatures of the reactive domain and stagnant fluid layer.

Therefore, it can be said that both S–PS–Ether FRRPP and PMAA–MAA–Water systems at 80°C can attain a flat temperature profile, and the manner at which it is happening has been elucidated here in a way that has not been predicted from previous quasi-steady-state mathematical modeling/computer simulation studies (Chap. 2 of Caneba 2010). This points to the study of a mass transfer-based mechanism for a more complete understanding of the reaction control aspects of the FRRPP process.

5.5 Nomenclature

5.5.1 Alphabets

5.5.1.1 Upper Case

A Heat transfer area, cm^2
T Absolute temperature, K

5.5.1.2 Lower Case

h Convective heat transfer coefficient, cal/(cm^2 s K)
k Thermal conductivity, cal/(g s K), and integer count in infinite series in Eqs. (5.30) and (5.31)

r Radial distance, cm
t Time, s
x Argument in Exponential Integral function, expressed in Eqs. (5.30) and (5.31)

5.5.2 Subscripts

1, 2, 3, . . ., i, . . ., 19, 20, 21, 22, 23, 59, 60, 61 Temperature grid points
b Bulk fluid
f Fluid
s Solid
ss Steady-state

5.5.3 Superscripts

None

5.5.4 Greek Symbols

α Dimensionless version of a from Eq. (1.2)
β Dimensionless version of b from Eq. (1.3)
γ Dimensionless activation energy, defined in Eq. (1.4)
δ Thermal conductivity ratio, defined in Eq. (5.18)
ε Thermal diffusivity ratio, defined in Eq. (5.12)
κ Relative boundary layer thickness, defined in Fig. 5.1
η Dimensionless radial distance, defined in Fig. 5.1
ρ Density, g/cm^3 or kg/m^3
θ Dimensionless temperature, defined in Eq. (1.5)
Θ Dimensionless temperature, defined in Eq. (5.3)
τ Dimensionless Time, defined in Eq. (5.4)
Φ Defined in Eq. (5.28)

5.5.5 Other Symbols

α_0 Defined in Eq. (1.18), cm^{-2} or m^{-2}
β' Defined in Eq. (5.6)
β_0 Defined in Eq. (1.19), cm^{-2} or m^{-2}
$\hat{C}_P$ Specific heat, cal/(g K)
$C\tilde{n}$ Defined in Eq. (1.13), dimensionless

γ' Defined in Eq. (5.7)
Nu Nusselt Number, dimensionless
$\dot{q}$ Reaction heat source per volume, cal/(cm^3 s)
Φ' Defined in Eq. (5.34)
r_0 Reactive particle radius, cm or m

References

Alharthi M (2010) Mathematical modeling and computer simulation of dynamic thermal behavior of FRRPP and related systems. M.S. Thesis, Michigan Technological University, Houghton
Bird RB, Stewart WE, Lightfoot EN (2007) Transport phenomena, 2nd edn. Wiley, New York
Caneba GT (2010) Free-radical retrograde-precipitation polymerization (FRRPP): novel concept, processes, materials, and energy aspects. Springer, Heidelberg. ISBN 978-3-642-03024-6
Riggs JB (1994) "An Introduction to Numerical Methods for Chemical Engineers", 2nd Edition, Texas Tech University Press, Lubbock, TX
Spanier J, Oldham KB (1987) An atlas of functions, Chap 37. Hemisphere, New York
Tirumala VR (2003) Ph.D. dissertation, Michigan Technological University, Houhgton
Tirumala V, Dar Y, Wang H-H, Mancini D, Caneba GT (2003) Adv Polym Technol 22:126
Tirumala V, Divan R, Mancini D, Caneba (2003c) "Lithographically-Assisted Synthesis of High Aspect-Ratio Hydrogel Microstructures", this paper was partly presented at the Fifth International Workshop on High Aspect Ratio Miscrstructure Technology (HARMST), Monterey, CA, June 15–17
Tirumala V, Mancini D, Caneba GT (2004a) "Synthesis of Ultrafast Response Microgels for MEMS Applications", *Smart Structures and Materials*, SPIE Conference, 5389, 221–228
Tirumala V, Mancini D, Caneba GT (2004b) "In Situ Fabrication of Thermoreversible Microgels" Proceedings of the *IEEE International Conference on Intelligent Sensing and Information Processing*, M. Palaniswami, C. Chandrasekhar, GK. Vengayamoorthy, S. Mohan, MK. Ghantasala (Eds.), pp. 196–200, Chennai, India, January 4–7
Tirumala V, Guo L, Caneba GT, Mancini D, Thiyagarajan P, Barker JG (2004c) "USANS Investigation of Poly(N-isopropylacrylamide) Gels prepared from Synchrotron-Radiation-Induced Polymerization on a Retrograde-Precipitation Environment", Proceedings of the *American Conference on Neutron Scattering*, June 6–10, College Park, Maryland
Tirumala V, Divan R, Mancini DC, Caneba GT (2005a) *Microsystems Technologies Journal*, 11 (4-5), 347–352
Tirumala V, Caneba GT, Mancini DC, Wang H-H (2005b) U.S. Patent No. 6,869,983, March 22
Tirumala VR, Caneba GT, Mancini DC, Wang HH (2006) *Journal of Applied Polymer Science*, 102(1), 429

Chapter 6
Conventional Emulsion-Based Polymerizations

An emulsion is the name typically given to a small particle size dispersion of nonaqueous liquids or solids in a continuous aqueous matrix, typically stabilized by surface-active molecules. An emulsion is also referred to as latex. Polymer emulsions are typically synthesized through a process called emulsion polymerization (Dar et al. 2006).

Emulsion polymerization is a heterogeneous reaction process used to synthesize polymer emulsions. In this process, unsaturated monomers are dispersed in an aqueous phase with the aid of emulsifiers and polymerized using a suitable initiation mechanism. Free radical initiators are most commonly used to synthesize polymer emulsions. The resulting emulsion, also referred to as a polymer latex, is a dispersion of polymer particles in water.

Emulsion polymerization typically involves the polymerization of a nonaqueous monomer that is slightly soluble in water. Water is used as the continuous medium for the dispersion as well as the heat sink for the heat of polymerization. Inverse emulsion polymerization is the term used for the polymerization of a water-soluble material in a nonaqueous dispersion medium.

Miniemulsion polymerization is another type of emulsion-like polymerization process that consists of stable oil in water emulsions with average droplet diameter of 80–400 nm, with initiation of polymerization in the miniemulsion droplets. Microemulsion polymerization occurs within thermodynamically stable surfactant-rich microemulsions with particles sizes in the range of 100 nm or smaller. Other related heterogeneous polymerization techniques include suspension polymerization and precipitation or dispersion polymerization. These differ in choice of continuous medium, particle size of the dispersed phase, mechanism of stabilization, and type of polymerization mechanism used.

Polymerizations within emulsion and latex particles normally involve the use of surfactants. If the initiator is soluble in the monomer-rich phase, then the polymerization process is technically a suspension type, which could result in 10–1,000 μm or larger polymer particles. For an oily monomer phase, the emulsion polymerization process involves the use of a water-soluble initiator, which results in much smaller 0.05–5 μm polymer particles (Rodriguez et al. 2003).

G. Caneba and Y. Dar, *Emulsion-based Free-Radical Retrograde-Precipitation Polymerization*, DOI 10.1007/978-3-642-19872-4_6,

The kinetics of suspension polymerization wherein surfactants are used to disperse the monomer-rich phase that includes the monomer, initiator, and solvent is the same as that of conventional bulk or solution polymerization processes. It should be noted that suspension polymerization is typically used to produce bead-sized polymers that have sizes in the 1–5 mm range through the use of protective colloids, such as poly(vinyl alcohol), instead of amphiphilic surfactants. What makes both systems classifiable as suspension polymerization is that they involve either bulk or solution polymerization kinetic mechanisms in their own respective size scales.

6.1 Ideal Emulsion Polymerization

6.1.1 Ideal Emulsion Polymerization Mechanism

The mechanism of emulsion polymerization is heavily dependent on the role of the surfactant and the manner of distribution of initiator molecules within the fluid system. Ideal emulsion polymerization is subdivided into three time intervals, based on the Harkins model (Poehlein 1986). Interval 1 is the particle initiation time regime, wherein initiator dissolves in the water, surfactant molecules form micelles, and monomer molecules segregate into 1–10 μm droplets and within micelles. As the initiator molecules decompose into radicals, they enter the micelles and propagate into growing polymer radicals. In the ideal situation, growing polymer radicals that are found within a micelle filled with monomer-swollen polymer material quickly recombine with other radicals within the particle until only one propagating radical is left. This means that polymer species within micelles/growing particles with even number of radicals cease to propagate; thus, statistically the number of propagating polymer species is half the total number of growing particles. Due to the relatively large surface area-to-volume ratio of the growing reactive particles, they readily absorb monomer molecules to the point that monomer concentration is maintained at a constant value, as long as there are separate domains of monomer/solvent phases dispersed within the fluid. This is the end of Interval 1, wherein conversions can reach up to about 2–10%.

Interval 2 begins when all surfactant molecules have formed micelles, and the concentration of polymer radicals is also constant. With constant monomer/solvent concentrations within growing particles, the rate of monomer consumption becomes pseudo-zero-order up to a conversion of about 70–80% (Rodriguez et al. 2003). The number of growing monomer-swollen particles is ideally half of the total particle population. As the level of surfactant concentration falls below the saturation amount for maintenance of micelles, monomer-swollen polymer particles are more stabilized by colloidal forces. The end of Interval 2 occurs when all monomer droplets are depleted.

Interval 3 starts when all the monomer/solvent-dispersed phase material has been incorporated within growing emulsion particles; monomer consumption results in a pseudo-first-order reaction, until all the monomer is depleted. Sometimes, when monomer depletion does not occur in a reasonable amount of time, a chase initiator solution is admixed into the reactor fluid.

One of the features that make emulsion polymerization different from suspension polymerization is that initiation occurs in the aqueous phase while propagation and termination occur within oily polymer/monomer/solvent domains. The other unique feature is the existence of growing emulsion particles that contain only one polymer radical, which can be terminated by the entry of another radical from an initiator or another growing emulsion particle.

6.1.2 Smith–Ewart Model Equations of Ideal Emulsion Polymerization

The Smith–Ewart (S–E) representation of ideal emulsion polymerization applies to Interval 2, and is based on Case 2 particle growth kinetics (Poehlein 1986). The Case 2 kinetics is bound by the upper-limit and lower-limit models. These models provide mathematical expressions for the number of growing particles, N, vs. time in the polymerization system. In turn, the propagation rate of polymerization, R_P, is related to N, because

$$R_P = k_P[M]_P[P\cdot] = k_P[M_P]\left(\frac{\bar{n}N}{N_A}\right), \tag{6.1}$$

where $[M]_P$ is the monomer concentration within the particles, $\bar{n}$ is the number of free radicals per particle, and N_A is the Avogadro's number. Note that in the ideal S–E Case 2 representation of the emulsion particle system, $\bar{n} = 0.5$.

The upper-limit model pertains to having all radicals generated during Interval 1 forming particles. Thus,

$$\frac{dN}{dt} = \rho_i, \tag{6.2}$$

where ρ_i is the rate of initiation of free radicals in the aqueous phase.

For the Case 2 model, within time Interval 2, the total number of particles, N; the growth rate of the volume of swollen polymer particles, μ; and ρ_i are all constants. The particle volume and surface area of age $(t–\tau)$ for a particle are equal to

$$v_{\tau,t} = \frac{4}{3}\mu r^3 = \mu(t-\tau), \tag{6.3}$$

$$S_{\tau,t} = 4\pi r^2 = (36\pi)^{\frac{1}{3}}[\mu(t-\tau)]^{\frac{2}{3}}. \tag{6.4}$$

The cumulative surface area for the total number of particles in the system is

$$A_{\mathrm{t}} = a_{\mathrm{S}}[S] = \int_0^t S_{\tau,t}\rho_{\mathrm{i}}\mathrm{d}\tau = \int_0^t (36\pi)^{\frac{1}{3}}[\mu(t-\tau)]^{\frac{2}{3}}\rho_i \mathrm{d}\tau = (36\pi)^{\frac{1}{3}}(0.6\rho_i)\mu^{\frac{2}{3}}t^{\frac{5}{3}}, \tag{6.5}$$

where a_{s} is the surface area occupied by a mole of surfactant and $[S]$ is the surfactant concentration. It should also be noted that

$$N = \rho_{\mathrm{i}} t_1 \tag{6.6}$$

wherein each radical starts a particle at time, t_1.

Combining Eqs. (6.2)–(6.6), the expression for the total number of particles is obtained as

$$N = 0.53\left(\frac{\rho_{\mathrm{i}}}{\mu}\right)^{0.4}(a_{\mathrm{S}}[S])^{0.6}. \tag{6.7}$$

This means that the total number of growing particles scales with the surfactant concentration to the 0.6, and with the rate of initiation to the 0.4 power.

In the lower-limit model, new particles are formed at a rate proportional to the rate of radical generation and amount of emulsifier associated with micelles relative to those associated with particles. The result for the number of particles is similar to Eq. (6.7), except that the front factor is 0.37 instead of 0.53.

Case 2 S–E emulsion polymerization kinetic mechanism is a good representation for hydrophobic monomers, such as styrene and (meth)acrylates. It breaks down for vinyl acetate because of its partial solubility in water. It also breaks down for vinyl chloride because the monomer is relatively insoluble in the polymer. Based on Eqs. (6.1) and (6.3)–(6.7), it is evident that the rate of propagation can be increased through increases in surfactant concentration and initiation rate. In bulk, solution, and suspension polymerizations, the increase in initiation rate is compensated by the increase in terminations rate, which keeps the polymer molecular weight from attaining relatively high values. In emulsion polymerization, since initiation occurs within the aqueous phase while termination occurs within the particle phase, molecular weights can be increased to relatively high values (10^6 g/mol or higher) without requiring a relatively low rate of propagation.

In Interval 3, polymerization reverts to pseudo-first-order, because the polymer concentration is fixed within the particles and in the overall fluid system. It is at this point wherein additional monomer can be added to the system, in order to form block and graft copolymers. Such seeded emulsion polymerizations are also used to produce larger particles and core–shell latex systems (Kowalski and Vogel 1984; Kowalski et al. 1991).

6.2 Emulsion Polymerization Recipes

In conventional emulsion polymerization process, the medium is water and hydrophobic monomers, such as styrene, methyl methacrylate, butyl acrylate, or ethylene, are used.

In a conventional sense, surfactants are compounds that comprise a hydrophilic head and a hydrophobic tail (Fig. 6.1).

The most popular classification of surfactants is based on its ionic characteristics; either they are anionic, cationic, or nonionic. Since ions are normally found in aqueous fluids, ionic characteristics of surfactants are found in the hydrophilic head; thus, an anionic surfactant would have negatively charged species in the hydrophilic heads. Because of the requirement of charge neutrality in an overall fluid system, an anionic surfactant would have its positive counterion within its vicinity. This counterion is subject to various ion-exchange mechanisms either with other types of counterions in the fluid or on solid surfaces. It is possible for nonionic species to be hydrophilic, because of their polar and hydrogen-bonding interactions with water molecules.

Early types of industrial surfactants were based on alkylbenzene sulfonates (ABS), whereby aromatic compounds were first alkylated followed by reaction of the aromatic ring with sulfuric acid. Upon neutralization with a convenient base, the result is an anionic ABS surfactant material. Later, cationic and nonionic types were introduced in the market. Even so, one should realize that these and most of the modern surfactants are oligomeric in size (see Fig. 6.2 for examples of anionic and nonionic surfactants).

Surfactants are popularly known for their detergency properties. Their appeal is based on the observation that while they are dispersible in water, they can efficiently remove oily contaminants from various surfaces, such as apparel, building materials, appliances, etc. This was found to be due to the capability of surfactants to form mesoscopic structures called micelles, in which surfactant molecules self-organized into spherical, cylindrical, and even lamellar domains. In these domains surfactant molecules arrange themselves like infantry soldiers of a Roman legion in defensive positions, wherein the hydrophilic heads of each molecule are facing the wide expanse of the aqueous phase while the hydrophobic tails that harbor oily material are facing inward amongst other hydrophobic tails of other molecules. In a fluid system under constant Brownian motion, one would expect that when there are not enough surfactant molecules per volume, micelles would not form. What was observed was the existence of a threshold concentration of surfactant as the

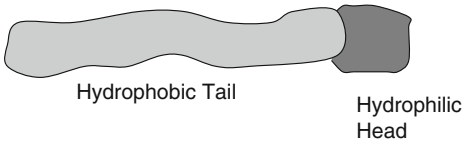

Fig. 6.1 Representation of a surfactant molecule, which comprises a hydrophobic (oil-loving) tail and a hydrophilic (water-loving) head

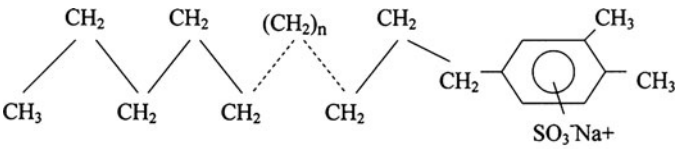

SODIUM ALKYL-ORTHOXYLENE SULFONATE
(n = from 2 to 10)

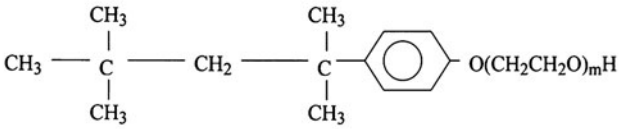

ETHOXYLATED OCTYLPHENOL (NONIONIC)
(m = from 2 to 100 – average value)

Fig. 6.2 Examples of anionic (*top*) and nonionic (*bottom*) surfactants

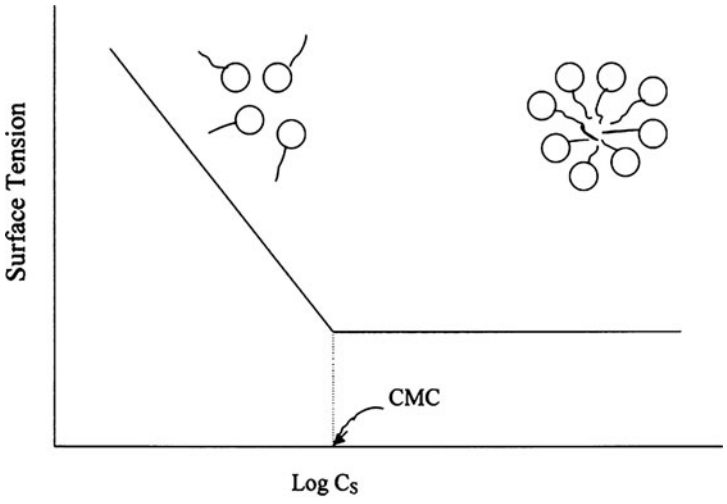

Fig. 6.3 Determination of the critical micelle concentration (CMC) based on a change in the slope of the surface tension vs. surfactant concentration

lower limit before micelle formation can occur. This is called the critical micelle concentration (CMC). As a general rule, the lower the CMC, the more effective a surfactant is, because less surfactant material is needed to form micelles. The CMC is also associated with the change in slope of the surface tension of the fluid with concentration, again due to the transition in structural assembly of the molecular system (Fig. 6.3).

Another property of surfactants has to do with their tendency to form oil-in-water (O/W) or water-in-oil (W/O) emulsions, through the so-called hydrophile–lipophile balance (HLB) number. The HLB number is defined in such a way that a value of 7 is the boundary, and below that the surfactant tends to form W/O emulsions. For emulsion polymerization, high HLB oligomeric surfactants are used, and they are mostly of the anionic type.

Water-soluble initiators used in emulsion polymerization can form radicals when they decompose thermally, in the same way as oil-soluble conventional initiators do. Examples of these initiators include benzoyl peroxide, lauroyl peroxide, their hydroperoxide counterparts, etc. Chase initiator solutions are typically aqueous solutions of *t*-butyl hydroperoxide (TBHP), which is only slightly soluble in water (Wicks Jr. et al. 1992). If low temperature operation and/or high initiator decomposition rates are desired, the so-called redox initiation is employed. In the redox system, the oxidizing material, which could also serve as a water-soluble thermally based initiator, is reacted with a reductant. An example redox system involves the following kinetic mechanism for the formation of primary radicals:

$$\underset{(1)}{{}^{-}O_3S-O-O-SO_3^{-}} + \underset{(2)}{Fe^{2+}} \rightarrow \underset{(3)}{{}^{-}O_3S-O^{\cdot}} + \underset{(4)}{SO_4^{2-}} + \underset{(5)}{Fe^{3+}}$$

$$\underset{(1)}{S_2O_8^{2-}} + 2\,\underset{(6)}{S_2O_3^{2-}} \rightarrow \underset{(7)}{S_4O_6^{2-}} + 2\,\underset{(8)}{{}^{-}O_3S-O\cdot}$$

$$\underset{(5)}{Fe^{3+}} + 2\,\underset{(6)}{S_2O_3^{2-}} \rightarrow \underset{(9)}{Fe^{2+}} + \underset{(7)}{S_4O_6^{2-}}$$

It is evident that the radical source is Species (**8**). Species (**1**), the oxidizer, comes from a persulfate salt (such as Potassium Persulfate or $K_2S_2O_8$), while the reductant, Species (**2**), comes from Ferrous Sulfate.

It is important that the reductant is stored separately from the oxidizer mixture. Also, it is preferable the reductant solution is added into the reactor before the rest of the reaction mixture is admixed into the reactor to start the polymerization.

6.3 FRRPP Effects on Ideal Emulsion Polymerization

In order to implement emulsion polymerization with FRRPP recipes, a solvent/precipitant is added with the monomer in the oily phase. We can imagine the Harkins model in this type of system, in which initiation occurs in the aqueous phase, and the resulting radicals migrate into the micelles containing monomer and solvent/precipitant. As soon as some polymer is produced, this is where emulsion-FRRPP would bifurcate from conventional emulsion polymerization.

The typical experimental procedure involves loading the monomer/poor-solvent/initiator/water/surfactant mix into the reactor and heating it to the operating

temperature (typically 60–120°C depending on the system) and pressure (typically up to 7 atmospheres depending on the system). The monomer is allowed to react with the initiator till all the initiator in the reactor has decomposed (>6 initiator half-lives). During this period, some or all of the solvent could be removed from the reactor to perturb the phase equilibrium and allow any trapped radicals to keep reacting.

The conversion profile of such a system shows that the conversion rises quickly and asymptotically to a low value (around 20–40%) initially (without any solvent removal). The molecular weights are typically low (3–20 kDa). The conversion jumps up to about 100% and the molecular weight to several hundred kilodaltons once all the solvent is removed. The rise in conversion and molecular weight can be correlated to the amount and rate of solvent removal.

Once all the initiator has decomposed and all the solvent has been removed, the system consists of a polymer emulsion with trapped radicals within the polymer particles. The procedure until this point has been called the first stage. At this point a second monomer is added to the reactor. This marks the beginning of the second stage. The best results are obtained when the second monomer is added as a pre-emulsion mix with water/surfactant. Almost all of the second monomer gets converted to polymer within 2–3 h. This stage of the reaction is relatively uncontrolled and possibly results in a lot of radical termination.

The resulting reactor product is a small particle size (of the order of 100 nm) polymer emulsion. The polymer itself appears to be a mixture of diblock and triblock materials with some contamination from prematurely terminated first-stage homopolymer. The triblock material could result from termination by combination leading to a midblock consisting of the second-stage monomer, and end blocks consisting of the first-stage monomer.

In the first stage of polymerization, once an initiator fragment enters the dispersed monomer–(non)solvent phase, the kinetics follow the traditional FRRPP route (Caneba 2010). The type and amount of initiator need to be adjusted to account for efficiencies associated with termination in the aqueous phase. This can be influenced by inherent primary termination as well as the probability that some initiator fragments will not enter the dispersed phase which will ultimately lead to alternate reaction routes including initiation in the aqueous phase, termination in the aqueous phase, and chain transfer to other species including surfactant.

Once polymer radicals and molecules are initiated in the dispersed phase, the polymer chains undergo a coil-to-globule transition and eventually form polymer particles. Due to the small size of the dispersed phase domains, the size of the precipitated polymer particles is physically constrained to be small. This is a key advantage of conducting FRRPP in emulsion. Without the use of emulsion FRRPP, there is no constraint on the size of the precipitated polymer domains without the use of a suitable stabilizer in the nonaqueous polymerization medium. Once the nonaqueous solvent has been removed, there are several factors that help preserve trapped radicals in polymer particles. These factors and other details on the polymerization process are presented in subsequent sections.

References

Caneba GT (2010) Free-radical retrograde-precipitation polymerization (FRRPP): novel concept, processes, materials, and energy aspects. Springer, Heidelberg. ISBN 978-3-642-03024-6

Dar YL, Farwaha R, Caneba GT (2006) Free-radical polymerization. In: Encyclopedia of chemical processing. Taylor and Francis, London

Kowalski A, Vogel M (1984) U.S. Patent No. 4,469,825, 4 Sept 1984

Kowalski A, Wilczynski JJ, Blankenship RM, Chou C-S (1991) U.S. Patent No. 5,030,666, 9 July 1991

Poehlein G (1986) "Emulsion Polymerization", in: Encyclopedia of Polymer Science and Technology, Vol. 6, pp. 1–51

Rodriguez F, Cohen C, Ober C, Archer LA (2003) Principles of polymer systems, Chap 5. Taylor and Francis, New York

Wicks Jr, ZW, Jones FN and Pappas SP (1992) "Polymer Coatings – Science and Technology. Volume 1: Film Formation, Components, and Appearance", SPE Monograph Series, Wiley Interscience, New York

Part II
Emulsion FRRPP (EFRRPP)

Genius is eternal patience.
Michelangelo

Free Radical Retrograde Precipitation Polymerization (FRRPP) provides the ability to trap polymer radicals and access them to build block copolymers and related architectures without the use of any chemical additive or mediator. This is a feature that provides a lot of value but due to the requirements of using retrograde precipitation, the medium of delivery of the polymers is potentially limited to the type of solvents used for the retrograde precipitation. The following chapters describe an industrially practicable approach to use FRRPP that allows the practitioner to switch from a retrograde precipitation solvent system to an aqueous emulsion system. This greatly increases the practical applicability of the materials derived from this process as an aqueous delivery medium is more widely applicable.

The following chapters demonstrate how the process was developed and optimized to deliver controlled architecture polymers using FRRPP but in an aqueous medium.

EFRRPP combines the benefits of free radical polymerization with those of emulsions. Free radical polymerization is a well-understood polymerization pathway and is commonly practiced for the industrial synthesis of high polymers. Free radical polymerization is broadly applicable and provides access to a large number and type of monomers. There is significant flexibility in choice of solvents, initiators, and operating conditions that have supported its popularity. The mechanism of free radical polymerization is well understood, which allows for effective transfer across scales and trouble shooting.

Polymerization in emulsion offers several advantages as compared to bulk or solution polymerization. The reaction proceeds at low to intermediate viscosity from the beginning all the way to the final product. The ability to control and maintain a low viscosity enables efficient transfer of the heat of polymerization out of the reaction medium. It also enables the production of high polymer concentrations that are often greater than 50% by weight of the final product. Further advantages include the ability to achieve high monomer conversion and relatively short cycle time. An additional benefit is delivery of the final product without any

hydrocarbon-based solvent in it. This is highly desirable due to the drive for sustainability and lower reliance on hydrocarbon-based solvents to protect the environment.

Due to the many advantages offered by emulsion polymerization, this process is applied on an industrial scale to produce a variety of products such as pressure sensitive adhesives, paints, carpet and textile binders, binders for nonwoven products (e.g. diapers), paper coatings, polymers for glass fiber sizing, and polymer additives for personal care products.

Part II on Emulsion FRRPP is organized to provide an overview of the process followed by deeper insight into the key factors influencing a successful outcome. Chapter 7 describes an initial approach developed to transform a non-aqueous dispersion polymerization into an aqueous controlled architecture polymer dispersion. This approach worked well but had some limitations from an industrial perspective. Therefore a modified approach was developed. This modified approach is introduced in Chapter 8.

Chapter 9 summarizes some conceptual and theoretical aspects of EFRRPP that provide insight into the potential mechanisms and key parameters that influence the synthesis of controlled architecture polymer emulsions. This includes basic observations on the confinement of polymer chains in emulsion particles and the potential effects on polymerization kinetics. This part also summarizes the experimental details used in Chapter 10. Experimental details include materials, procedure for polymer synthesis, and the procedure and parameters used for polymer characterization.

Chapter 10 summarizes selected experimental work that demonstrates the capabilities of EFRRPP. This work also provides experimental insight into the effect of different parameters on the process and product. Examples with polystyrene and poly methyl methacrylate-based block copolymers are presented in this part.

Chapter 11 is focused on control experiments conducted to rule out autopolymerization as an alternate mechanism for this process. Chapter 12 provides a summary of the key observations and conclusions from Chaps. 7 to 11.

The data and observations presented show that EFRRPP presents a relatively straightforward pathway to block-copolymer materials that can find use in a variety of applications.

Chapter 7
Initial Approach

An emulsion-based FRRPP system was developed due to the benefits of delivering a controlled architecture polymer in an aqueous dispersion (Caneba and Wang 2001). In order to deliver aqueous dispersions of these materials, the following basic five-step approach was initially developed and used.

Step 1: Polymerize the Stage I monomer via the FRRPP process in a monomer–polymer–(non) solvent system.
Step 2: Emulsify the entire system through careful selection of a surfactant package and processing conditions.
Step 3: Remove the (non) solvent under carefully regulated conditions to preserve a stable emulsion.
Step 4: Add pre-emulsified comonomer(s) to the emulsions to polymerize Stage II to achieve a block copolymer while maintaining conditions where the polymer radicals remain trapped and available for copolymerization.
Step 5: Repeat step 4 for additional monomers if possible.

This procedure allowed the synthesis of an intermediate product that was synthesized by polymerization above the LCST. This was then transformed into a polymer dispersion containing living radicals that could be used to synthesize controlled architecture polymers. The factors that are potentially responsible for radical trapping and preservation are also presented within this chapter.

7.1 PS-PBA from Emulsified PS–S–Ether System

Efforts were made to increase conversion from low limiting conversions found in PS–S–Ether systems, as shown in the first FRRPP monograph (Chaps. 3–5 of Caneba 2010). One of the approaches, which resulted in the formation of block copolymers, involved the emulsification of the PS–S–Ether reactive FRRPP system after limiting conversion. In the following parts of this chapter, it will be shown

G. Caneba and Y. Dar, *Emulsion-based Free-Radical Retrograde-Precipitation Polymerization*, DOI 10.1007/978-3-642-19872-4_7,

how continued controlled chain propagation was achieved toward the formation of block copolymers in a bench-scale reactor system.

7.2 Recipe

The recipe was formulated in order to result in a total of 270 ml in the 300-ml Parr reactor system shown in Fig. 2.3.4 of the first FRRPP monograph. The following approximate proportions were used for the various components during the formation of high conversion PS radicals in emulsion fluid system (Stage I):

1. 40 wt.% organic material relative to water
2. 15 wt.% styrene in organic fluid phase by volume
3. 1 wt.% initiator relative to styrene
4. 3 wt.% surfactant relative to weight of organic phase

The reaction system was subdivided into stages with the following component added into the reactor.

Stage Ia: 70–115 ml Ether
10.5–17 ml Styrene (S) Monomer
95–154 mg AIBN Initiator
Stage Ib: 88–142 ml Distilled Water
1.8–2.9 g Sodium Dodecyl Sulfate (SDS) or Sodium Lauryl Sulfate (SLS) Surfactant
Stage II: 25 ml *n*-Butyl Acrylate (BA) Monomer
10 ml Distilled Water
Stage III: 2 ml Methacrylic Acid (MAA) Monomer
14 ml Distilled Water

All monomers were passed through inhibitor removal columns, and all fluids were bubbled with nitrogen gas for at least 15 min.

7.3 Procedure

At the start, the empty reactor was purged with Nitrogen gas in order to remove Oxygen from the ambient air. Then, 80 ml Ether was pumped into the reactor. The reactor was heated to 80°C and brought to a pressure of 80 psig. Then, the experiment proceeded according to Table 7.1.

Stage II was started by introduction of 25 ml BA and 10 ml flush distilled water into the reactor at room temperature. Then, the reactor temperature was raised to 60°C linearly for 2 h. After 6 h and 45 min at 60°C, the reactor fluid was brought to room temperature in 15 min.

Table 7.1 Procedure for Stage I of FRRPP of Styrene in Ether followed by emulsification with distilled water

Time (h:min:s)	Comment(s)
0:00:00	Started to inject 10.5 ml Styrene and 95 mg AIBN into the reactor at a constant follow rate
0:05:00	Done injecting Styrene and AIBN. $P = 75$ psig, $T = 80°C$
5:15:00	Stage Ia completed. Started loading 1.8 g SDS in 88 ml distilled water to start Stage Ib
5:27:00	Done loading 1.8 g SDS in 88 ml distilled water
9:14:00	Opened valve from top of the reactor through the condenser, in order to slowly remove Ether from the reactor pot into a receiver flask
9:42:00	Started seeing condensed Ether into receiver flask. $P = 43$ psig
13:38:00	Removed 20 ml Ether from reactor into receiver flask. $P = 10$ psig
15:53:00	Removed a total of 25 ml Ether from reactor into receiver flask. $P = 8$ psig
16:36:00	Removed a total of 32 ml Ether from reactor into receiver flask. $P = 2$–3 psig. Started blowing top of reactor fluid with Nitrogen gas, in order to remove more Ether. A total of 35 ml Ether was collected in the receiver flask. Finally, raised reactor pressure to 60 psig with Nitrogen gas
16:41:00	Reactor was cooled to 20°C in 15 min. This concluded Stage Ib and the entire Stage I process

At the start of Stage III, 16 ml Stage II fluid (2 ml MAA in 14 ml distilled water) was injected into the reactor at room temperature. The additional monomer was allowed to soak into the emulsion particles for 30 min. Then, the reactor temperature was linearly ramped up to 60°C for 30 min. After 8 more hours, the reactor fluid temperature was dropped to room temperature in 15 min. This ended the entire polymerization run.

7.4 Results and Discussion

The emulsification of the PS–S–Ether system has been noted to result in the dispersion of the organic phase in the aqueous phase, thereby facilitating the subsequent slow removal of Ether to approach high conversions with acceptable coagulum levels.

The development of PS molecular weight has been shown to follow a rather unusual pathway (Schlom Personal communication), as depicted in Fig. 7.1. Before the emulsification, there existed a single MW peak with peak MW in the order of 6,600 Da. Upon emulsification and during slow removal of Ether, a small high MW peak appeared at a peak MW of 250,000–350,000 Da. Continuation of Ether removal did not result in the significant changes in the molecular weights of the low and high MW peaks, thereby maintaining a bimodal MWD until the point when the reactor pressure reached almost atmospheric. Instead, the low MW peak was losing mass while the high MW peak was gaining mass, as can be seen in the

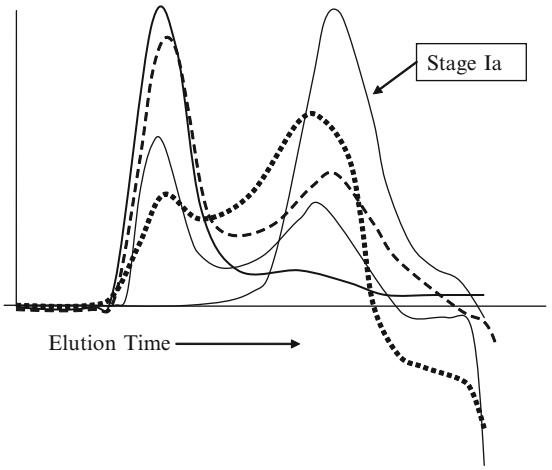

Fig. 7.1 Development of the molecular weight distribution of PS radicals during emulsification and Ether removal after Stage Ia. The low MW peak at elution volume of 18.5 ml (6,600 Da) that was developed during Stage Ia was losing mass in favor of an increase in mass of the high MW peak (250,000–350,000 Da). At the end of Ether removal, most of PS material went into the high MW peak

opposite vertical shifts of these two peaks. Towards the end of Ether removal, only the high MW peak existed, with small remaining low MW material becoming mostly reactor coagulum.

Upon addition of Stage II BA monomer, the MW increased further to the order 10^6 Da, indicating that live PS radicals were preserved after Ether removal. The Stage II product was also observed exhibited a slow dissolution in a good solvent, indicating a very high MW polymer.

Solvent exchange is a critical step in order to transition from Stage Ia, which consists of a nonaqueous dispersion (e.g. polystyrene in diethyl ether) to Stage Ib and ultimately the final product, which comprise of aqueous dispersions with water as the continuous phase.

Solvent exchange involves the removal of the nonaqueous solvent (e.g. diethyl ether or *n*-pentane) and replacing it with water. This has to be done without introducing any instability and preserving the trapped radicals in the polymer particles. It also has to be done while avoiding drastic and catastrophic changes in reactor fill volume to avoid undesirable and catastrophic changes in temperature and composition and to ensure that control is maintained over reactor operating conditions at all times. Any destabilizing effects can lead to small- or large-scale coagulation rendering the reactor contents worthless.

The solvent exchange process has two independent processes:

1. Addition of water containing a carefully selected surfactant/stabilizer package to the reactor and forming a polymer/monomer in nonaqueous solvent in water dispersion (see Fig. 7.2).
2. Removing the nonaqueous solvent through either lowering the pressure or application of vacuum based on the relative boiling points of the solvent and water.

The rate of water/surfactant addition has to be balanced with solvent removal to ensure that the rate of change of volume in the reactor is maintained within desired levels to ensure no undesirable heat/mass transfer effects take place.

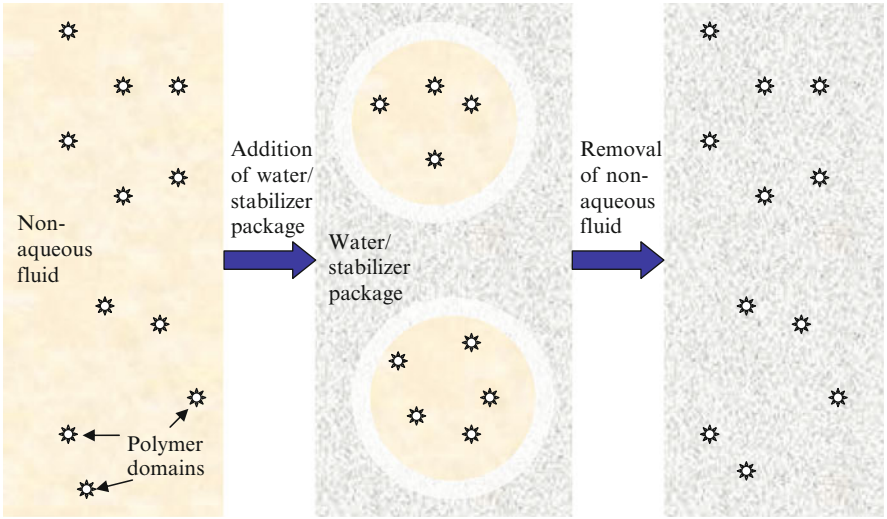

Fig. 7.2 Schematic showing a polymer in oil in water dispersion being transformed into a polymer in water dispersion

It is important to select a solvent that is lower boiling than water. For solvents that form azeotropes or have higher boiling points, more complex removal strategies can be considered including addition of nonreactive solvents that form lower boiling azeotropes with the solvent that needs to be removed.

This initial approach was successful in producing an emulsion product with appearance and properties consistent with a poly-styrene and poly-(*n*-butyl acrylate) block copolymer. This was conducted to prove the ability to replace a nonaqueous dispersion medium with water and obtain the desired product in aqueous dispersion.

However, this process may not be industrially practicable as the emulsification of a large amount of fluid into a stable emulsion as is needed to go from Stage Ia to Stage 1b is a challenging process to scale-up. The final product needs to have a relatively narrow particle size distribution and it should be possible to produce the dispersion with the desired particle size and distribution with a high degree of reproducibility. Even small deviations from the desired ideal process can lead to coagulum in the reactor and eventually lead to premature termination of any trapped radicals and lack of second stage conversion.

In order to overcome this issue, the process was modified so that an intermediate emulsification step was not needed. This modified process is described in Chap. 8.

References

Caneba GT (2010) Free-radical retrograde-precipitation polymerization (FRRPP): Novel concept, processes, materials, and energy aspects. Springer, Heidelberg. ISBN 978-3-642-03024-6

Caneba GT, Wang B (2001) Low VOC latex paints from a precipitation polymerization process. Clean Prod Process 3:55

Chapter 8
Modified Approach

The process described in Chap. 7 was modified in order to achieve an industrially practicable process with the desired final product properties. The five steps described in Chap. 7 were modified into the five-step process below, which essentially was an exchange of steps 1 and 2 in the original process.

Step 1: Emulsify the entire system through careful selection of a surfactant package and processing conditions to produce an aqueous dispersion/emulsion with water as the continuous phase and the monomer/(non) solvent as the dispersed phase.

Step 2: Polymerize the stage 1 monomer via the FRRPP process in a monomer–polymer–(non)solvent system that is itself dispersed in an aqueous dispersion.

Step 3: Remove the (non)solvent under carefully regulated conditions to preserve a stable emulsion.

Step 4: Add preemulsified comonomer(s) to the emulsions to polymerize stage II to achieve a block copolymer while maintaining conditions where the polymer radicals remain trapped and available for copolymerization.

Step 5: Repeat step 4 for additional monomers if possible.

The following sections present the most effective way to achieve success in each step including validation work to verify the proposed process in each step. Validation includes experiments and theoretical considerations in the design of the process.

G. Caneba and Y. Dar, *Emulsion-based Free-Radical Retrograde-Precipitation Polymerization*, DOI 10.1007/978-3-642-19872-4_8,

Chapter 9
Impact of Process Parameters on EFRRPP

The ability to deliver controlled architecture copolymers from FRRPP in an emulsion form requires a working knowledge of the stabilization of emulsions containing several components through the choice of suitable surfactant package and emulsification conditions. This chapter describes work that was done to make complex emulsions that included polymer in oil-in-water dispersions that were ultimately modified to polymer-in-water emulsions, as well as the manipulation of preemulsified systems that provided stable final products. Some additional details are provided in Dar and Caneba (2002, 2004).

9.1 Theoretical Considerations to Form and Maintain Stable Emulsions for EFRRPP

This section describes different aspects that need to be considered to make a stable emulsion.

9.1.1 Formation of a Stable Emulsion

It is critical that, in order to develop an industrially practicable process, a stable emulsion with reproducible particle size distribution and other emulsion characteristics can be produced in a manner that is suitable for operation at different laboratory and industrial scales. Since the critical scale of operation for emulsion polymerization is influenced by the size and number of polymer particles as well as the size and number of the reservoirs of monomer in the reactor, it is of vital importance to create and maintain the desired size and ratio of the polymer particles to the monomer reservoirs throughout the process. The choices of stabilizer package, mixing conditions, temperature, as well as pressure play a key role in the process.

G. Caneba and Y. Dar, *Emulsion-based Free-Radical Retrograde-Precipitation Polymerization*, DOI 10.1007/978-3-642-19872-4_9,

9.1.1.1 Choice of Surfactant and Stabilizer Package

The choice of stabilizers influences all five steps of the FRRPP process. A significant amount of theoretical and experimental work is available describing surfactants as well as stabilizers for nonaqueous dispersions. Surfactants are surface active molecules that stabilize an interface by lowering its interfacial tension and consequently its free energy. Once an aqueous/nonaqueous interface is created by using a suitable process, the surfactant self-locates itself at the interface and preserves it. Stabilizers have different mechanisms of action. They can work to structure the continuous phase. This can be accomplished by providing very high zero-shear viscosity to minimize the movement and coalescence of the dispersed phase particles. This can also be accomplished by tethering the particles to one another through stiff polymer chains leading to a reduction in particle mobility leading to lower rates of coalescence. Addition of selected soluble species to the continuous phase can reduce the solubility of components of the dispersed phase in the continuous phase. This reduces the rate of transport of molecules out of the dispersed phase domains and leads to higher stability by preserving the size and composition of the dispersed phase domains.

9.1.1.2 Mixing Optimization

Mixing plays an important role in emulsion processes and consequently in EFRRPP. It is critical to choose appropriate mixing processes and equipment to get the most suitable mixing conditions in the reactor system of choice. Poor mixing in two-phase reaction systems leads to nonuniform heat and mass transfer, which can lead to undesirable effects. Mixing and shear play a critical role in EFRRPP. The shear in the reactor should be high enough for a good emulsion and keep the reactor well mixed. However, the rate of mixing should not be so high as to cause entrainment and foaming – a consequence of air being drawn in through the mixing vortex and being stabilized as foam by the surfactant. Foaming leads to emulsion destabilization and precipitation. Excessive shear can also destabilize the dispersion through excessive particle collisions or shear-induced breakup of dispersed liquid phases. The ideal mixing configuration and process would provide adequate shear with sufficient turbulent mixing and minimize foam formation due to entertainment of gas bubbles.

There are many different types of impeller blade shapes and geometries available and used for making and processing dispersions and emulsions. Some examples include a 45° pitched blade turbine, a 30° pitched blade turbine, a Cowles dispersion blade, and a radial dispersion blade. Different impellers can be used in combination to provide desired mixing effects based on reactor geometry, the desired level of micro/macro mixing, and the properties of the medium being mixed. Another important factor is the use of baffles to promote vertical mixing in the reactor. A combination of baffles and one or more type of mixing blades is

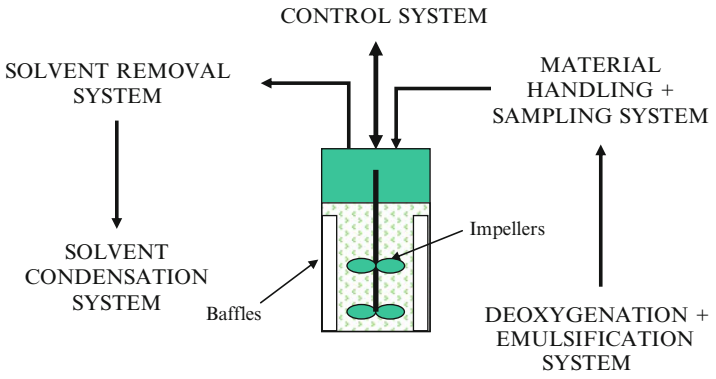

Fig. 9.1 Optimal configuration of the reactor system to provide the best possible mixing

usually a good choice for providing adequate mixing. The mixing speed is a key parameter that provides sufficient mixing power while minimizing entrainment. The actual mixing elements and geometries used vary significantly based on many factors including reactor size, height-to-diameter ratio, surface-to-volume ratio, viscosity of the fluids, and level of reactor filling. A poor choice of mixing configuration can lead to excessive vortex formation even at low mixing speeds leading to massive amounts of entrainment, foaming, and emulsion destabilization.

Figure 9.1 shows an example of an optimal mixing composition with baffles, a pitched blade turbine impeller at the bottom of reactor, and a radial dispersion blade about one third of the way up from the bottom of the reactor. This configuration provided a high level of mixing without undue entrainment of air.

9.1.1.3 Impact of Temperature

Temperature is one of the most important parameters for EFRRPP. It has three different and independent modes of action on the process.

1. Reaction kinetics: The reactor temperature influences the kinetics of the polymerization process as well as reagent choice including choice of initiator. It is important to choose an initiator that decomposes in a reasonable amount of time with high efficiency to maintain the balance between a high enough radical flux to initiate polymerization and the ability to maintain that flux over the time needed to achieve adequate stage I conversion. Oil-soluble as well as water-soluble initiators can be used with appropriate choice of half-life and relative concentrations. One of the most critical parameters in choosing the other reagents is to ensure that no reagents are chosen that have a high rate of chain transfer to or from any of the other reagents at the reaction temperature.
2. Temperature influences the choice of stabilizer for the emulsion. This is especially valid for nonionic surfactants as their interfacial activity is temperature

sensitive – most nonionic temperatures are ineffective above a certain temperature called their cloud point temperatures. It is important to ensure that the stabilizer has a cloud point that is 10–20° above the reaction temperature to keep batch-to-batch variations and any excursions in reactor temperature into account. In the example system described in Chapter 10, nonionic akylphenol ethoxylate surfactants were found to be essential to stabilize emulsions of diethyl ether in water under the reaction conditions.

3. The choice of temperature determines whether a reaction system can proceed under FRRPP conditions or not. During stage I, the temperature has to be above the lower critical solution temperature (LCST) to ensure that the FRRPP process is the polymerization route. It is recommended to maintain a temperature at least 10–20° above the LCST to ensure that the system is well within the two-phase region above the LCST.

9.1.1.4 Impact of Pressure

Pressure plays a key role in this process. In several cases (e.g., styrene, polystyrene, and diethyl ether), the choice of a temperature suitable for FRRPP could be above the boiling point of the solvent. This requires the polymerization to proceed at higher than atmospheric pressure to contain the volatile solvent and preserve the composition of the liquid phase. The pressure needs to be sufficiently high to ensure that the vapor pressure of the solvent is well below boiling conditions. A very high vapor pressure creates excessive solvent condensate and recycling into the reactor, which can create pools of solvent that need to be reemulsified. This can frequently lead to emulsion instability as well as nonuniformity in the type of dispersed phase domains in the reactor. There is no real upper limit to the pressure other than limitations of the pressure vessels used and cost constraints. Pressure also has an impact on the LCST of the polymerization process. An increase of 1 atm. can lead to a rise in LCST by about 0.5°C.

9.1.2 Maintaining Emulsion Stability Through Solvent Exchange

Solvent exchange is a critical step in order to transition from stage I, which is usually a nonaqueous dispersion (e.g., polystyrene in diethyl ether) to stage II and ultimately the final product, which is an aqueous dispersion with water as the continuous phase.

Solvent exchange involves the removal of the nonaqueous solvent (e.g., diethyl ether or *n*-pentane) and replacing it with water. This has to be done without introducing any instability and preserving the trapped radicals in the polymer particles. It also has to be done while avoiding drastic and catastrophic changes in reactor fill volume to avoid undesirable and catastrophic changes in temperature and composition and to ensure that control is maintained over reactor operating

conditions at all times. Any destabilizing effects can lead to small- or large-scale coagulation rendering the reactor contents worthless.

For the initial process, the solvent exchange process has two independent processes:

1. Addition of water containing a carefully selected surfactant/stabilizer package to the reactor and forming a polymer/monomer in nonaqueous solvent in water dispersion (see Fig. 9.2).
2. Removing the nonaqueous solvent through either lowering the pressure or application of vacuum based on the relative boiling points of the solvent and water.

The rate of water/surfactant addition has to be balanced with solvent removal to ensure that the rate of change of volume in the reactor is maintained within desired levels to ensure no undesirable heat/mass transfer effects take place.

It is important to select a solvent that has lower boiling point than water. For solvents that form azeotropes or have higher boiling points, more complex removal strategies can be considered including addition of nonreactive solvents that form lower boiling azeotropes with the solvent that needs to be removed.

The modified process is different from the steps shown in Fig. 9.2 since it starts with an emulsified initial system. The modified process is shown in Fig. 9.3.

The time taken for solvent removal and addition of water is a critical parameter. The removal of solvent and addition of the aqueous continuous phase is a complex process and can lead to several issues. This can be seen by considering the styrene/polystyrene/ether system as an example. In this case, a pressure of about 5 atm. of nitrogen pressure can be chosen for the reaction to ensure that the contents of the

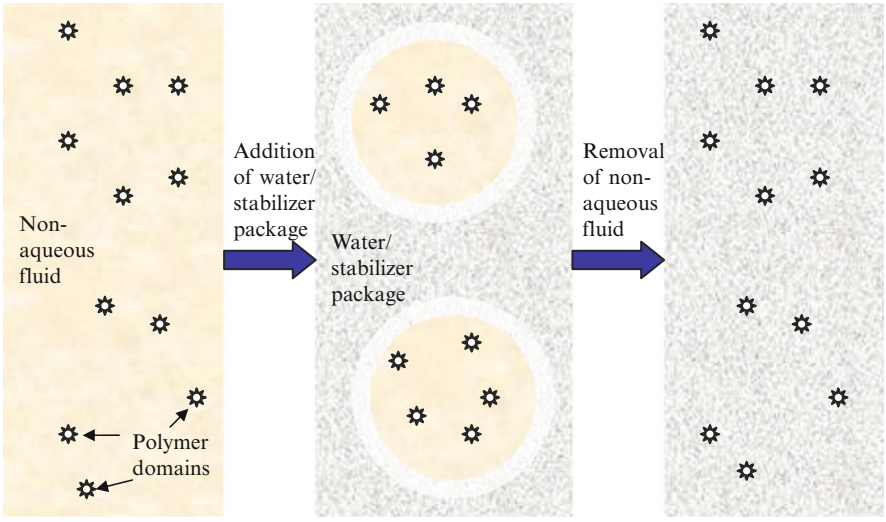

Fig. 9.2 (Reproduced from Chap. 7) Schematic showing a polymer-in-oil in water dispersion being transformed into a polymer in water dispersion

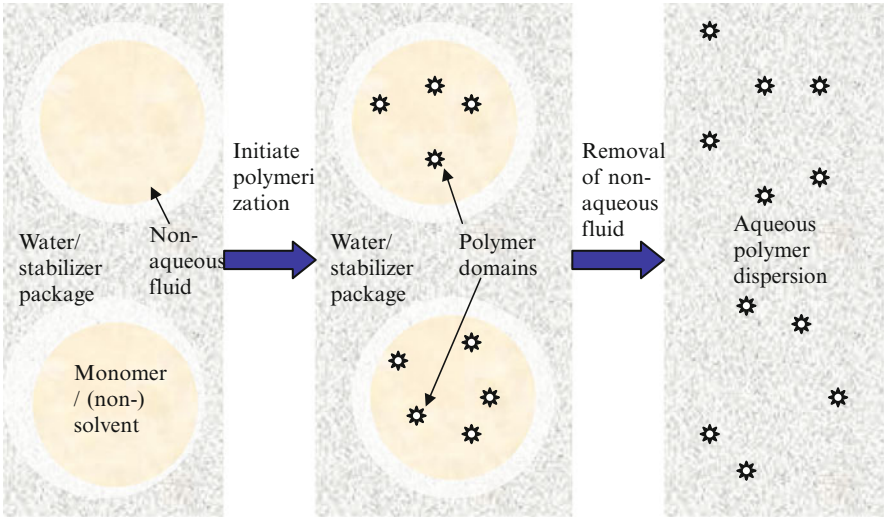

Fig. 9.3 Schematic showing the modified EFRRPP process starting from an emulsified initial system

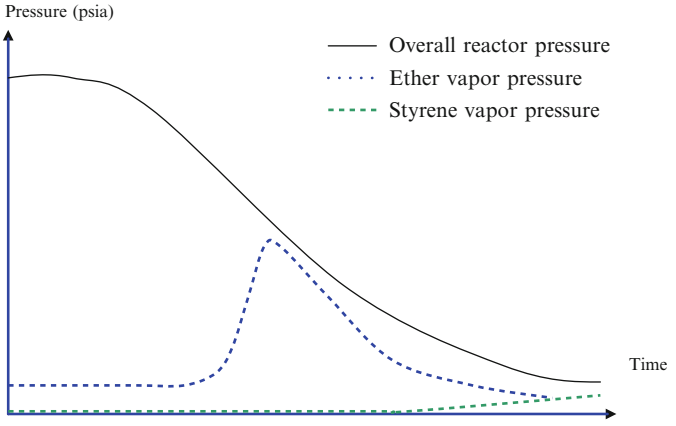

Fig. 9.4 Schematic representation of the overall pressure in the reactor and the vapor pressure of the monomer and (non)solvent

reactor stay nonvolatile and that the vapor pressure of ether is well below that at boiling conditions. The overall reactor pressure and the vapor pressure of ether as well as styrene in the reactor headspace are shown schematically in Fig. 9.4 as a function of time. If the reactor pressure is decreased in a controlled manner over a defined period of time while maintaining isothermal conditions, the partial pressures of volatile components in the reactor headspace will increase as the

nitrogen blanket is removed. Once the volatile components themselves are being removed, the partial pressure eventually starts to decrease.

The vapor pressure of diethyl ether stays close to zero until the pressure starts coming close to the boiling point of ether at the chosen reaction temperature. The vapor pressure of ether then increases as the ether volatilizes from the reaction medium. The maximum ether pressure is a function of the rate of volatilization and the rate of removal from the reactor headspace out of the reactor. An excessively slow rate of removal will lead to the partial pressure of ether being almost equal to the overall reactor pressure.

The removal of the volatile nonsolvent changes the composition of the dispersed phase in the reactor. An excessively fast removal can lead to undesirable reaction kinetics, dispersion instability, and other undesirable effects. Very slow removal can lead to the accumulation and pooling of recondensed nonsolvent in the reactor, which in turn leads to instability and undesirable effects on reactor kinetics due to the introduction of a new species of dispersed phase in the reactor.

In order to calculate the optimum time for removal of the nonsolvent and addition of water, a suitable approach is to use surface renewal theory to estimate the conditions that minimize the perturbation of critical parameters upon solvent removal. A schematic of the reactor surface is shown in Fig. 9.5 to illustrate how this can be accomplished.

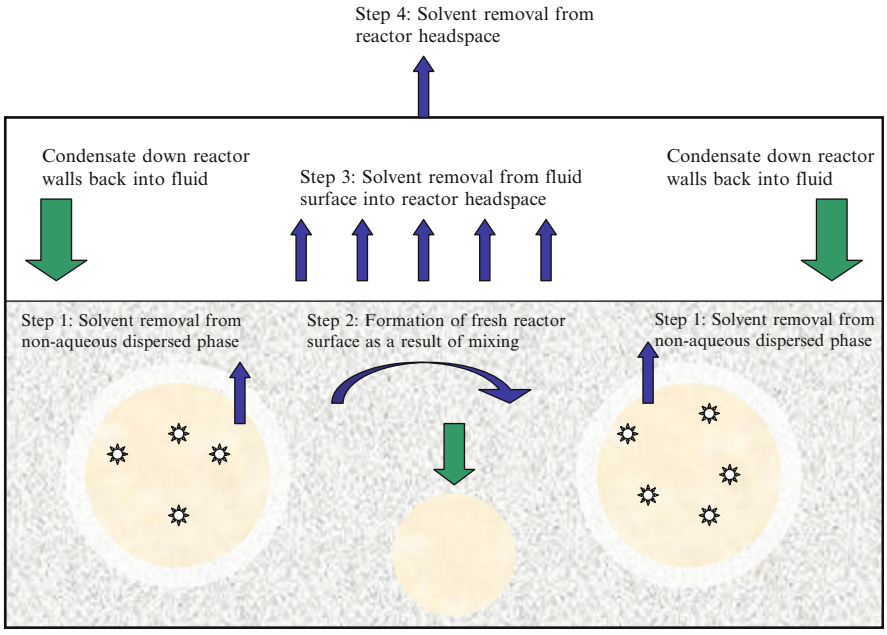

Fig. 9.5 Surface renewal as a critical step in the removal of solvents from the reactor

As shown in the Fig. 9.5, there are four critical mass transport steps in the removal of solvent from the reactor.

Step 1: Nonsolvent diffuses out of the nonaqueous dispersed phase into the continuous phase.
Step 2: The surface composition of the reactor fluid surface is renewed at a rate controlled by mixing parameters.
Step 3: The nonsolvent volatilizes from the reactor surface into the headspace.
Step 4: The headspace is depressurized resulting in the removal of the solvent.

Of all the steps above, step 4, or the rate of depressurization is not critical until the pressure is low enough to result in an increase in the vapor pressure of the nonsolvent. At that point, it is important to balance that rate of removal with the rate of volatilization of the solvent from the fluid surface to minimize the condensate that sends the solvent back into the fluid resulting in monomer and solvent pooling and the resulting undesirable effects.

Step 2 is directly related to the rate of mixing and the level of turbulence in the reactor. Step 1 is significantly impacted by steps 3 and 4 as well as by the solubility of the dispersed phase components in the continuous phase. A faster rate of removal of solvent from the continuous phase will drive a faster rate of diffusion into the continuous phase.

In order to control the solvent removal process to minimize solvent pooling and resulting instability, steps 1, 3, and 4 need to be balanced. Step 2 is a key rate-limiting step and is the only one that cannot be controlled only through pressure. The mixing rate and parameters are limited by maintaining an adequate level of shear while minimizing foam formation and entrainment (as described in Chapter 9.1.1.2). This implies that the rate of surface renewal can be calculated within a reasonable limit based on mixing speed, the level of turbulence, reactor size/shape, and fill level. Assuming that all solvent on the reactor surface volatilizes instantaneously requires that the reactor be depressurized at a rate fast enough to balance surface renewal. This means that the timescale of pressure drop is on the order of several millibars over seconds or even less implying that the overall solvent exchange process can take place over a timescale of minutes or at most a few hours.

This process was experimentally verified for an example 1 l reactor system, where it was calculated that at 400 rpm, assuming the surface renewed once per revolution, the time for surface removal was ~0.15 s. Assuming a surface depth of several nanometers and instant volatilization of the entire solvent from the surface at every surface renewal by maintaining a fast enough pressure drop, the overall time to be used for pressure to drop from the starting pressure to atmospheric was estimated to be about 1–2 h. Thus, the time for solvent exchange is a critical factor and needs to be carefully regulated and controlled for a robust process.

The rate of surface renewal was calculated using Eq. (9.1) below. This is based on the assumption that step 3 (volatilization of surface solvent) is instantaneous to balance the removal of solvent from the headspace and that the rate of solvent

removal from the headspace is fast enough to minimize/elimination of condensation along the walls and return to the reactor (Fig. 9.5).

Time for surface renewal (t) – time taken for one revolution of the impellers is described by Eq. (9.1).

$$t(\mathrm{s}) = \frac{60}{\mathrm{rpm}}. \tag{9.1}$$

For 400 rpm, this was 0.15 s. In this time, the entire volume of ether in the surface was transferred to the vapor phase. Assuming a surface depth of d, the amount of ether transferred to the vapor phase was estimated using Eq. (9.2).

$$v = \pi R^2 df \tag{9.2}$$

where v is the volume of ether instantaneously removed from the surface, R is the radius of the reactor, d is the surface depth, and f is the volume fraction of ether in the interface.

If v is the volume removed at every interval t, the time taken for overall solvent removal can be calculated by Eq. (9.3) assuming a nearly constant rate of solvent removal.

$$T = t\frac{V}{v} \tag{9.3}$$

where T is the time taken for removal of the overall solvent and V is the overall volume of solvent to be removed. The terms v and t have been described above.

Based on the model styrene–ether system described above with ether being a volatile component of low density actively being transported out of the reactor, the volume fraction of ether in the surface is considered to be close to 1. The interface depth is assumed to be about 200 nm. For the 300 ml reactor system described previously, the time taken to remove 100 ml of ether can be calculated to be about 4 h or faster. This means that if the time taken is longer than 4 h, the ether in the headspace will condense on the reactor walls and return back to the liquid phase leading to potential instability. A removal time of less than 4 h long will prevent this from happening as long as the ether is not removed "catastrophically," i.e., without destabilizing the dispersion.

9.1.3 Theoretical Observations on Polymer Confinement and Impact on Polymer Mobility and Radical Trapping

Once the nonsolvent is removed from the reactor, the reaction medium is essentially a dispersion of polymer particles and monomer reservoirs in the reaction medium.

Since this is no longer in the FRRPP regime (there is no LCST), it is very important to understand the state of polymer chains in the particle and the impact on chain mobility, polymerization kinetics, and the persistence of any radicals within the polymer particles.

Experimental data generated has provided the following observations:

1. Polymer radicals within emulsion particles have long persistence times, possibly up to several hours.
2. Based on calculations from kinetic data, there are a very large number of such radicals in the reactor, possibly 10–1,000 times the number of emulsion particles. At least one such radical exists in each emulsion particle.
3. These radicals are available for reaction with additional monomer and lead to block copolymer-like materials upon reacting with a different monomer.
4. The molecular weights of the polymer molecules obtained from this process correlate with the emulsion particle sizes. The correlation is that the theoretical radii of gyration corresponding to the molecular weights of the polymer chains based on melt-like conditions are always higher than the sizes of the particles that they are present in.

The above observations suggest that the polymer chains in the emulsion particles are physically immobilized, which is what leads to the kinetics effects observed. This is similar to observations of the gel effect or the Trommsdorf effect in free radical polymerization processes. There are several factors that can lead to this confinement.

The polymer chains within emulsion particles are in an environment that can be closely compared to a polymer melt, except at the particle surface. However, the molecular weight of the polymer chains is such that the radius of gyration corresponding to a melt-like environment is actually larger than the experimentally observed polymer particles. The polymer chains cannot achieve this larger radius due to their confinement to the emulsion particles by virtue of being in a precipitating environment.

The extent of this confinement can be visualized by comparing the size that the polymer chain would prefer to assume by virtue of its confinement in the polymer-rich environment, and the size that it is actually confined to, by virtue of being constrained within the emulsion particle. The size that the polymer chain would like to assume in a melt-like environment is the size that the chain would assume if the particle size was large enough to accommodate the random space expansion dynamics of the chain. The calculations described below are based on polystyrene. The radius of gyration for a polymer chain in a melt environment can be calculated using Eq. (9.4) (de Gennes 1979).

$$R_g = a(\mathrm{DP})^{0.5}. \tag{9.4}$$

The parameter a is 3.11×10^{-10} (Nierlich et al. 1978) and DP is the degree of polymerization of the polymer molecule. The actual size of the polymer chains is

limited to be equal to or less than the size of the polymer particles. This size can be calculated from the experimentally measured particle size. For the purpose of calculation, an upper limit of the particle size can be calculated for a given number of polymer chains with a given average chain length with the assumption that the chains are packed into a domain size defined by the bulk density of the polymer (e.g., bulk density of polystyrene = 1.047 g/cc, Sigma-Aldrich Catalog 2001). The radius of the particle and its dependence on degree of polymerization are described in Eq. (9.5).

$$R_{\mathrm{p}} = \left(\frac{3}{4\pi} \frac{\mathrm{MW}_{\mathrm{monomer}} N_{\mathrm{Chains}} \mathrm{DP}_{\mathrm{average}}}{\rho} \right)^{\frac{1}{3}}. \tag{9.5}$$

In Eq. (9.5), $\mathrm{MW}_{\mathrm{monomer}}$ is the molecular weight of the monomer, N_{Chains} is the number of chains in the particle, ρ is the bulk density of the polymer, and $\mathrm{DP}_{\mathrm{average}}$ is the average degree of polymerization of the chains in the particle.

In reality, this particle size may be a little larger than the calculated number due to water inclusions in the particle and the density at the small size scale being less than the bulk polymer density. Both sizes can be compared by plotting the volumes based on the calculated radii and comparing them as a function of increasing molecular weight. This comparison is shown in Fig. 9.6.

As seen in Fig. 9.6, there is a crossover point observed where the volume that the chain would theoretically assume (chain volume) in a nondimensionally constrained system becomes larger than the particle volume. If the molecular weight

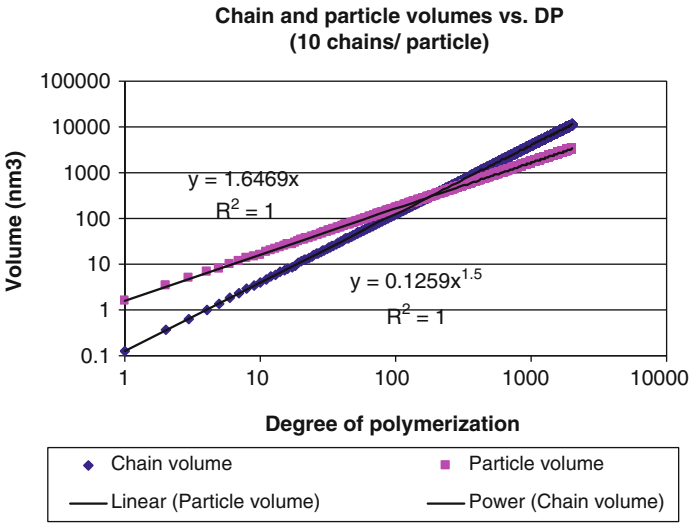

Fig. 9.6 Impact of degree of polymerization leading to a crossover of the volume a polymer chain would occupy in bulk and the volume it is constrained to occupy by virtue of being "confined" in an emulsion particle

of the chains is higher than that at the crossover point, the chain would effectively be confined to a size that is smaller than that at theta conditions. This, in effect, would be a confined condition for the chain. Thus, depending on the degree of polymerization of the chains, the chains can have a size that would be similar to that assumed in polymer melts or a size that would be comparable to that under precipitation conditions. For large molecular weight, this can be an effective confinement mechanism for the polymer chains.

This confinement can have a significant impact on the dynamics of the polymer chain in the particle. The polymer chain can have a higher degree of entanglement as compared to melt conditions due to the confined space as the chain is forced to explore a smaller space.

In addition to the confinement effect due to physical size limitations, another consequence of the fact that the chain dimensions are equal to the particle dimensions implies that several chain segments for each polymer chain in the particle form the particle interface. The presence of chain segments at the particle–liquid interface results in surface tethering (Li 1996). This is a surface effect where energy costs associated with renewing interfaces lead to the persistence of elements that are positioned at interfaces for longer timescales than in the bulk. This implies that a polymer chain with chain segments at the interface is "tethered" or pegged at the points on the interface on the timescale of reptation in the melt. If the chain has a significant number of elements at the interface, it could effectively be tethered to the point of immobility.

Surface tethering combined with an increased number of entanglements can lead to a significant loss in segmental mobility. This is most likely a significant contributing factor in the immobilization of polymer radicals within emulsion particles that lead to radical persistence in stage II of EFRRPP.

The crossover point observed in Fig. 9.6 has not been noted in the scientific literature to the best of the authors' knowledge. Further calculations around this crossover point are shown in Figs. 9.7 and 9.8. Figure 9.7 describes the crossover degree of polymerization as a function of the number of polymer chains in each particle, assuming that each chain has the same degree of polymerization. Figure 9.8 describes the crossover degree of polymerization as a function of particle size for a fixed number of polymer chain in every particle, assuming the same degree of polymerization for each chain in the particle.

Based on the calculations in Figs. 9.7 and 9.8, the crossover DP has very well-defined functionality, as shown in Eqs. (9.6) and (9.7).

$$\mathrm{DP}_{\mathrm{Crossover}} \sim N_{\mathrm{chains}}^{2}, \tag{9.6}$$

$$\mathrm{DP}_{\mathrm{Crossover}} \sim D_{\mathrm{particle}}^{2}. \tag{9.7}$$

N_{chains} is the number of chains in each particle and D_{particle} is the particle size. Equations (9.6) and (9.7) are not really independent as the particle size is a function of the number of chains in the particle for a given DP, as calculated here. However,

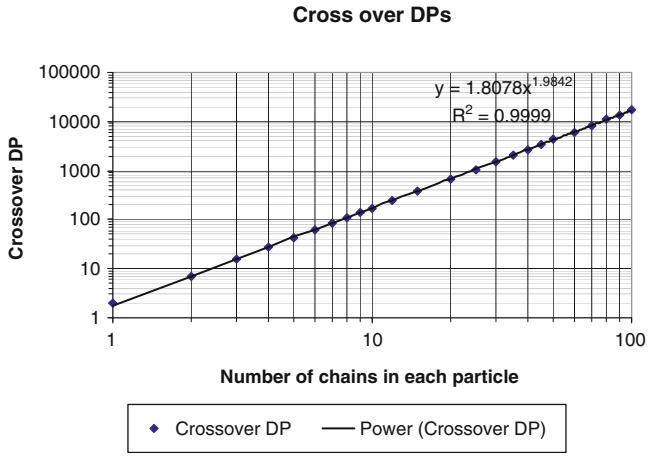

Fig. 9.7 Crossover degree of polymerization as a function of the number of polymer chains in each particle

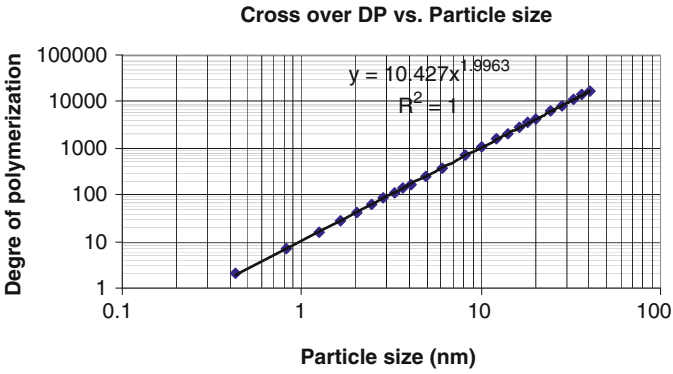

Fig. 9.8 Crossover degree of polymerization as a function of particle size

both Eqs. (9.6) and (9.7) present different aspects of the calculated crossover point. In a real system, the crossover DP can increase either as the particle size increases or as the number of chains in the particle increases, i.e., for a lower DP for the same particle size. This would imply that for confinement conditions to occur, both the particle size and the number of chains in each particle should be within the defined limit for a given average degree of polymerization in the particle.

The relationship between the number of chains in a particle and the particle size is not linear, which makes the dependence observed in Eqs. (9.6) and (9.7) significant. The number of polymer molecules per particle as a function of particle size is plotted for a number of different degrees of polymerization in Fig. 9.9. A constant density equal to the bulk polymer density is assumed for the purpose of calculation.

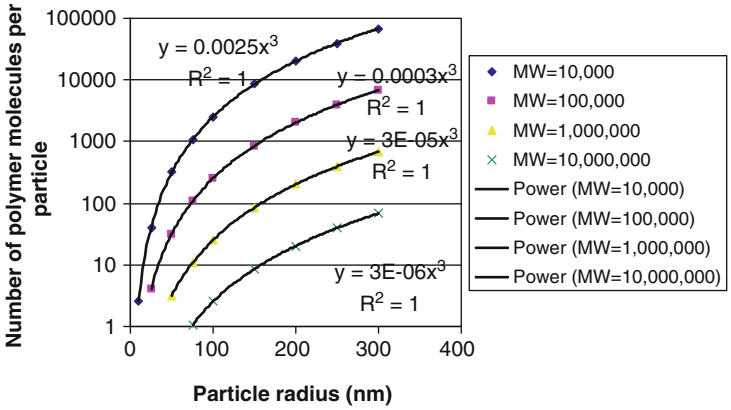

Fig. 9.9 Number of polymer molecules per particle as a function of particle size

The scaling relationship shown in Fig. 9.9 is described in Eq. (9.8).

$$N_{\text{chains}} \sim D^3_{\text{particle}}. \tag{9.8}$$

Thus, the crossover point described in Eqs. (9.6) and (9.7) is a much stronger function of particle size than the number of chains.

The change in degree of confinement with degree of polymerization can be represented as a calculated parameter called the Confinement Index (CI). The scaling relationships that influence this parameter are described in Eqs. (9.9) and (9.10).

$$\text{CI} \sim \text{DP}^{0.5}, \tag{9.9}$$

$$\text{CI} \sim D^{1.5}_{\text{particle}}. \tag{9.10}$$

A significant factor that affects the dynamics of polymer chains in such an environment is the presence of lower molecular weight diluents within the emulsion particles. All the effects described previously will show greatly reduced impact on the polymer chain dynamics if low molecular weight diluents that swell the polymer are present at a significant level. These could include monomers and suitable solvents. The presence of a precipitant may have an enhancing effect on the factors described earlier. To be able to study the impact of the confinement effects described earlier, it is critical to conduct experiments at monomer starved conditions.

An additional factor that can impact this process is the finite size of the emulsion polymer particles. Many investigators have assumed that a polymer chain in an emulsion particle can be virtually indistinguishable from one in a polymer melt for most practical purposes. However, in addition to the confinement and tethering effects described above, there are two consequences of the finiteness of the particles

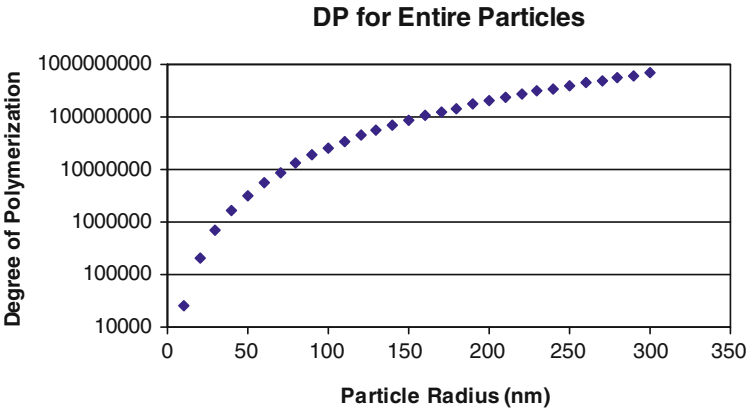

Fig. 9.10 Degree of polymerization as a function of particle size if the entire particle consisted of a single polymer chain

that may also have significant bearing on the state of polymer chains in the polymer particles.

The first consequence is that the particle size limits the maximum possible DP within the particle. This is because even if all the polymer segments within the particle were joined to form just one large polymer chain, the maximum molecular weight of the chain would be limited by the particle size. This is further illustrated in Fig. 9.10.

The effects observed in Stage II of FRRPP correspond to particle radii of tens to hundreds of nanometers typically. These correspond to upper limits in degree of polymerization in the range of tens of thousands to tens of millions for a single chain that constitutes the entire particle. The degrees of polymerization observed in experimental systems are typically about 1–2 orders of magnitude lower than these values for this range of particle size. This implies that there are hundreds to thousands of polymer chains per polymer particle.

The second consequence of the finite particle size is on free volume. The free volume for polymer particles is a very finite quantity. Of specific interest is hole free volume, which is the available volume in the bulk that is in addition to the minimum volume occupied by the polymer chains and increases with temperature. For example, the hole free volume for Polystyrene (V^*) was estimated by Zielinski and Duda (1992) as 0.8296 cc/g.

Fluctuations in hole free volume are believed to be the driving force for the diffusion of polymer chains. Resistance to diffusion comes from entanglements and surface renewal cost. Hole free volume is typically about 5% or less of the total available volume. Since the total volume is a small finite quantity for small particles, the total hole free volume and any thermal fluctuations are bound to very small finite quantities. The ability of a polymer chain to diffuse needs the physical availability of a large enough fluctuation in hole free volume that allows a polymer segment to move into it. A very small finite free volume will have a significant

impact on the overall size of the holes and the ability to generate a large enough hole to allow polymer segments to diffuse into it. This can further limit the diffusion of polymer segments within small particles.

Another important factor that contributes to polymer mobility is the very high surface-to-volume ration for very small particles. For a given DP, the smaller the particle size, the more the number of chains that have at least one segment on the surface leading to stronger tethering effects, as described previously. It has been shown that polymer segments on interfaces have much lower mobility due to high energy costs associated with surface renewal. For the particle sizes and molecular weights observed in FRRPP emulsions, it can be estimated that nearly all the polymer chains have segments at the particle–liquid interface. This contributes to a higher level of tethering and would reduce polymer self-diffusivities with very small particles for a given DP.

In summary, the polymer physics at the scale of small emulsion particles suggests that diffusion of polymer chains is greatly reduced under the polymerization conditions being studied and this can lead to the persistence of radicals in Stage II even after the nonsolvent has been removed from the system. This can obviously be changed by undesirable events including monomer flooding as well as large/catastrophic changes in particle size.

9.2 Experimental Methods Used in Studies of EFRRPP

This section provides details on experiments conducted that were used to test/verify the theoretical considerations described in Chapters 7 and 9 and to demonstrate the ability of the FRRPP process to synthesize block copolymer emulsions in different monomer systems. Experimental details include materials and sources, polymer synthesis detail, and characterization approaches and techniques.

9.3 Materials

Table 9.1 describes the materials used for experimental studies of the modified EFRRPP process as described in Chap. 8.

9.3.1 Polymer Synthesis

The polymerization was conducted in a stage-wise manner, where FRRPP was used to synthesize and trap polymeric radicals in stage I and these radicals were further reacted with additional monomer to obtain polymer molecules with different

Table 9.1 Materials used for experimental studies

Ingredient	Chemical	Source
Stage 1 (Formation and trapping of PS radicals) $T = 75$ or 80°C		
Monomer	Styrene	Aldrich Chemicals
Nonsolvent for PMMA/PS	Diethyl ether	Fisher Chemicals
Initiator	V-50 (2,2′-Azobis (*N*,*N*′-amidinopropane) dihydrochloride) VA-044 (2,2′-Azobis (*N*,*N*′-dimethyleneisobutyramidine) dihydrochloride)	Wako Chemicals
Water	DI water	NSC
Surfactant	IGEPAL CA-897 (octyl phenol ethoxylate, nonionic surfactant)	Rhodia
Stage 2 (Addition of second monomer and copolymerization) $T = 60$ or 75°C		
Monomer	Styrene	Aldrich Chemicals
Monomer	*N*-Butyl acrylate	Aldrich Chemicals
Surfactant	IGEPAL CA-897	Rhodia
Water	DI water	NSC

architectures in stage II or beyond. The procedure for stages I and II are provided below for an example laboratory synthesis.

Stage I. Uninhibited monomer (37 ml) and diethyl ether (300 ml) were purged with subsurface nitrogen for 15 min. Water (100 ml) and 7.6 g surfactant solution (IGEPAL CA-897, Rhodia) in a round bottom flask were deoxygenated by evacuating for 1 min and breaking the vacuum with Argon, the process of which was repeated twice. As a final step, the water–surfactant mixture was completely deoxygenated by freezing it in a dry-ice acetone mixture while keeping it under vacuum. The vacuum was maintained while allowing it to thaw completely to let any dissolved gases escape. The vacuum was then replaced with an Argon blanket. Water (500 ml) and initiator solution (0.4792 g) (2,2′-azobis (*N*,*N*′-amidinopropane) dihydrochloride or V-50, Wako chemicals) were purged with nitrogen for 20 min. The ether and MMA were added to the water surfactant mixture by canula transfer. A preemulsion was made using a high shear homogenizer blade. The admixture was kept oxygen free by maintaining a constant flow of Argon saturated with ether through the round bottom flask. This preemulsion was inverted into an emulsion by diluting with the initiator–water mixture (350 ml) by canula transfer. This emulsion was transferred into a shot bomb and then loaded into the reactor with 20 psig of nitrogen overpressure. The transfers were effected using nitrogen pressure. The reactor was heated up to 80°C in 25 min. The pressure was regulated at 60 psig. The take-off valve was opened after 1 h and ether was stripped from the reactor at such a rate as to be completely removed in 3 h. Samples were taken at irregular intervals to determine conversion and molecular weight.

Stage II: Water (55 ml) and IGEPAL CA-897 surfactant solution (Rhodia) (2.95 g) in a round bottom flask were deoxygenated by the same process as described above in stage I. MMA (95 ml) was deoxygenated by purging with subsurface nitrogen for 15 min. A preemulsion was made by adding the MMA to

the water surfactant mixture under high shear. This was diluted with 50 ml water. The resulting emulsion was loaded into reactor over 5 min. The reactor was cooled to 60°C in 10 min and the pressure was set at 60 psig. Samples were taken to determine conversion and molecular weight.

The laboratory scale setup for polymerization included either a 300-ml or a 1-l mantle-heated high-pressure reactor vessel purchased from Parr Instruments, Inc. (Moline, IL) and high-pressure metering pumps purchased from Fluid Metering, Inc. (Oyster Bay, NY). A canula purging and fluid-transfer system was used to purge the reagents of oxygen as well as to transfer fluids between vessels. When larger volumes of liquid were used, a jacked glass–resin kettle was used with an overhead stirrer.

9.3.2 Characterization

All polymer samples were characterized for conversion, molecular weight, and based on properties of interest. Samples were taken at intermediate reaction points and from the end product. They were analyzed for particle size if desired and then air-dried for further analysis. Conversion was determined gravimetrically. The solids were analyzed by proton NMR for composition, DSC for degree of blockiness vs. randomness, and for chain length distribution by gel permeation chromatography (GPC). Extraction processes were also used to test the product samples to determine whether they contained homopolymers of both monomers. To determine the presence of homopolymer, the product was dried at room temperature and a weighed amount was soxhlet extracted using a liquid which was a good solvent for one homopolymer but a poor solvent for another homopolymer. The residue in the thimble was soxhlet extracted using a good solvent for the other homopolymer but a poor solvent for one already extracted. The homopolymer should dissolve in a good solvent. The solvent was evaporated and the solid was air-dried. The parameters for the techniques used are described in the sections below.

9.3.2.1 Conversion

Conversion was determined gravimetrically by weighing the sample obtained, and then air/vacuum drying the sample. The dry residue was weighed and used to calculate conversion.

9.3.2.2 Size Exclusion Chromatography/Gel Permeation Chromatography

Samples were dissolved in THF, filtered with 0.45 μm PTFE filters, and analyzed under GPC conditions listed in the Table 9.2.

Table 9.2 GPC conditions

Column: SHODEX KB-806M 9104919 & KF-G (guard column 201050)	Mobile phase: THF
Injector: WATERS 717 PLUS	Column temp.: 35°C
Detector: RID-6A, 486 MS UV detector at 254 nm	Standards: Polystyrene
Pump: WATERS 515	Run time: 17 min
Injection No.: 2 @ 50 µl	Flow rate (isocratic): 1 ml/min

9.3.2.3 Differential Scanning Calorimetry

Differential scanning calorimetry (DSC) was performed on air-dried sample using TA Instruments (Model DSC 2920). DSC determines the temperature and heat flow associated with material transitions as a function of time and temperature. It also provides quantitative and qualitative data on endothermic and exothermic processes of materials during physical transitions that are caused by phase changes, melting, oxidation, and other heat-related changes. Liquid nitrogen was used for cooling. Nitrogen gas was used as a carrier gas. Empty aluminum pan was used as reference. Dry film was exactly weighed (5–20 mg) into the DSC aluminum pan (hermetically sealed). Appropriate lid was placed onto the pan and sealed using the crimper. The method used for operation was as follows:

1. Hold for 1 min at 25°C
2. Cool from 25°C to −80°C at 20°C/min
3. Hold for 5 min at −80°C
4. Heat from −80°C to 150°C at 10°C/min
5. Cool from 150°C to −80°C at 20°C/min
6. Hold for 5 min at −80°C
7. Heat from −80°C to 150°C at 10°C/min

Universal Analysis software was used to analyze the data.

9.3.2.4 Particle Size

Particle size was measured using Brookhaven Instruments 90Plus Particle Size Analyzer. The 90Plus Analyzer is used for the measurement of particle sizes from 2 nm to 3 µm by photon correlation spectroscopy or quasi-elastic light scattering (QELS). The computerized analysis uses MAS Particle Sizing Software Beta Version 1.13 (MAS OPTION), which makes the size measurements and automatically calculates the translational diffusion coefficient and particle diameter. A very dilute sample solution of about 0.005% by weight was prepared and placed in a cuvette clear on all four sides. The cuvette was placed in the sample chamber and sample information was entered into the software. When the sample concentration is correct, the count rate will be 100,000–300,000 counts/s. If the count rate is not within this range, the sample must be diluted or concentrated until the count rate is correct. The instrument parameters are listed in Table 9.3.

Table 9.3 BI 90Plus parameters

Runs	5
Temperature (°C)	25
Liquid	Aqueous
Angle	90°
Run duration	1 min
Dust cut off	30
Refractive index of particles Real	1.590

Table 9.4 Solvents and nonsolvents for polymer

	Solvent	Nonsolvents
Polystyrene	THF, ethyl acetate, MEK	Alcohol, ether, acetone, saturated hydrocarbon
Poly(*n*-butyl acrylate)	Butanol, THF, ketones	Ethyl acetate, methanol, ethanol
Poly(methyl methacrylate)	Ethyl acetate, ethanol/ water, IPA/MEK	Absolute ethanol, ether

9.3.2.5 Soxhlet Extraction

Soxhlet extraction was carried out using an apparatus consisting of 500 ml one-necked round bottom flask equipped with thimble in the extractor chamber, condenser on top of extraction chamber, and heating mantle. The solvents and nonsolvents for the polymers subject to extraction are listed in Table 9.4 (Immergut and Brandrup, 1989).

9.3.2.6 Gel Permeation Chromatography-Infrared Analysis

Gel permeation chromatography-infrared (GPC-IR) is an analytical tool which combines the separation and detection strength of liquid chromatography/gel permeation chromatography with the identification strength of infrared spectroscopy. This provides an opportunity to map compositional distribution across the molecular weight range.

GPC separation of the sample is usually conducted using a suitable solvent (e.g., THF) as the mobile phase under the following conditions.

GPC Columns: PLgel 10 μm Mixed & Styragel HR-1
Run time: 30 min
Injection: 100 μl
Detection-1: Waters 2487 Dual Wavelength UV detector
Detection-2: Shimadzu RID-6A Refractive Index detector
Column temp: Room temperature
Flow rate: 1 ml/min

9.3.2.7 Nuclear Magnetic Resonance Spectroscopy

Proton nuclear magnetic resonance (NMR) spectroscopy was conducted on each final polymer product and other polymers as needed for comparison. To prepare the samples, about 15 mg of dry polymer was dissolved in about 1.5–2 g of deuterated chloroform. After the entire polymer had dissolved, the samples were transferred to 7 mm NMR tubes and analyzed on a 400 MHz Bruker NMR. The results were analyzed using Bruker 1D WinNMR software. Deuterated chloroform was the reference for calibration.

9.3.3 Selection of Surfactants

A comprehensive study of the stability of emulsions of styrene and methyl methacrylate in ether and pentane was undertaken to identify suitable surfactants or surfactant combinations which would lead to a stable emulsion. Sodium dodecyl sulfate (SDS) had been used as the surfactant on all the previous runs and had not worked very well. It had been recommended to try nonionic surfactants or their combination with SDS to improve emulsion stability. The surfactants tried were sodium dodecyl sulfate (SDS) and an alkyl ethoxylate (BRIJ 76, Uniquema) for MMA/Styrene in pentane, and SDS and octyl/nonyl-phenol ethoxylates (IGEPAL CA/CO series, Rhodia) for the styrene–ether system. The system was emulsified using a high shear homogenizer (Ultra Turrax T8, IKA Laboritechnik). The stability of the emulsions was observed visually and under an optical microscope. It was observed that the nonionics greatly increased the stability of the emulsions in combination with SDS. Further, they were even more effective when used without SDS. Another criterion in surfactant selection was the high temperature of operation (80°C). This temperature necessitated the selection of surfactants with high HLB (hydrophile-lipophile balance) numbers, which would correspond to cloud points above 100°C. Based on these considerations and on the particle sizes observed, IGEPAL CA-897 was chosen as the surfactant of choice for the styrene–ether system.

A model reactor run was carried out in a resin kettle with the mixing modifications developed in the study on mixing (next section) for a styrene/heptane emulsion in water made using the homogenizer with CA-897 to observe the impact of shear on emulsion stability. The shear led to accelerated creaming, but did not seem to lead to any widespread separation of the organics. Heptane was used instead of ether as it has a similar density to pentane and ether, but has a much higher flash point and boiling point.

9.3.4 Selection of Dispersion Conditions

For EFRRPP, based on a detailed laboratory study, it was concluded that the use of baffles is absolutely essential for most reactor designs to prevent entrainment due to

vortex formation. The combination that worked the best in test reactor configurations was a pitched blade turbine at the tip of the mixing shaft placed close to the reactor base with a radial dispersion blade about a third of the way up the reactor fill-line combined with four full baffles. This system gave excellent oil-in-water dispersion at low mixing speeds, the least dead spots, and the least entrainment.

References

Dar YL, Caneba GT (2002) Transport phenomena aspects of the free-radical retrograde-precipitation polymerization (FRRPP) process. Chem Eng Commun 189:571

Dar YL, Caneba GT (2004) Free-radical retrograde-precipitation polymerization: mathematical modeling of styrene polymerization in diethyl ether. Chem Eng Commun 191:1634

de Gennes PG (1979) Polymer physics. McGraw Hill, New York, NY

Immergut EH, Brandrup J (1989) Polymer handbook, 3rd edn. Wiley, New York, NY

Li Z (1996) Polymer thin films on selected surfaces. Ph.D. Dissertation, State University of New York at Stony Brook, NY

Nierlich M, Cotton JP, Farnoux B (1978) J Chem Phys 69:1379

Sigma-Aldrich Catalog (2001) Sigma-Aldrich Corporation, Milwaukee, WI

Zielinski JM, Duda JL (1992) AIChE J 38:405

Chapter 10
Radical-Containing Polymer Emulsions

This chapter describes the study of the radical-containing polymer-in-water dispersions obtained using the techniques described in the previous chapter. The studies include verification of the presence of radicals in the system through theoretical estimation. Some of the concepts and data presented here are adapted from Caneba and Dar (2002), Dar and Caneba (2001), Dar et al. (2003), and Caneba et al. (2002).

10.1 PS Radical-Containing Emulsions from Monomer Pre-emulsions

This section describes experiments conducted to synthesize emulsions with polystyrene as the stage I monomer and use entrapped radicals to initiate stage II polymerization. Intermediate samples were taken during the reactions and used to calculate conversion, molecular weight, particle size, and characterization of copolymer microstructure. The kinetics data were also used to estimate the population of trapped radicals.

10.1.1 Estimation of Radical Populations from Kinetics Data

In previous work, it has been demonstrated that FRRPP can be used to trap polymer free radicals and use them to make copolymers. These copolymers are obtained at high (100%) yield in a small particle size aqueous dispersion. The molecular weight of these copolymers is a function of the number of radicals successfully trapped in the reactor as well as the amount of monomer available to these radicals. It has been shown that the molecular weight shows some variation with system parameters such as temperature and reactant concentration. The total number of radicals trapped in the system as well as the number of radicals trapped in each dispersion

G. Caneba and Y. Dar, *Emulsion-based Free-Radical Retrograde-Precipitation Polymerization*, DOI 10.1007/978-3-642-19872-4_10,

particle are critical parameters for evaluating the radical trapping and utilization capability of FRRPP.

There were two metrics used to measure the effectiveness of FRRPP to trap radicals and generate copolymer. The first metric was the total number of radicals trapped in the reactor as a fraction of the maximum number of radicals generated, called the instantaneous trapping efficiency. The second one was the total number of radicals trapped in every emulsion particle.

The data necessary to calculate these metrics were generated from the polymerization of styrene in ether. Additional styrene was loaded in the second stage to observe the activity of any trapped radicals. The results indicate that close to 100% of the polymer radicals initiated are trapped and 5–30% of the initiator led to trapped radicals. The number of trapped (nonterminated) radicals per dispersion particle was calculated to be of the order of 10^2–10^4. This is a very large number to be trapped in such a small space (~100 nm) in the absence of chemical trapping agents. This strongly suggests a unique and novel radical trapping mechanism that differentiates this technology over others.

Styrene polymerization was carried out in ether with the aim of maximizing the number of trapped radicals. Additional styrene was added in the second stage to observe the impact on the kinetics. This was done to see if the slow addition of a reactive good solvent would solvate the polymer particles and make the trapped radicals more accessible. The use of styrene as the good solvent made it possible to get a quantitative measurement of the real molecular weights of the polymer radicals using size exclusion chromatography (this is difficult for copolymers).

Two experiments were conducted to study this effect – one at 60°C (PS-1) and one at 75°C (PS-2). A lower half-life initiator (VA-044) was used in PS-1 to keep the overall reaction times comparable. The half-life of VA-044 at 60°C is about 61 min. In experiment PS-2, a smaller styrene charge (one third) was used, but the amount of initiator was the same as used in previous experiments. This tripled the initiator-to-monomer ratio.

The materials used for the reactions are listed in Table 10.1. The experimental conditions and details are listed in Table 10.2. Details and data from two additional styrene polymerizations (PS-3 and PS-4) are also included for the purpose of comparison. In both these experiments, a second styrene charge was slow added before ether was removed.

Conversion, molecular weight distribution, and particle size data were gathered for each of these experiments. This was used to calculate the performance metrics for each experiment.

The overall results for each experiment are summarized in Table 10.3.

The results show that the addition at lower temperature as well as the lower monomer charge (despite the higher initiator-to-monomer ratio) lead to higher molecular weights. This indicates a lower efficiency of radical trapping in both these experiments as compared to the earlier ones. The molecular weight of the precipitates in all the experiments was comparable to the product molecular weight, indicating that the precipitate was formed in the later stages of polymerization due to stabilization issues.

Table 10.1 Materials used for each stage of FRRPP

Ingredient	Chemical	Source
Stage 1 (formation and trapping of PS radicals) $T = 75$ or 80°C		
Monomer	Styrene	Aldrich Chemicals
Nonsolvent for PMMA/PS	Diethyl ether	Fisher Chemicals
Initiator	V-50 (2,2′-Azobis (*N*,*N*′-amidinopropane) dihydrochloride) VA-044 (2,2′-azobis (*N*,*N*′-dimethyleneisobutyramidine) dihydrochloride)	Wako Chemicals
Water	DI water	NSC
Surfactant	IGEPAL CA-897 (octyl phenol ethoxylate, nonionic surfactant)	Rhodia
Stage 2 (addition of second monomer and copolymerization) $T = 60$ or 75°C		
Monomer	Styrene	Aldrich Chemicals
Surfactant	IGEPAL CA-897	Rhodia
Water	DI water	NSC

Table 10.2 Variation in experimental conditions

Exp.	Experimental details
PS-3	Styrene was the first-stage monomer. $T = 80$°C. $P = 70$ psig (initial). 1% initiator (V-50) (w/w monomer). Start loading 3× the original charge of styrene in the reactor after 8 initiator half-lives (4 h), and over 11 initiator half-lives (5.5 h). Ether removal started after 19 initiator half-lives (10 h)
PS-4	Styrene was the first-stage monomer. $T = 75$°C. $P = 70$ psig (initial). 1% initiator (V-50) (w/w monomer). Start loading 3× the original charge of styrene in the reactor after 4 initiator half-lives (4 h), and over 4.5 initiator half-lives (4.5 h). Ether removal started after 10 initiator half-lives (10 h)
PS-1	Styrene was the first-stage monomer. $T = 60$°C. $P = 70$ psig (initial). 1% initiator (VA-044) (w/w monomer). Ether removal started after 4 initiator half-lives (4 h) and removed over 4 h. Second styrene charge (2× original charge) loaded in one shot after 8 initiator half-lives (8.5 h)
PS-2	Styrene was the first-stage monomer. Initial styrene charge reduced to 33% of the typical charge $T = 75$°C. $P = 70$ psig (initial). 3% initiator (VA-044) (w/w monomer). Ether removal started after 4 initiator half-lives (4 h) and removed over 3.5 h. Second styrene charge (2× original charge) loaded in one shot after 8 initiator half-lives (8 h)

Table 10.3 Summary of results

Exp.	Overall conversion (%)	M_n (Daltons)	PDI[a]	Particle size (nm)
PS-1	100	585,973	2.9	107
PS-2	95	731,817	1.9	98
PS-3	72	232,000	2.3	157
PS-4	80	193,000	2.7	150

[a]Polydispersity Index

The conversion, molecular weight, and particle size data from experiments PS-1 through PS-4 were used to calculate the instantaneous trapping efficiency and the number of radicals per particle. In order to do this, it was necessary to estimate

the total number of living (trapped) and terminated polymer chains at a given time. This was easy for the polystyrene/ether system since there does not appear to be a significant premature termination. All the chains that get trapped in the initial stages of polymerization appear to be trapped right up to the later stages of polymerization. The number of chains in a peak in a given molecular weight distribution can be calculated by knowing the mass of polymer in that peak (from conversion data) and dividing it by the number average molecular weight of the peak.

The instantaneous trapping efficiency (ITE) is a measure of the fraction of trapped radicals based on the maximum possible number of available radicals in the system and includes the effect of initiator efficiency. The ITE is actually a product of two efficiencies. The first is the intrinsic initiator efficiency (IE). This is a measure of what fraction of the primary initiator fragments successfully overcomes the cage effect to initiate a polymer radical. The second efficiency is the trapping efficiency (TE). This is a measure of what fraction of the initiated polymer radicals actually gets trapped. The trapping efficiency is the actual quantity of interest, but since there is no straightforward way of estimating the initiator efficiency, the overall instantaneous efficiency is the only variable that can be calculated from the available data. Thus,

$$\text{ITE} = \frac{\text{Number of trapped radicals at any time}}{2 \times \text{Number of initiator molecules decomposed at the time}}. \tag{10.1}$$

$$\text{ITE} = \text{IE} \times \text{TE}. \tag{10.2}$$

A factor of 2 in the denominator on the right-hand side of Eq. (10.1) is used because each initiator molecule decomposes into two primary initiator fragments. The denominator of Eq. (10.1) equals the maximum possible number of radicals generated in the polymerization. The ITE includes the word instantaneous as it measures the number of trapped radicals as fraction of the maximum number of generated radicals at any given instant.

The number of trapped radicals per particle can be calculated by using the particle size analysis data and the total number of radicals in the system.

$$\text{Trapped radials/particle} = \frac{\text{Total number of trapped radicals}}{\text{Total number of particles}}. \tag{10.3}$$

The total number of particles can be calculated by measuring the particle size at the end of a typical experiment. If the conversion is high, the particles consist of mainly polystyrene stabilized by surfactant. This can be used to calculate the weight of every particle using the density of polystyrene and then to calculate the total number of particles by dividing the total weight of polymer by the weight of one particle. Since the total number of particles in a dispersion polymerization process is determined in the particle nucleation phase, this number should stay constant once nucleation is complete, or once all of the initiator has decomposed. This implies that the estimation of number of particles from the final stages of polymerization can be used for most of the samples.

The metrics calculated in this way have an overall error of up to 40% associated with them based on the factoring of errors in the experimental data. However, they can be successfully used to provide a semiquantitative estimate of the success of a particular experimental strategy.

The instantaneous trapping efficiency with time is shown in Fig. 10.1. It can be seen that it is of the order of 5–30%. More than 99% of the initiator has decomposed by seven half-lives so any increase observed in the initiator efficiency after that is due to error. It can be seen that PS-2 has a lower trapping efficiency. This experiment had a lower styrene charge in the first stage with the same amount of initiator as used in other experiments. This means that the initiator-to-monomer ratio was three times that of other experiments. The apparent fall in efficiency could be due to significant primary termination during the early stages of polymerization.

The number of radicals per particle for these experiments is shown in Fig. 10.2. This number is of the order of 10^2–10^4 depending on the experiment. This is a high number indeed considering that particle sizes are of the order of 100 nm. The presence of such a large number of polymer radicals per polymer particle is evidence of a unique and novel trapping mechanism that leads to polymerization control in FRRPP. If this number were of the order of 1 radical per particle, it would have indicated that the isolation of radicals by virtue of being in different particles could play a significant role in controlling their termination. Since this number is 2–4 orders of magnitude higher than 1, it strongly suggests the presence of a trapping mechanism inherent to the system. Understanding the nature, capabilities, and limitation of this mechanism has been one of the main goals of this investigation.

The extremely large number of trapped radicals per particle for all experiments suggests the presence of an inherent and novel trapping mechanism that controls polymerization. It also shows that the separation of these radicals into different particles is not the dominant mechanism of polymerization control.

Fig. 10.1 Instantaneous trapping efficiency vs. time

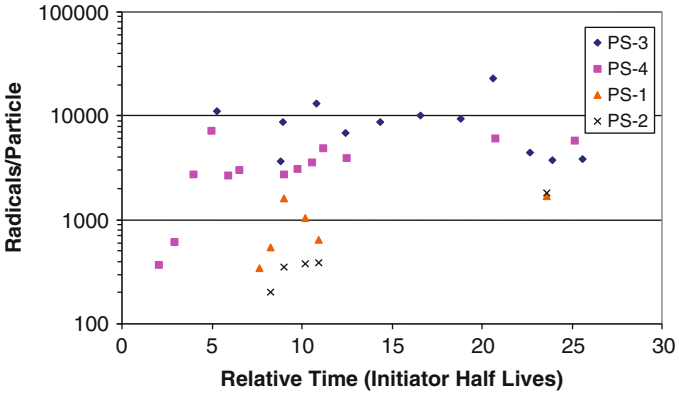

Fig. 10.2 Number of trapped radicals/particle vs. time

10.1.2 Investigation of Impact of Molecular Weight and Number of Trapped Radicals

The molecular weights of these copolymer materials are a function of the number of radicals successfully trapped in the reactor as well as the amount of monomer available to these radicals. In the experiments described previously, the molecular weights of the products have been several hundred thousand to several million Daltons. The maximum limit of the number (or percentage) of radicals that can be trapped in a given experiment is a critical parameter for this system. The determination of this parameter would provide an estimate of the range of molecular weights available from it. To this end, work was conducted to reduce the molecular weight of the polymers produced by FRRPP by trapping more radicals.

Producing lower molecular weight materials would help in discovering the limits of this process as well as in augmenting the versatility of this method. These materials could then be used in applications not suited for higher molecular weight polymers.

Two approaches were used to try and reduce molecular weight. The first approach was to use more initiator to initiate a larger number of free radicals, which could possibly result in a higher number of trapped radicals. The second approach involved increasing the half-life of the initiator. This would slow down the rate of decomposition and possibly increase the efficiency of the initiator by minimizing primary termination.

The work described here was targeted toward producing lower molecular weight polymers by increasing the half-life of the initiator. This would possibly reduce primary termination by spreading out the initiation step over a longer time. This approach reduced the molecular weight of the final product by a factor of 3.

An estimation of the number of trapped radicals indicated that up to 20% of the radicals produced by the initiator were available for polymerization in the second

stage. Almost 100% of the polymer radicals actually initiated by the initiator were successfully trapped for polymerization with additional monomer.

Lower molecular weight polymer was produced by using a longer initiator half-life. The half-life was increased to 62 min from 28 min by lowering the reaction temperature to 75°C from 80°C. This strategy was used to produce lower molecular weight Polystyrene–*block*–Poly(*n*-butyl acrylate) (PS:PBA, PSPBA-1). This material was synthesized under standard FRRPP conditions with the exception that the reaction temperature was lowered.

Two more experiments were carried out with PS where, once the first-stage charge was polymerized; more styrene was added in the second stage to observe the impact on the kinetics. This was done to see if the slow addition of a reactive good solvent would dissolve the polymer in the reactor and make the trapped radicals more accessible to monomer. The use of styrene as the second monomer made it possible to get a good estimate of the real molecular weights of the polymer radicals using size exclusion chromatography (this is difficult for copolymers). The first experiment was carried out at 80°C (PS-3) and the second one was carried out at 75°C (PS-4) (See Tables 10.2 and 10.3 for experimental details).

The materials used for the reactions are listed in Table 10.4. The experimental conditions for the experiments are listed in Table 10.5. Details and data from two previously discussed experiments (PSPBA-2 for PS:PBA and PSPBA-3 for PS:PBA with initiator slow addition) with the original set of FRRPP conditions are also included for the purpose of comparison.

The conversion data for experiments PSPBA-2, PSPBA-3, and PSPBA-1 are shown in Fig. 10.3. The time is given relative to initiator half-life. The trend lines shown in the figure are not data fits, but are intended to clearly identify the points that belong to the same dataset. There is some error in measurement that leads to the observed variation in conversion (and the conversion apparently greater than 100% in some instances).

The first-stage conversion is close to 100% in all the cases after ether removal. The second-stage monomer (preemulsified with water and surfactant) was added to the reactor well after all the initiator had been exhausted. The steep rise in

Table 10.4 Materials used for each stage of FRRPP

Ingredient	Chemical	Source
Stage 1 (formation and trapping of PS radicals) $T = 75$ or 80°C		
Monomer	Styrene	Aldrich Chemicals
Nonsolvent for PS	Diethyl ether	Fisher chemicals
Initiator	V-50	Wako chemicals
Water	DI water	NSC
Surfactant	IGEPAL CA-897 (octyl phenol ethoxylate, nonionic surfactant)	Rhodia
Stage 2 (addition of second monomer and copolymerization) $T = 60$ or 75°C		
Monomer	*N*-Butyl acrylate	Aldrich chemicals
Surfactant	IGEPAL CA-897	Rhodia
Water	DI water	NSC

Table 10.5 Variation in experimental conditions

Exp.	Experimental details
PSPBA-1	Styrene was the first-stage monomer. $T = 75°C$. $P = 70$ psig (initial). 1% initiator (w/w monomer). Ether removal started after 4 initiator half-lives. *N*-BA (2:1 molar ratio with respect to styrene) loaded after 7.5 initiator half-lives over a period of 2 min. $T = 60°C$, $P = 50$ psig for the second stage
PSPBA-2	Styrene was the first-stage monomer. $T = 80°C$. $P = 70$ psig (initial). 1% initiator (w/w monomer). Ether removal started after 1–2 initiator half-lives. *N*-Butyl acrylate loaded after 12 initiator half-lives. Styrene:*n*-BA ratio used was 1:3. $T = 60°C$, $P = 50$ psig for the second stage
PSPBA-3	Styrene was the first-stage monomer. $T = 80°C$. $P = 70$ psig (initial). 1% initiator (w/w monomer) in reactor initially. 2% initiator (w/w monomer) added to the reactor over 2 initiator half-lives. Ether removal started after 7.5 initiator half-lives. *N*-BA (2:1 molar ratio with respect to styrene) loaded after 15 initiator half-lives over a period of 2 min. $T = 60°C$, $P = 50$ psig for the second stage

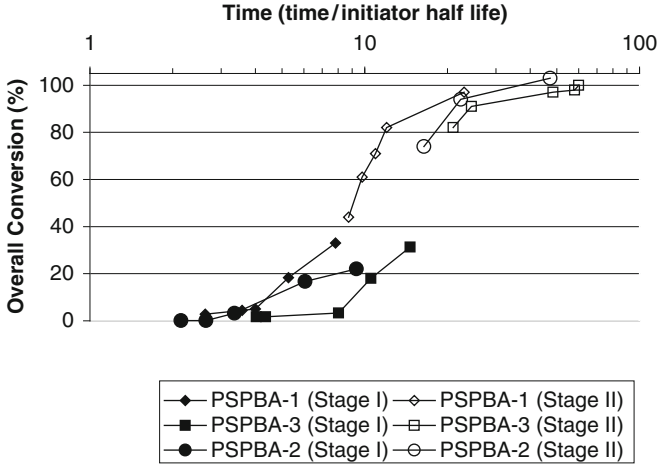

Fig. 10.3 Conversion vs. time data for experiments PSPBA-1, 2, and 3

conversion within a time of about 1–2 h provides strong evidence in favor of a significant population of trapped radicals in the reactor. The final overall conversion is about 100% in all the cases.

The conversion data for the experiments with the slow addition of styrene is shown in Fig. 10.4. These results indicate that the conversion increases somewhat with the addition of styrene. The actual numerical value of the conversion remains almost constant over this period, but if there were no reaction, the value would have decreased due to the addition of material in the reactor. A steep rise in conversion is seen with ether removal. The rise in conversion is coincident with ether removal at both the operating temperatures.

The overall results for these experiments are summarized in Table 10.6. The first-stage molecular weights for both PSPBA-1 and PSPBA-3 show a significant decrease in comparison to PSPBA-2, due to the higher amount of initiator (PSPBA-3) and the higher initiator efficiency in leading to high molecular weight polymer (PSPBA-1). The peak molecular weights as well as the number average molecular weights declined by a factor of 2–3. The PSPBA product had a comparable molecular weight to PSPBA-3, but showed a much narrower molecular weight distribution.

Experiment PS-4 shows lower intermediate and final molecular weights with a higher conversion than PS-3. This indicates a higher percentage of living radicals at the lower temperature. The actual values of molecular weight are higher than PSPBA-1 or PSPBA-3, but those products were copolymers so their molecular weights are based on polystyrene standards and the true molecular weights are likely to be in the same range as PS-3 and PS-4.

These results show that the use of a lower temperature (PSPBA-1, PS-4) does lead to lower molecular weight, possibly due to a higher probability that an initiator

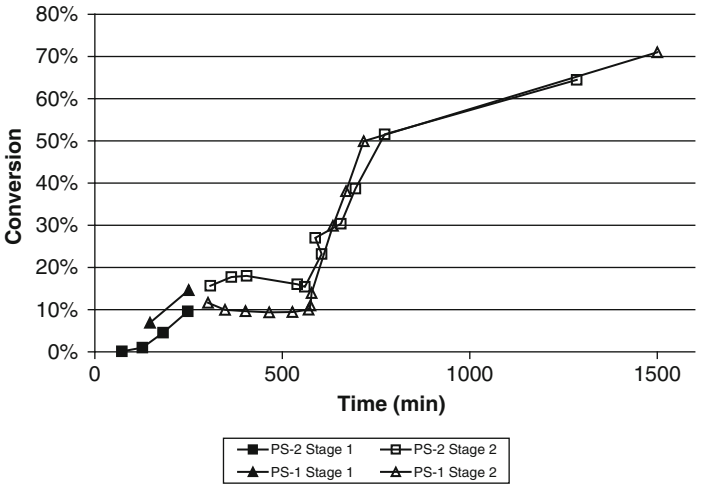

Fig. 10.4 Conversion vs. time for PS-3 and PS-4. Styrene was slow added in both experiments prior to ether removal to observe the impact on the reactor kinetics

Table 10.6 Results summary

Experiment	Monomer (stage I/stage II)	Overall conversion (%)	M_n (Daltons)	PDI[a]
PSPBA-2	Styrene/*n*-BA	100	252,000	4.5
PSPBA-3	Styrene/*n*-BA	100	84,000	11
PSPBA-1	Styrene/*n*-BA	97	101,000	4.7
PS-3	Styrene/Styrene	72	232,000	2.3
PS-4	Styrene/Styrene	80	193,000	2.7

[a]Polydispersity index

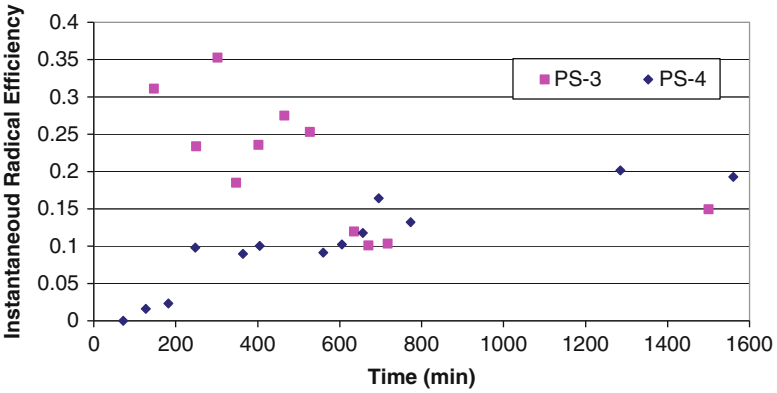

Fig. 10.5 Instantaneous radical efficiency vs. time. Instantaneous radical efficiency is defined as the ratio of the population of radicals estimated at a given time to the maximum available population of radicals at that time. The maximum available population is effectively constant after 5–6 initiator half-lives, which is 150–180 min for PS-3 and 300–360 min for PS-4. The scatter in the data reflects the precision as well as experimental error

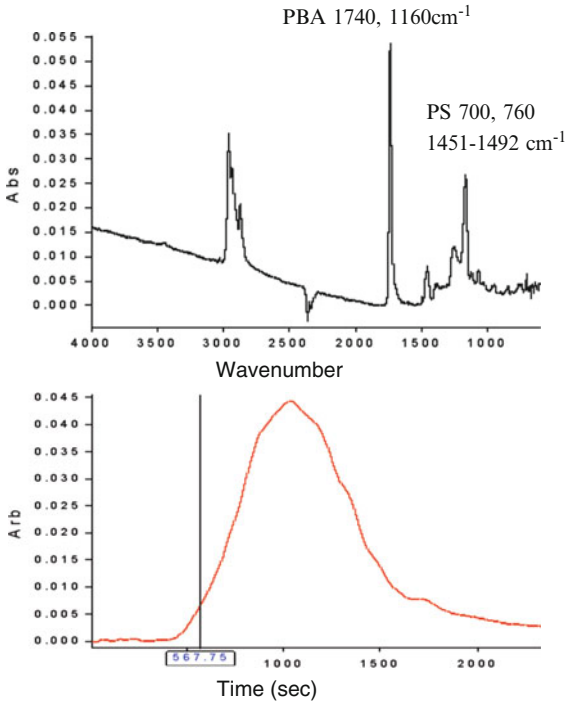

Fig. 10.6 Slice 1 from a PS–PBA GPC-IR chromatogram

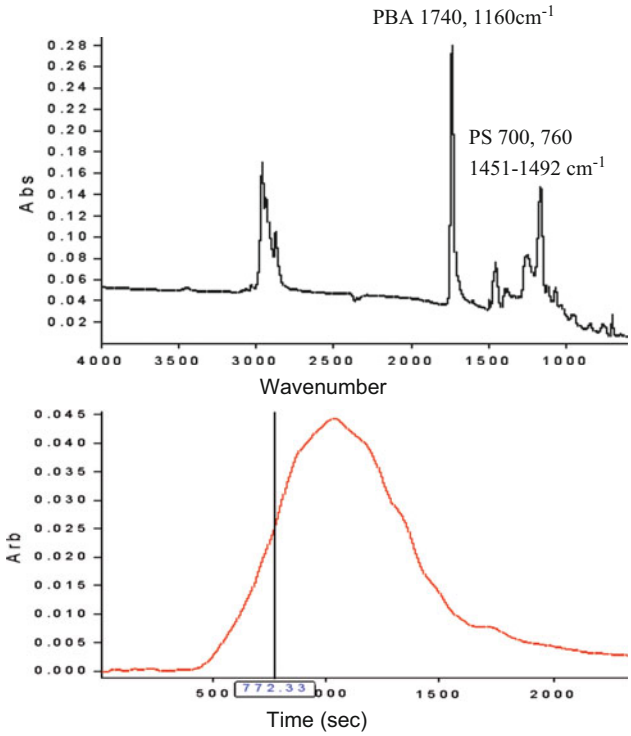

Fig. 10.7 Slice 2 from a PS–PBA GPC-IR chromatogram

molecule will generate a polymer radical due to lower primary termination. The use of a higher concentration of initiator slow added to the reactor also leads to a lower molecular weight. However, the continuous initiator slow add appears to have a negative impact on the population of trapped radicals and may lead to primary termination. This is reflected by higher peak molecular weight values observed in this approach.

The conversion and molecular weight data from experiments PS-3 and PS-4 were used to obtain semiquantitative estimates of the population of trapped radicals in the reactor. An estimate of the percent radicals trapped as opposed to the maximum possible amount generated (assuming an initiator efficiency of 1.0) was also obtained. The results (Fig. 10.5) show that about 10–20% of the maximum possible radicals generated had been trapped in either of these reactions. The radical population is higher initially in experiment PS-3, which is to be expected due to the shorter initiator half-life. However, the ultimate population of trapped radicals appears to be higher in the experiment run at the lower temperature. This is based on the observation that the molecular weights obtained were 20% lower for a conversion that is 10% higher. This observation is supported by the observation of lower molecular weights in experiment PSPBA-1, though a quantitative

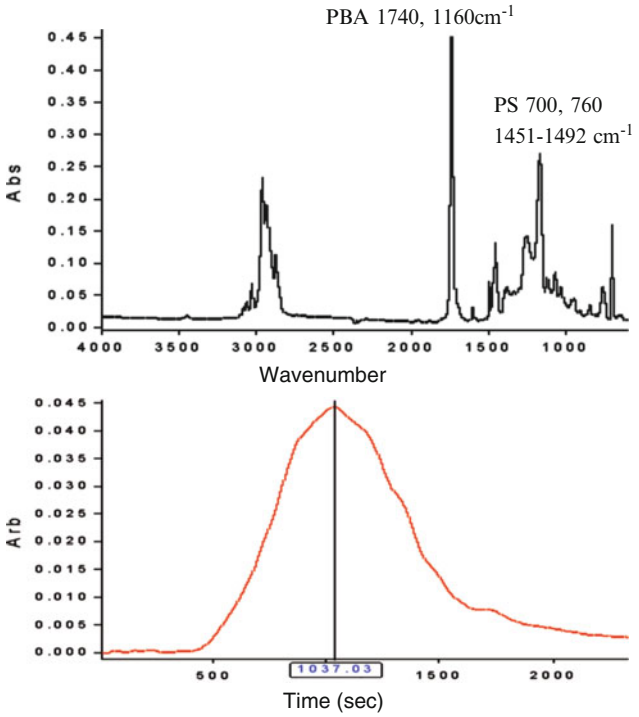

Fig. 10.8 Slice 3 from a PS–PBA GPC-IR chromatogram

correlation is not possible for that experiment as it is a copolymer and the molecular weights are based on polystyrene standards.

The results indicate that there was a significant increase in the number of radicals trapped due to lowering the temperature as well as higher initiator loading, as reflected by a lower molecular weight of the final product. A combination of these factors can be used to trap more radicals and lower the molecular weight of these materials to a few decades of thousands. It was observed that 10–20% of the initiator fragments resulted in trapped radicals. The actual initiation efficiency is higher since the intrinsic initiator efficiency (resulting from the cage effect) is less than 1.

10.1.3 Characterization of Polymer Microstructure and Composition

Some of the results from polymer microstructure and composition analysis are presented here as examples to support the conclusion that the products obtained after stage II were block copolymers.

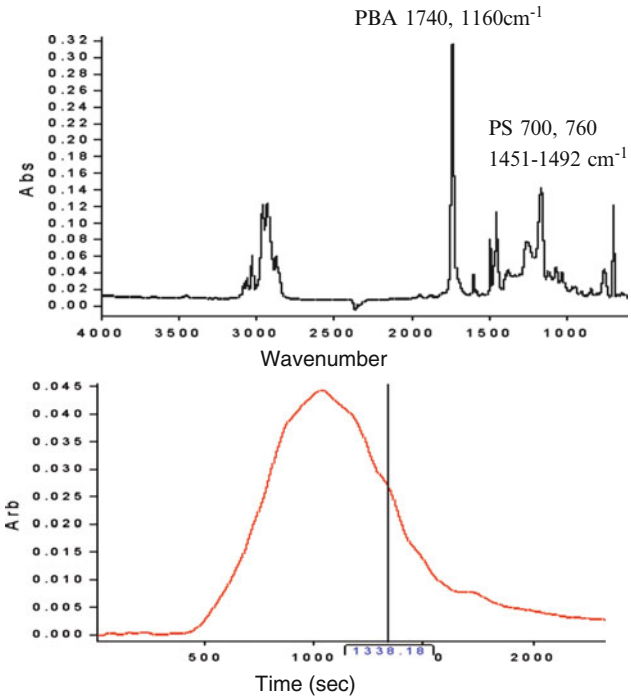

Fig. 10.9 Slice 4 from a PS–PBA GPC-IR chromatogram

10.1.3.1 GPC-IR Analysis

The data generated from GPC-IR analysis is shown in Figs. 10.6–10.10 for an example PS–PBA system. The figures show the composition of the PS and PBA in four different slices of the GPC chromatogram. The presence of similar amounts of PS and PBA in all slices of the chromatogram demonstrates the presence of block copolymers vs. homopolymers of PS and PBA in two different peaks that merged to form one peak.

Each of the series of figures has two charts. The chart at the bottom is the chromatogram for the final product from stage 2 of a PS–PBA reaction and shows a slice from the chromatogram used for IR analysis. The IR spectrum in the top half of the figure shows the relative amounts of PS and PBA present in the reactor. The relative amounts of the PS and PBA can be estimated by looking at the relative intensities of the peaks associated with each polymer as indicated on the chromatogram.

10.1.3.2 Differential Scanning Calorimetry

DSC was used to verify whether the polymer obtained at the end of stage II showed two distinct glass transitions vs. an average of the glass transition temperature of the two monomers. Figure 10.11 shows an example DSC chromatogram for a PS–PBA

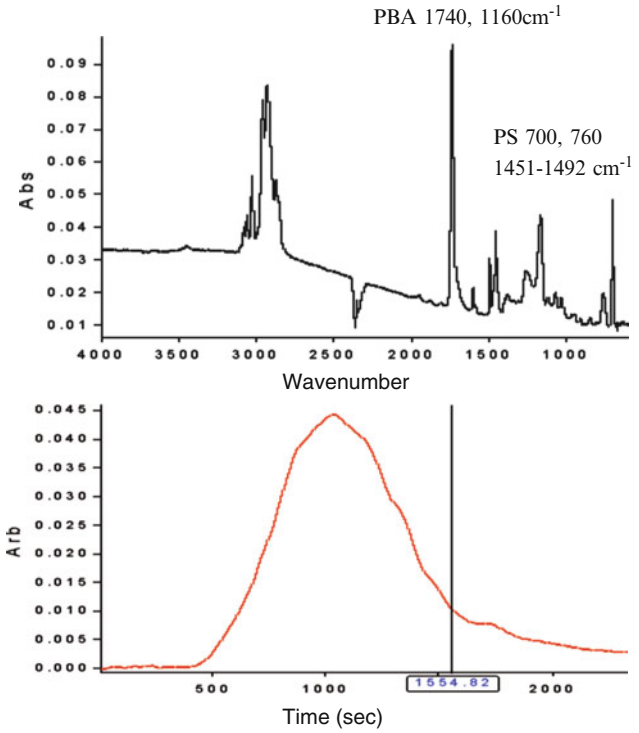

Fig. 10.10 Slice 5 from a PS–PBA GPC-IR chromatogram

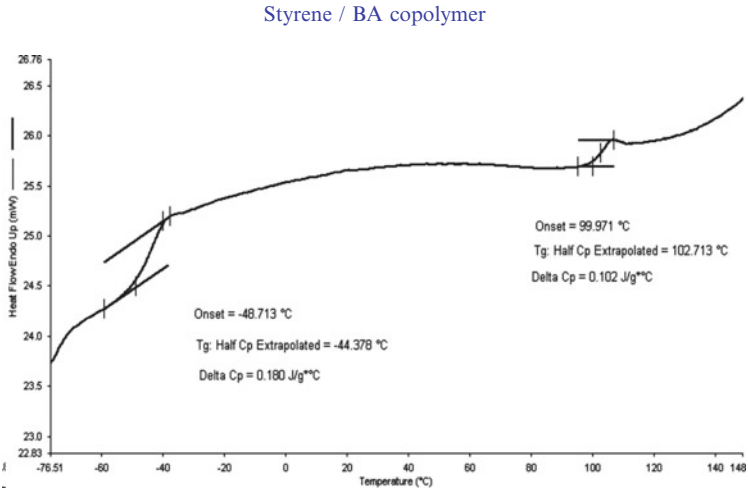

Fig. 10.11 DSC chromatogram showing two different T_gs for the copolymer product consistent with the T_gs of pure polystyrene and pure poly(*n*-BA)

copolymer. The chromatograph shows two distinct T_gs that are consistent with the T_gs of the individual homopolymers.

10.2 PMMA Radical-Containing Emulsions from Monomer Pre-emulsions

The experiments described in Chapter 10.2 used methyl methacrylate (MMA) instead of styrene as the first stage and sometimes additionally as the second stage monomer. The ability of EFRRPP to synthesize PMMA based block copolymers is examined and compared to results in section 10.1 where styrene was used as the first monomer. The impact of initiator loading was also studied. The ability to synthesize controlled architecture polymer emulsions with PMMA as well as polystyrene as the stage I polymer is important because this demonstrates the ability to use different monomer types.

10.2.1 Synthesis of Copolymers with methyl methacrylate as the Stage I Monomer

An experiment (PMMAPBA-2) was conducted with methyl methacrylate as the first-stage monomer and *n*-butyl acrylate as the second-stage monomer to demonstrate the ability of EFRRPP to synthesize block copolymers with first stage monomers other than styrene. Details and results for experiment PSPBA-2, previously described in section 10.1, are also included for comparison. The reagents used are listed in Table 10.7 and the experimental conditions are listed in Table 10.8.

Table 10.7 Materials used for each stage of FRRPP

Ingredient	Chemical	Source
Stage 1 (Formation and trapping of PS/PMMA radicals) $T = 80°C$		
Monomer	Styrene (PSPBA-2)/methyl methacrylate (PMMAPBA-2)	Aldrich Chemicals
Nonsolvent for PS/PMMA	Diethyl ether	Fisher Chemicals
Initiator	V-50	Wako Chemicals
Water	DI water	NSC
Surfactant	IGEPAL CA-897 (octyl phenol ethoxylate, nonionic surfactant)	Rhodia
Stage 2 (addition of second monomer and copolymerization) $T = 60°C$		
Monomer	*N*-Butyl acrylate	Aldrich chemicals
Surfactant	IGEPAL CA-897	Rhodia
Water	DI water	NSC

Table 10.8 Variation in experimental conditions

Experiment	Experimental details
PSPBA-2	Styrene was the first-stage monomer. $T = 80°C$. $P = 70$ psig (initial). 1% initiator (w/w monomer). Ether removal started after 1–2 initiator half-lives. *N*-Butyl acrylate loaded after 12 initiator half-lives. Styrene:*n*-BA ratio used was 1:3. $T = 60°C$, $P = 50$ psig for the second stage
PMMAPBA-2	MMA was the first-stage monomer. $T = 80°C$. $P = 70$ psig (initial). 1% initiator (w/w monomer). Ether removal started after 3–4 initiator half-lives. *N*-Butyl acrylate loaded after 11 initiator half-lives. MMA:*n*-BA ratio used was 1:2.5. $T = 60°C$, $P = 50$ psig for the second stage

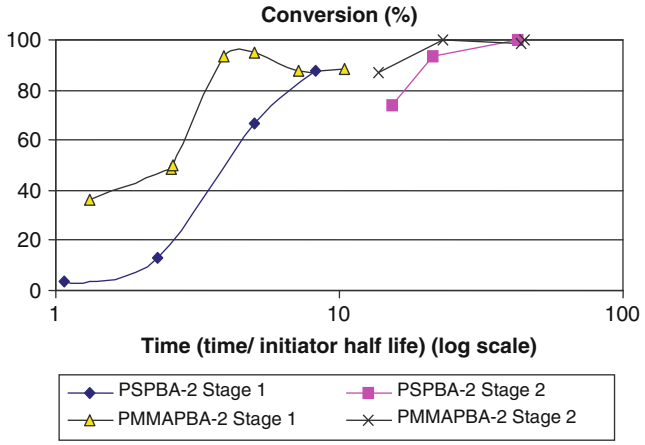

Fig. 10.12 Conversion vs. time data for PSPBA-2 and PMMAPBA-2

The conversion and molecular weight data for these experiments are shown in Figs. 10.12 (conversion data) and 10.13 (molecular weight data). The time is given relative to initiator half-life. The half-life of V-50 at 80°C is 28 min (from product literature). The conversion data in Fig. 10.12 reflect the observations for the earlier experiments. The trend lines shown in the figure are not data fits, but are intended to clearly identify the points that belong to the same dataset. It can be seen that the conversion in both experiments rises with ether removal during the first stage. The initial conversion in the MMA system is much higher than in the corresponding styrene system. This could be due to aqueous phase polymerization of MMA, as MMA is much more water-soluble than styrene is. The final first-stage conversions for both experiments are about 90%. In the case of the MMA reaction, the onset of ether removal was delayed to 3–4 initiator half-lives.

The existence of trapped radicals can be clearly deduced from the second-stage kinetics. The conversions shown in Fig. 10.12 are based on total monomer content. Thus, a 100% conversion in the second stage would have four times the solid content as compared to a 100% conversion in the first stage for PSPBA-2 (styrene: *n*-BA is 1:3). It can be seen that more than 80% of the *n*-BA added to the reactor

is consumed within 2–3 initiator half-lives (60–90 min). Since the *n*-BA was added after 11–12 initiator half-lives, there is no significant amount of initiator in the reactor. Further, there is no evidence of the spontaneous homopolymerization of *n*-BA under the reaction conditions as reported in the literature or in Chapter 11. Thus, the fast reaction of *n*-BA could only have been initiated by trapped polymeric radicals in either case. This observation is further supported by efforts to extract *n*-BA homopolymer as well as size exclusion chromatography (SEC)/gel permeation chromatography (GPC) analysis with ultraviolet (UV)/refractive index (RI) as well as infrared (IR)/refractive index (IR) dual-detection in the case of polystyrene/poly(*n*-BA). All three cases do not indicate any significant amount of *n*-BA homopolymer in the product.

The molecular weight results (Fig. 10.13) follow a trend similar to the conversion results. It can be seen that the molecular weight shows an increase after the addition of *n*-BA. As seen in previous reactions, the molecular weight appears to decrease with the incorporation of increasing amounts of *n*-BA. This is possibly due to smaller radii of gyration for the copolymer molecules as compared to the homopolymers. The data for the MMA run (PMMAPBA-2) have not been presented here as the molecular weight distributions obtained were multimodal due to the presence of some prematurely terminated PMMA homopolymer (estimated to be about 20%).

The overall results for these experiments are summarized in Table 10.9. The polymer compositions were determined using proton NMR. The compositions are close to stoichiometric design in either case. The reaction product was obtained in the form of a stable small particle size emulsion. There was some coagulation evident in the reactor in each case. This can be possibly improved by using a better surfactant package.

Both products were characterized using DSC and TGA. PSPBA-2 product showed the glass transition temperatures for *n*-BA (around −40°C) and styrene (around 90°C). PMMAPBA-2 showed the glass transition temperature for *n*-BA,

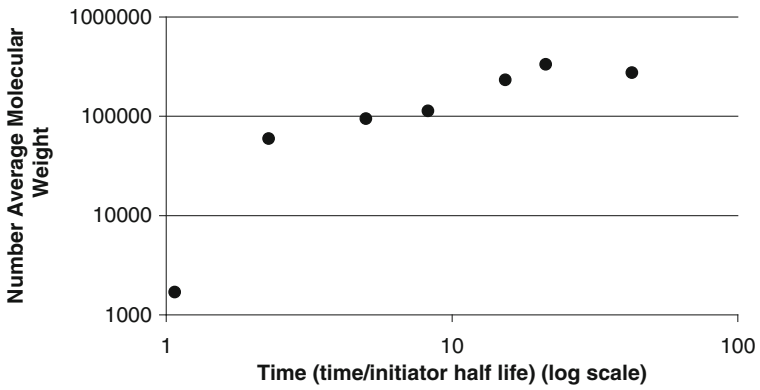

Fig. 10.13 Molecular weight vs. time data for PSPBA-2

Table 10.9 Results summary for reactor products

Experiment	Overall conversion (%)	M_n	Dispersion particle size
PSPBA-2	100	274,830	148 nm
PMMAPBA-2	100	N/A	66 nm

Table 10.10 Results for extraction of *n*-BA-rich segments using *n*-butanol

Experiment	Sample	% Weight fraction	Styrene:*n*-BA ratio (from NMR)
PSPBA-2	Supernatant	78.8	15:85
	Precipitate	21.2	68:32
PMMAPBA-2	A significant amount of material could not be extracted. This could be due to some compatibility of poly(*n*-BA) with PMMA or cross-linking		

and a temperature intermediate to *n*-BA and MMA at about 65°C (T_g for PMMA is about 100°C).

The products were used to cast films on glass slides from solution (5 wt% polymer in THF). The styrene/*n*-BA product forms a white opaque film, whereas the MMA/*n*-BA product forms a clear film with faint cloudiness.

Extraction of n-BA-rich segments: This was done by using *n*-butanol, which is a poor solvent for polystyrene and is only slightly better than a theta solvent for *n*-butyl acrylate. Solid polymer was added to *n*-butanol at a concentration of about 1%. This material was tumble-mixed for at least 72 h. This procedure was a way of effecting a rough precipitation with a butyl acrylate-rich supernatant and a PS or PMMA-rich precipitate. This was done for both experiments.

The results are tabulated in Table 10.10. For PSPBA, the results indicate that both the supernatant and precipitate contained significant amounts of PS as well as PBA. The precipitate was richer in polystyrene segments, whereas the supernatant was richer in poly(*n*-butyl acrylate). The fact that both streams contained substantial amounts of styrene and *n*-butyl acrylate within the polymer chains supports the presence of block copolymers after extraction.

The conversion, size exclusion chromatography, and particle size data obtained for experiments PSPBA-4, PSPBA-5, PSPBA-2, and PMMAPBA-2 were used to calculate the approximate efficiency of initiator in each experiment. It was also used to calculate the approximate number of trapped radicals per emulsion particle. This was done to determine whether the number of trapped radicals was comparable to the number of emulsion particles. A small number of radicals per particle (close to 1) would mean that the isolating effect of emulsion particles could play a role comparable to the effect of precipitation in isolating radicals from each other. A large number of radicals per particle would indicate that occlusion by precipitation is the more significant factor in controlling polymerization in FRRPP. The results for these calculations are shown in Table 10.11.

The data indicate that that there are around 1,000 radicals per emulsion particle. This is comparable to the number of high molecular weight molecules in each particle and is only slightly less than the total number of molecules in each particle. The trapping efficiency is quite low and reflects the fraction of total initiator in the

Table 10.11 Calculations for radical trapping efficiency and number of trapped radicals per emulsion particle

Experiment	Emulsion particle size (nm)	Number of radicals/Particle	Trapping efficiency (%)
PSPBA-4	163	1,030	3
PSPBA-5	122	817	5
PSPBA-2	148	1,930	9
PMMAPBA-2	66	859	3

reaction that results in the formation of high molecular weight trapped radicals. If the inherent initiator efficiency for the process were about 20%, the fraction of molecules initiated which could be trapped and grown to high molecular weight could be more than 50%.

It should be noted that the data obtained are approximate due to the large amount of uncertainty and error associated with the average numbers for molecular weight, particle size, and fraction of living vs. dead radicals used. However, the results should be accurate within an order of magnitude, i.e., the number of radicals per particle can range from several hundred to several thousand, and the trapping efficiency could be off by about 25–50%. An exact estimate of the error is not possible due to the same reasons responsible for the approximate nature of the data.

The results from this set of experiments provide strong insight into the potential of EFRRPP. They show that FRRPP can be used to make not only polystyrene/*n*-butyl acrylate block copolymers, but also methyl methacrylate/*n*-butyl acrylate block copolymers. The block size ratio of these materials is very close to stoichiometric design. There is some polydispersity observed, both in molecular weight and in block size. One of the reasons for this can be seen from the kinetic data. Once the *n*-BA is added to the reactor, it reacts very quickly. Flooding of emulsion particles with the second monomer can lead to conventional free radical kinetics as well as quick termination of any previously trapped radicals. This could be avoided by adding the *n*-BA (or another second-stage monomer) slowly to the reactor. A nonsolvent (like ether) could also be added to moderate the kinetics.

The reaction products are in the form of a stable small particle size emulsion (50–200 nm particle size). There does not seem to be any significant amount of *n*-BA homopolymer in either the styrene or the MMA reaction systems. There does not seem to be any significant polystyrene homopolymer in the styrene system, but there appears to be some low and intermediate molecular weight MMA homopolymer in the MMA experiment. This contamination could be further reduced by process optimization including the use of lower temperatures.

The calculations to determine the number of trapped radicals per emulsion particle indicate that the ratio is significantly greater than 1. This means that occlusion via precipitation plays a much more important role in trapping radicals than the isolating influence of the particles themselves. However, it has been previously noted that the formation of a stable/small particle size dispersion is critical to the further growth of any trapped radicals. This could be due to the

favorable impact of small particle size on polymerization kinetics through heat and mass transport.

10.2.2 Examination of Other Parameters with methyl methacrylate as the Stage I Monomer

Higher initiator loading was used to reduce the molecular weight in two experiments to make Polystyrene–*block*–Poly(*n*-butyl acrylate) (PS:PBA, PSPBA-3) and Poly (methyl methacrylate)–*block*–Poly(*n*-butyl acrylate) (PMMA:PBA, PMMAPBA-1). These materials were synthesized under standard FRRPP conditions with the exception that three times the amount of initiator was loaded into the reactor. To maximize the impact of the additional initiator, the initial initiator charge was kept the same as earlier (1% initiator w/w monomer). An additional 2% initiator (w/w monomer) was loaded into the reactor in aqueous solution over the next 1–2 h (2–4 initiator half-lives). This was done to reduce primary termination. The materials used for the reactions are listed in Table 10.12. The experimental conditions for the experiments are listed in Table 10.13. Details and data from two other experiments (PSPBA-2 and PMMAPBA-2) are also included for the purpose of comparison. These experiments are similar to the ones described in this section but did not have the additional initiator loading.

The conversion data for these experiments are shown in Fig. 10.14. The time is given relative to initiator half-life. The half-life of V-50 at 80°C is 28 min (from product literature). The trend lines shown in the figure are not data fits, but are intended to clearly identify the points that belong to the same dataset. There is some error in measurement that leads to the observed variation in conversion (and the conversion apparently greater than 100% in some instances).

The first-stage conversion is close to 100% in all the cases after ether removal. This corresponds to an overall conversion of about 25% for PSPBA-2 and 33% for PMMAPBA-2, PSPBA-3, and PMMAPBA-1. The second-stage monomer

Table 10.12 Materials used for each stage of FRRPP

Ingredient	Chemical	Source
Stage 1 (Formation and trapping of PMMA radicals) $T = 80°C$		
Monomer	Methyl Methacrylate/Styrene	Aldrich Chemicals
Nonsolvent for PMMA/PS	Diethyl ether	Fisher Chemicals
Initiator	V-50	Wako Chemicals
Water	DI water	NSC
Surfactant	IGEPAL CA-897 (octyl phenol ethoxylate, nonionic surfactant)	Rhodia
Stage 2 (addition of second monomer and copolymerization) $T = 60°C$		
Monomer	*N*-Butyl acrylate	Aldrich Chemicals
Surfactant	IGEPAL CA-897	Rhodia
Water	DI water	NSC

Table 10.13 Variation in experimental conditions for (Styrene/MMA) and *n*-BA copolymerization

Experiment	Experimental details
PSPBA-2	Styrene was the first-stage monomer. $T = 80°C$. $P = 70$ psig (initial). 1% initiator (w/w monomer). Ether removal started after 1–2 initiator half-lives. *N*-Butyl acrylate loaded after 12 initiator half-lives. Styrene:*n*-BA ratio used was 1:3. $T = 60°C$, $P = 50$ psig for the second stage
PMMAPBA-2	MMA was the first-stage monomer. $T = 80°C$. $P = 70$ psig (initial). 1% initiator (w/w monomer). Ether removal started after 3–4 initiator half-lives. *N*-Butyl acrylate loaded after 11 initiator half-lives. MMA:*n*-BA ratio used was 1:2. $T = 60°C$, $P = 50$ psig for the second stage
PSPBA-3	Styrene was the first-stage monomer. $T = 80°C$. $P = 70$ psig (initial). 1% initiator (w/w monomer) in reactor initially. 2% initiator (w/w monomer) added to the reactor over 2 initiator half-lives. Ether removal started after 7.5 initiator half-lives. *N*-BA (2:1 molar ratio with respect to MMA) loaded after 15 initiator half-lives over a period of 2 min. $T = 60\ °C$, $P = 50$ psig for the second stage
PMMAPBA-1	MMA was the first-stage monomer. $T = 80°C$. $P = 70$ psig (initial). 1% initiator (w/w monomer). 2% initiator (w/w monomer) added to the reactor over 4 initiator half-lives. Ether removal started after 6 initiator half-lives. *N*-BA (2:1 molar ratio with respect to MMA) loaded after 13 initiator half-lives over a period of 2 min. $T = 60°C$, $P = 60$ psig for the second stage

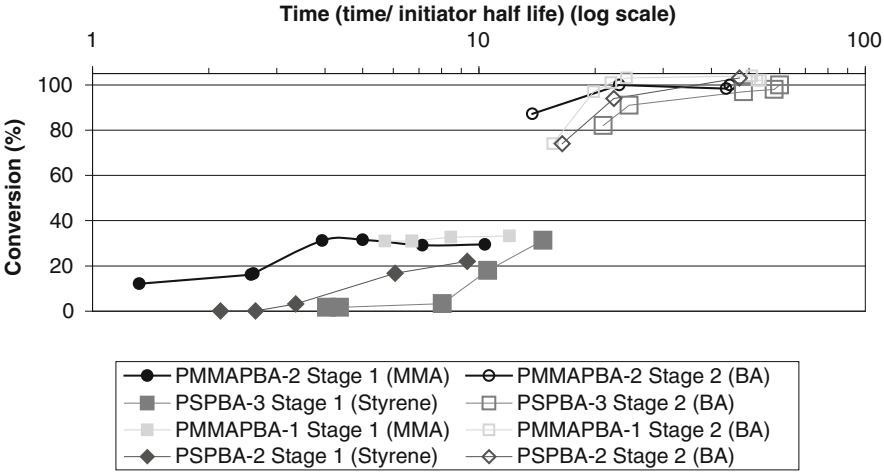

Fig. 10.14 Conversion vs. time data for experiments PSPBA-2, PMMAPBA-1, PSPBA-3, and PMMAPBA-2. The *n*-BA was added in one shot for all the experiments. Initiator slow addition was used only in PSPBA-3 and PMMAPBA-1

(preemulsified with water and surfactant) was added to the reactor well after all the initiator had been exhausted. The steep rise in conversion within a time of about 1–2 h provides strong evidence in favor of a significant population of trapped radicals in the reactor. The final overall conversion is about 100% in all the cases.

Table 10.14 Results summary for (Styrene/MMA):*n*-BA reactor products

Experiment	Monomer	Overall conversion (%)	M_n (Daltons)	PDI[a]
PSPBA-2	Styrene	100	252,117	4.5
PMMAPBA-2	MMA	100	250,000[b]	–
PSPBA-3	Styrene	100	83,835	11
PMMAPBA-1	MMA	100	195,730[b]	–

[a]Polydispersity Index
[b]Peak molecular weight

The overall results for these experiments are summarized in Table 10.14. The peak molecular weight listed is for the most significant mode in the product molecular weight distribution. This corresponds to the high molecular weight peak resulting from monomer addition to surviving radicals.

The first-stage molecular weights for both PSPBA-3 and PMMAPBA-1 show a significant decrease in comparison to PSPBA-2 and PMMAPBA-2, respectively, due to the higher amount of initiator. The molecular weight distribution in experiment PSPBA-3 showed a significant shoulder on the low molecular weight side that leads to the much higher polydispersity in the first as well as second stages. The final product does not show any signs of homopolymer contamination upon visual inspection. The composition of the copolymers was determined by extraction with *n*-butanol, as described in Section 10.2.1. The results were consistent with the analysis of the earlier products- there was no evidence of significant amounts of extracted *n*-BA homopolymer. It is conceivable that the shoulder contained trapped radicals as well, which reacted with the new monomer. This is because the molecular weight distribution is preserved after the addition of the butyl acrylate. The presence of lower molecular weight material brings the overall molecular weight down significantly as compared to PSPBA-2. The MMA system showed a similar trend, but with the presence of a distinct PMMA homopolymer peak.

Due to the wide polymer distributions obtained and the continuous (and somewhat approximate) nature of SEC data, it is not possible to derive an exact quantitative result of the population of trapped radicals. However, a qualitative result can be obtained based on the molecular weight numbers. In previous systems, about 5–10% of the initiator used successfully initiated polymer radicals. Of these radicals, almost 100% were successfully trapped into the second stage for the polystyrene system. Only about 50–70% were successfully trapped for the MMA system.

A good metric for improvement would be to observe an increase in the number of radicals initiated while keeping the overall efficiency of trapping them at least as high as it is currently. In the current dataset, the use of higher initiator loading dropped the average molecular weight for the PS or PMMA first-stage product. This factor was preserved (qualitatively) in the final product as well. This would mean that the number of radicals generated and successfully trapped in the first stage is higher than in the earlier reactions. However, the polydispersity of the distribution widened considerably (from 4 to 11). This indicates that though there were more radicals generated, a significant fraction were unable to grow to higher molecular weight in

the first as well as the second stage. The data in the MMA system are more difficult to analyze due to the heterogeneity of the distribution. However, the SEC chromatograms show a similar trend.

The results indicate that there was a significant increase in the number of radicals trapped due to the higher initiator loading, as reflected by a lower molecular weight of the final product. This increase was accompanied by a broadening of the molecular weight distribution that suggests a decrease in the efficiency of trapping for these radicals. All experiments showed high stage I and stage II conversions indicating a large number of radical generating species had reached stage II and participated in copolymer synthesis.

References

Caneba GT, Dar YL (2002) Free-radical retrograde precipitation copolymers and process for making the same. Submitted to the U.S. Patent and Trademark Office, January, Publication 2003/0153708

Caneba GT, Zhao Y, Dar YL (2002) ACS PMSE Preprints 88:436

Dar YL, Caneba GT (2001) FRRPP project report. Michigan Technological University, Houghton, MI

Dar YL, Xiao C, Schlom P (2003) Free radical retrograde precipitation polymer dispersions. PCT Application 2003059960

Chapter 11
Control Experiments to Test Autopolymerization of styrene and *n*-butyl acrylate

It is important to rule out the possibility that stage II monomers can homopolymerize under the reaction conditions to somehow lead to the effect observed in the experiments in Chap. 10. The presence of significant levels of homopolymerization could also lead to the possibility of chain transfer and radical initiation on the polymer backbone, which could still lead to potentially similar effects as would be produced by trapped polymer radicals.

In order to test the role of autopolymerization of the monomers on stage I and II conversion, styrene, MMA, and *n*-BA were heated for 4 h at 60°C as well as 80°C in the presence of surfactant and water. Inhibitor had been removed from the monomers prior to addition to ensure that any autopolymerization was detected. Samples were taken from the reaction at intermediate time intervals as well as at the end of the time at temperature.

No significant conversion was detected in any of the samples. This indicates that first and second stage monomer conversion is not because of any significant autopolymerization of the monomers at the reaction conditions used. It supports the presence of an alternate initiation source in the emulsion particles, which is most likely due to trapped polymer radicals.

Two further experiments were conducted that simulated the entire modified EFRRPP process by essentially following the whole process without the use of any free radical initiator. One experiment used methyl methacrylate as the first stage monomer while the other used styrene as the first stage monomer. Both experiments used *n*-butyl acrylate as the second stage monomer. The aim of these two experiments was to test whether any extraneous effects, such as the removal of the nonaqueous solvent, could potentially introduce free radical species into the system that would lead to the observed increase in conversion and molecular weight. There was no well-understood mechanism for this to take place but the experiments were conducted to test for any effects that might have been overlooked.

The results did not demonstrate any significant levels of conversion in either the first or the second stage of polymerization. This further supported the conclusion that autopolymerization did not play a significant role in the increase in conversion and molecular weight described in Chap. 10.

G. Caneba and Y. Dar, *Emulsion-based Free-Radical Retrograde-Precipitation Polymerization*, DOI 10.1007/978-3-642-19872-4_11,

Chapter 12
Summary

Based on all the experimental data and theoretical observations provided in Chaps. 7–11, the EFRRPP process allows the user to synthesize controlled architecture polymers. This is supported by observations made based on reactions kinetics data, as well as analytical techniques. This was demonstrated for Polystyrene as well as Poly (methyl methacrylate) polymers.

This allows practitioners to combine the benefits of free radical polymerization and emulsion polymerization while providing controlled architecture polymers such as block copolymers. Free radical polymerization has previously been used to synthesize controlled architecture polymers. The discussion below provides a comparison to some of the approaches that have been used and their relative features and benefits and has been adapted from Dar et al. (2005).

Free radical polymerization is a statistical process with several possible reactions that can take place at the same time and the likelihood of each reaction being determined by its kinetic rate coefficient. A lot of effort has been directed towards controlling the statistical nature of this process over the last two decades (Matyjaszewski 2003).

This includes several approaches that have been proposed to reduce the probability of termination by adding reversible termination agents, highly efficient chain transfer agents, or by reducing the diffusional mobility of polymers in poor solvents. The processes developed in recent years can be used to control polymer microstructure and composition with high yield, efficiency, and specificity. The ability to do this has led to a variety of novel materials, properties, and applications.

CFRP has been used successfully to produce block, graft, and other controlled architecture copolymers within the last decade for a variety of free radically polymerizable monomers. The main techniques include reversible addition fragmentation and transfer (RAFT) polymerization, stable free radical polymerization (SFRP) mediated by nitroxide/alkoxyamine-based radicals, atom transfer radical polymerization (ATRP), di-phenyl ethylene (DPE)-mediated polymerization, and novel precipitation/emulsion polymerization-based methods like free radical retrograde precipitation polymerization (FRRPP) (Dar and Caneba 2002).

G. Caneba and Y. Dar, *Emulsion-based Free-Radical Retrograde-Precipitation Polymerization*, DOI 10.1007/978-3-642-19872-4_12,

Nitroxide-mediated SFRP, diphenyl ethylene-mediated polymerization, ATRP, RAFT, etc., achieve polymerization control through the use of kinetic mediators or transfer agents, which protect a propagating free radical from undesirable transfer and termination reactions. The emulsion block copolymer method is unique in that it does not require the use of any chemical mediators to achieve this control. The proposed mechanism of polymerization control is physically trapping radicals by precipitation. This minimizes the reaction of the radicals with each other by severely restricting their mobility in the reaction medium.

The ability of these methods in delivering block copolymer structures has been well demonstrated. ATRP, RAFT, and SFRP could all be used to make diblock and triblock copolymers, as well as radial polymers using multiarm initiators. Since these methods are based on free radical polymerization, they give access to a wider variety of monomer systems than currently available through nonfree radical polymerization-based techniques. They can also lead to controlled polymerization under more industrially practicable conditions as compared to ionic polymerization.

Table 12.1 provides a summary of the different technology options available.

The unique feature and benefit of FRRPP is that it does not need a chemical mediator to control polymerization. This makes the process more affordable and allows it to be used for several different types of monomers.

Some of the key factors that influence the ability to trap radicals and sustain their activity over a lengthy period of time have been proposed to be:

1. Radical trapping due to precipitation above the lower critical solution temperature in a monomer/nonsolvent/polymer system.
2. Persistence of radicals in an aqueous emulsion due to a combination of several physical effects related to small particle size that cause the polymer chain to be at dimensions much smaller than at theta conditions, which would be more typical of a polymer melt or a large emulsion particle

   (a) Surface tethering
   (b) Finite free volume
   (c) Greater entanglements
   (d) Potential crosslinking of entire particles while keeping the overall molecular weight at a level that the polymer is still soluble
   (e) Increase of polymer chain length by propagation leading to an increase in theoretical radius of gyration in melt-like conditions with a correspondingly smaller increase in particle size leading to a confinement-like effect

The above factors work independently of each other to enable the trapping and longevity of radicals in the polymer particles.

Based on the observations and theoretical considerations described in Chaps. 7–11, insight can be derived into the overall path a polymer chain evolves through in an EFRRPP reaction. This path is schematically explained in Fig. 12.1.

Table 12.1 Summary of controlled free radical polymerization technology (Dar et al. 2005)

Name	Technology
ATRP	Transition metal mediators
RAFT	Thioesters, thiophosphates, xanthates, and other chain transfer agent mediators
SFRP	Nitroxides/alkoxyamines, functional nitroxides, imidazoline, piperizinones, morpholones and related mediators
DPE	Di-phenyl ethylene mediator
FRRPP	Physical immobilization of free radicals to reinitiate polymerization
Others	Telomerization, macromers by chain transfer, bimetallic chain transfer, electron donors, alkyl iodide mediators

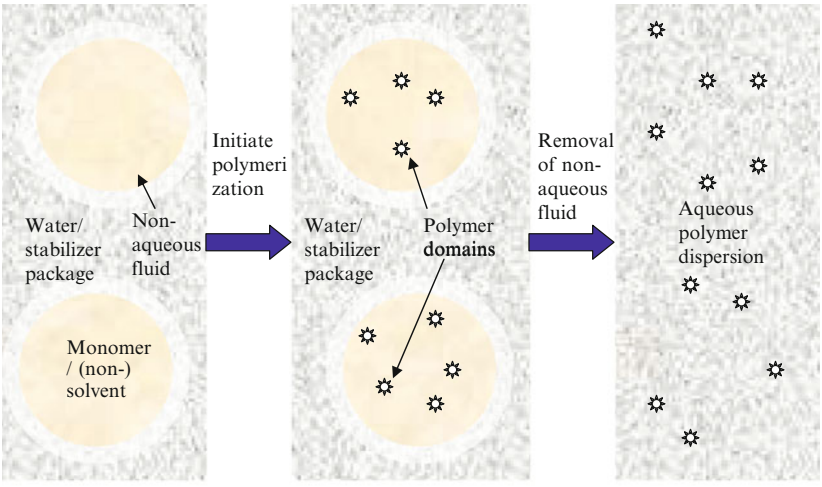

Fig. 12.1 A schematic of the modified EFRRPP process

Polymerization or the stage I monomer can be initiated within the aqueous phase or within the dispersed monomer/nonsolvent particles. The presence of the nonsolvent leads to precipitation of the polymer within the monomer nonsolvent domains. If the polymerization is initiated in the aqueous phase the polymer chain can enter the monomer/nonsolvent domains or the monomer/nonsolvent can be transported to the polymer through the aqueous phase. In either case, due to the significantly lower concentration of monomer as compared to the nonsolvent, and the high mutual solubility of the monomer and the nonsolvent, there should be a substantial amount of nonsolvent at any location where there is a monomer supply.

The precipitated polymer chain will continue to propagate and form polymer globules and eventually small precipitated polymer domains within reservoirs of monomer and nonsolvent. This is allowed to continue until most of the initiator is consumed. At this point, solvent removal is initiated and the transformation of the system from a dispersed FRRPP system to an aqueous polymer dispersion is initiated.

Solvent removal takes place based on the approaches described in Chap. 9 until all but a small amount of the solvent has been collected in a reservoir outside the reactor where it can be processed for recycling. At this point, if the solvent removal was carried out to ensure emulsion stability, the reactor consists essentially of a polymer emulsion. The stage I monomer is typically consumed to close to 100% conversion during this process.

Stage II monomer is pre-emulsified and slowly added to the reactor at this point. No additional initiator is added. The stage II monomer is observed to rapidly convert to high (>80%) conversion. This is most likely a consequence of the trapped polymer radicals present in the polymer domains that act to initiate copolymerization. The final product could potentially be used for additional polymerization stages (though this has not been thoroughly explored yet) or finished up for utilization in application.

An index to characterize the state of the polymer chains has been defined and used to understand the level of confinement that the chains experience. This index, called the confinement index (CI), is consistently less than 1 for the polymer produced in stage II based on the particle size of the emulsion and molecular weight of the polymer chains. A CI that is well below 1 would characterize chains that have very limited physical mobility and thus can lead to trapped polymer radicals.

The final steps for polymerization include adding a final initiator charge to consume the small amount of residual monomer remaining in the reactor and to pass the polymer emulsion through a filtration system to remove any coagulum or precipitate. The resulting polymer emulsion can be used as obtained for formulation in coatings, waterborne adhesives, or other such applications. An example is described in (Caneba and Wang 2001). It can also be dried for use as a solid block copolymer product.

The product obtained has the physical appearance and properties of a block copolymer of the stage I and stage II monomers. This has been verified by studying the molecular weight and distribution, the observation of two glass transition

temperatures, the physical properties, GPC-IR analysis, as well as by Soxhlet extraction and follow-up compositional analysis.

Several factors have been investigated during the development of EFRRPP to optimize the process and gain some understanding of the underlying mechanisms that drive a successful outcome. The use of different types of initiation, the impact of temperature, and pressure has been investigated and are relatively well understood. The solvent removal process has also been tested to determine the impact of speed of solvent removal and the impact of the different steps on the stability of the emulsion and the activity in stage II.

All the key factors needed for emulsion stability have been thoroughly investigated. This includes the use of different types of surfactant packages and the optimization of the type and amount of each surfactant in the mix. The impact of agitation including the mixing configuration, mixing speed, and overall volume of liquid in the reactor have also been tested and optimized to obtain emulsion stability, minimize coagulum, and eliminate foam formation. Foaming in the reactor is not desirable and can in turn lead to instability and coagulum.

Data has been presented with two stage I monomers – styrene and methyl methacrylate. These were chosen as they are well-understood monomers and have been studied widely in free radical polymerization systems. Stage II monomers used included styrene, methyl methacrylate, and *n*-butyl acrylate. In several cases, the same monomer that was used in stage I was also used in stage II as it allowed for semiquantitative conclusions based on kinetic data including conversion and molecular weight.

The level and impact of initiator was investigated as a way to influence the molecular weight of the stage I polymer. It was determined that lesser initiator led to higher molecular weight stage I polymer, as would be typically expected in a standard free radical polymerization system. Increasing the half life of the initiator by lowering reaction temperature or slow adding the initiator over stage I as opposed to adding all of it as an initial charge, both led to lower stage I molecular weights. This was possibly due to higher initiator efficiencies and lesser primary termination due to a lower radical flux. The stage I initiator had minimal impact on the molecular weight of the stage II polymer. The only factor that would have serious impact on stage II molecular weight would be the amount of stage II monomer used and the number of surviving initiating radicals from stage I.

The use of a seed polymer latex was also tested to see if it would impact the particle size distribution and the stability of the stage I and stage II emulsions. The results indicate that use of a seed polymer latex does have a small impact but this is not a critical factor in influencing the particle size or stability.

The number of trapped radicals was estimated through the definition of two parameters called a trapping efficiency (TE) as well as an instantaneous trapping efficiency (ITE). The ITE can be interpreted as the fraction of radicals trapped versus those that initiate polymerization whereas the TE is the fraction of radicals trapped versus the maximum number of radicals that could have been generated if the initiator efficiency was 100%. Instantaneous trapping efficiencies were of the order of 10–30% of the radicals generated whereas overall TEs, which take the

initiator efficiency into account, were estimated to be typically between 1 and 5%. In order to ensure that these could be calculated with some degree of accuracy, experiments were conducted with polystyrene as the first stage as well as the second stage polymer. This ensured that measurement of the degree of polymerization were accurate since they were based on polystyrene standards, and were consistent across the two stages. The number of trapped radicals per emulsion particle was also estimated and appeared to be a significantly high number of close to 1,000 radicals/particle. Due to the possibility of error in the parameters that were used to calculate this number, the actual number may have significant error associated with it but this error would be limited at most to one order of magnitude i.e. to ~100 to ~10,000 radicals per particle range. This is well above a single radical per particle, which indicates that significant residual initiation activity in each particle leads to the rapid and high second stage conversion in the experiments described in Chap. 10.

Other factors such as the ratio of nonsolvent to monomer were also tested and the impact was consistent with that of typical free radical processes. Additional factors have been tested separately and have been reported by Caneba in the first FRRPP monograph.

The investigation of the Emulsion FRRPP process presented here has been conducted with a view to developing an industrially practicable process that can deliver block copolymers in aqueous dispersion. There are a lot of additional opportunities to understand the mechanism and the effects that direct and influence this process. The impact of different parameters on the confinement of polymer chains, the influence of system parameters on the stability and population of trapped radicals, as well as the use of different monomer systems to develop polymer with different compositions and architectures are all areas that can be topics of future research and development.

References

Caneba GT, Wang B (2001) Low VOC latex paints from a precipitation polymerization process. Clean Prod Process 3:55

Dar YL, Caneba GT (2002) Transport phenomena aspects of the free-radical retrograde-precipitation polymerization (FRRPP) process. Chem Eng Commun 189:751

Dar YL, Farwaha R, Caneba GT (2005) Free radical polymerization. In: Lee SM (ed) Encyclopedia of chemical processing. Dekker, New York, pp 1057–1068

Matyjaszewski K (2003) Advances in controlled/living radical polymerization. ACS Symposium Series 854. American Chemical Society, Washington DC

Part III
Supplementary Topics

Without freedom of thought,
there can be no such thing as wisdom
Benjamin Franklin

This portion of the monograph pertains to additional FRRPP topics wherein emulsions were formed during the polymerization process, or applications using emulsions from FRRPP-based products.

Chapter 13
Cloudpoint Studies of PMMA–MMA–*n*-Pentane Systems

13.1 Cloudpoint Experiments

An attempt was made to determine the existence of LCST behavior for the PMMA–MMA–*n*-Pentane binary system at a reasonable temperature. For the cloudpoint studies, primary standard PMMA (HI $<$ 1.1) was purchased from Pressure Chemical Corp. (Pittsburgh, PA), with a molecular weight of 6,500 g/mol. As-received MMA was used in the determination of cloudpoint. The same apparatus was used in this study, as the one used for cloudpoint experiments in Sect. 1.1 of Caneba (2010). A constant proportion of PMMA relative to MMA of 52.4 g/g was used. The proportion of *n*-Pentane relative to MMA+PMMA was varied, by adding certain amounts of *n*-Pentane to aliquots of the PMMA–MMA mixture. The inverse- temperature cloudpoint was obtained by slowly raising the PMMA–MMA–*n*-Pentane temperature until the solution became turbid. The exact cloudpoint temperature was obtained at the onset of cloudiness. Thus, Table 13.1 shows cloudpoint temperature values of starting PMMA–MMA–*n*-Pentane mixtures used. It should be noted that at 28 wt% MMA, the system did not exhibit a clear LCST-based cloudpoint temperature, because the fluid was always turbid from room temperature up to 110°C. This supports the contention that an hourglass-shaped phase envelope was obtained from the PMMA–*n*-Pentane system.

After attainment of turbid mixtures, the temperature was allowed to go down slowly in order to observe when the fluid became clear again. This was rarely observed, until the point was reached close to room temperature when polymer deposited on the inner walls of the containers. This means that the system at least exhibited an hourglass phase envelope.

Taking only the results in Table 13.1, it is evident that PMMA–MMA–*n*-Pentane mixtures will exhibit reasonable retrograde precipitation temperatures, although they seem to be above 80°C. Still, additional observations indicate the occurrence of an hourglass phase envelope for this system.

G. Caneba and Y. Dar, *Emulsion-based Free-Radical Retrograde-Precipitation Polymerization*, DOI 10.1007/978-3-642-19872-4_13,

Table 13.1 Cloudpoint temperatures above the LSCT for PMMA–MMA–Pentane mixtures at MMA/PMMA of 52.4 g/g

Wt% MMA			
35 ± 1	40 ± 1	53 ± 1	72 ± 1
104 ± 1	107 ± 1°C	157 ± 1°C	176 ± 1°C

13.2 Interpretation of Cloudpoint Results

By virtue of the existence of an hourglass phase envelope in the PMMA–*n*-Pentane system, there is the possibility of some FRRPP-based reaction propagation control in the PMMA–MMA–*n*-Pentane system. Even if the true LCST is at a higher temperature than the reactor operating temperature, unsteady-state simulations shown in Chap. 5 indicate that reaction domains can attain uniform higher temperatures than the bulk fluid at relatively low monomer conversions. Moreover, the pathway to uniform higher temperature via hourglass phase envelopes has been discussed in Chap. 3.

The effect of the phase separation of the MMA–*n*-Pentane mixture as the temperature increases can enhance FRRPP-like behavior from the hourglass PMMA–*n*-Pentane phase behavior. This is especially true if emulsion polymerization is used with a surfactant that interacts more with *n*-Pentane compared to the MMA. This was indeed obtained with an aliphatic hydrocarbon hydrophobic portion of the surfactant used, such as Sodium Lauryl Sulfate or SLS (also called Sodium Dodecyl Sulfate or SDS). In order to explain the likely mechanism for emulsion polymerization with above-LCST behavior for the MMA–*n*-Pentane mixture, we would refer to the analysis of ideal emulsion polymerization in Sect. 6.1.

Even before the start of polymerization when a stream of MMA and *n*-Pentane was prepared as preemulsion, the use of SLS would have resulted in emulsions wherein *n*-Pentane molecules were adjacent to hydrophobic groups on the inside surfaces of the micelles. Then, the *n*-Pentane would have had to be completely covering the MMA molecules inside the micelles. We are also presuming that when initiator molecules decompose into radicals, they either absorb MMA/*n*-Pentane in them or they enter micelles with MMA/*n*-Pentane already present in them. In the latter case, inner micelle surfaces that are coated with *n*-Pentane would not allow entering radicals to propagate uncontrollably via conventional kinetics and easily terminate with others that are already in the vicinity. The reason is that entering radicals would phase separate when exposed to *n*-Pentane-rich environment. On the other hand, if the inside surfaces of the micelles are coated with MMA molecules through polar hydrophobic surfactant tails, entering polymer radicals would tend to propagate and terminate via conventional kinetics before FRRPP mechanism can take place in the interior of the micelles.

Reference

Caneba GT (2010) Free-radical retrograde-precipitation polymerization (FRRPP): Novel concept, processes, materials, and energy aspects. Springer, Heidelberg. ISBN 978-3-642-03024-6

Chapter 14
PMMA–PBA from Emulsion from PMMA–MMA–*n*-Pentane Systems

14.1 Single-Stage Semi-Batch Formation of PMMA

This section describes the FRRPP-based emulsion method used to generate PMMA radicals in the first-stage semi-batch reactor system.

14.1.1 Recipe and Apparatus

All monomers were passed through inhibitor removal columns, and all fluids were bubbled with nitrogen gas for at least 15 min. The following mixtures were prepared and called Stream numbers.

Stream 1.
Sodium Lauryl Sulfate (SLS) Surfactant, in powder form – 0.75 g
Distilled Water – 100 ml
Stream 2.
Methyl Methacrylate (MMA) Monomer – 10 ml
n-Pentane – 40 ml
Stream 3.
Distilled Water – 75 ml
V-50 Initiator – 0.2 g

The reactor system (Fig. 14.1) is similar to the one used in earlier works, such as the one shown in Fig. 2.3.4 of Caneba (2010).

14.1.2 Procedure

First, the reactor system was purged with Nitrogen gas in order to displace Oxygen from the air; afterwards, 20 psig of Nitrogen gas was left in the reactor. Stream 1 was loaded into the reactor and the reactor temperature was raised to 80°C. Then,

G. Caneba and Y. Dar, *Emulsion-based Free-Radical Retrograde-Precipitation Polymerization*, DOI 10.1007/978-3-642-19872-4_14,

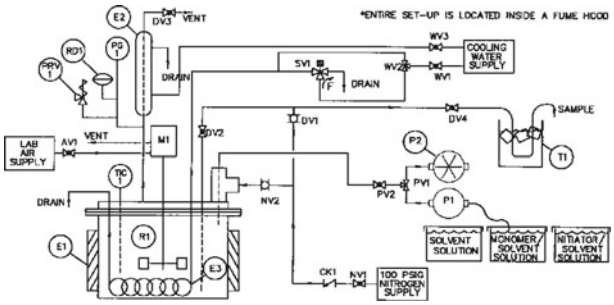

Tag #	Equipment Name	Description
AV1	Valve	Air Cooling for Mixer
CK1	Valve	Nitrogen Supply Check Valve
DV1	Valve	Nitrogen Bubbler Valve
DV2	Valve	Liquid Sampling Valve
DV3	Valve	Condenser Vent Valve
DV4	Valve	Liquid Sampling Valve
E1	Electrical Heater	Part of Parr Reactor
E2	Condenser	Vertical Reflux
E3	Cooling Coil	316 SS
M1	Magnetic Stirrer	Air Cooled Stirrer
NV1	Valve	Nitrogen Shut-off Valve
NV2	Valve	Nitrogen Purge Valve
P1	Pump	Liquid feed type
P2	Pump	Vacuum type
PRV1	Valve	Pressure Relief, 225 psig rating
PV1	Valve	Pump Select Valve
R1	Reactor	300 ml Parr Reactor, Cat. No. 4560
RD1	Rupture Disk	1000 psig rating
SV1	Valve	3-Way Solenoid type
T1	Bath	Ice-water
T1C1	T/C Controller	Controls SV1 valve
WV1	Valve	Cooling water shut-off
WV2	Valve	SV1 bypass
WV3	Valve	Condenser shut-off

Fig. 14.1 Semibatch reactor system (including component tags, names, and descriptions) used in the single-stage emulsion polymerization of MMA in Pentane

Stream 2 was loaded into the reactor. To start the polymerization reaction, the following procedure was followed (Table 14.1).

Samples were dried, by airdrying first and then completely drying in a vacuum oven at 50°C and full vacuum for 1–2 h.

14.1.3 Results

Sample fluids that were taken from the reactor formed nice lattices. Conversion values were obtained from gravimetric measurements, and they indicate almost complete monomer conversion to polymer for Samples #2–7.

Table 14.1 Procedure for single-stage emulsion polymerization of MMA in Pentane

Time (h:min)	Comment(s)
0:00	Started to inject 50 ml of Stream 3, followed by injection of 4.6 ml distilled water as line flush
0:13	Done injecting Stream 3 and line flush
0:31	$P = 70$ psig, $T = 80°C$. Took Sample #1
0:46	Took Sample #2
1:13	Took Sample #3
1:43	Took Sample #4
2:37	Took Sample #5
3:37	Took Sample #6
4:37	Took Sample #7, which is also the product sample. Finally, the reactor was cooled to room temperature and shut down for cleaning

14.2 Multistage Batch Reactor Experiments

14.2.1 Stage 1

Stage 1 involved the formation of PMMA latex.

14.2.1.1 Recipes

All monomers were passed through inhibitor removal columns, and all fluids were bubbled with Nitrogen gas for at least 15 min.

Experiment 1 (5/30/91 Experiment)

Stream 1: Prepared as pre-emulsion
Sodium Lauryl Sulfate (SLS) Surfactant, in powder form – 0.75 g
Distilled water – 100 ml
Methyl Methacrylate (MMA) Monomer – 10 ml
n-Pentane – 40 ml
Stream 2.
Distilled water – 75 ml
V-50 Initiator – 0.2 g

Experiment 2 (6/7/91 Experiment)

Recipe for this experiment was the same as that of Experiment 1.

14.2.1.2 Apparatus

The polymerization system used in these experiments is similar to the 300-ml pressurized Parr reactor system shown in Fig. 2.3.4 of Caneba (2010).

14.2.1.3 Procedures

Experiment 1

At the start, the empty reactor was purged with Nitrogen gas in order to remove Oxygen from the ambient air. Then, all of Stream 1 was pumped into the reactor followed by 4.6 ml Distilled Water as line flush. The reactor was heated to 80°C and brought to the saturation temperature of 34 psig. Then, the experiment proceeded according to Table 14.2.

Note that the reactor temperature was maintained at 80°C even during Stage 2 of the polymerization run.

Experiment 2

This experiment used the same recipe and procedure as those of Experiment 1, except when indicated in Table 14.3 below.

Table 14.2 Procedure for Stage 1 of Experiment 1

Time (h:min:s)	Comment(s)
0:00:00	Started to inject 50 ml of Stream 2, followed by injection of 4.6 ml distilled water as line flush
0:19:00	Done injecting Stream 2 and line flush
0:26:00	$P = 38$ psig, $T = 80$°C. Reactor had a small leak which was used for *n*-Pentane removal by isolating reactor from Nitrogen supply
9:21:00	$P = 2$–4 psig, $T = 80$°C. Increase P to 12 psig through the Nitrogen supply and open overhead valve through condensers (with water cooling lines closed) to blow off remaining *n*-Pentane
10:48:00	Close overhead vapor valve. $P = 12$ psig
11:48:00	This was the end of Stage 1 and the beginning of Stage 2

Table 14.3 Procedure for Stage 1 of Experiment 2

Time (h:min:s)	Comment(s)
0:00:00	Started to inject 50 ml of Stream 2, followed by injection of 4.6 ml distilled water as line flush.
0:12:30	Done injecting Stream 2 and line flush. $P = 36$ psig
9:50:00	$P = 0$ psig
15:34:00	$P = 0$ psig, $T = 80$°C. Increase P to 10 psig through the Nitrogen supply and open overhead valve through condensers (with water cooling lines closed) to blow off remaining *n*-Pentane
16:07:00	Close overhead vapor valve. $P = 10$ psig, and this ended Stage 1

14.2.2 Stage 2

14.2.2.1 Experiment 1

For Experiment 1, Stage 2 proceeded according to Table 14.4 with the temperature still at 80°C.

14.2.2.2 Experiment 2

For Experiment 2, Stage 2 proceeded according to Table 14.5.

14.2.3 Stage 3

A third-stage reaction was done with Experiment 2 only, and the procedure is shown in Table 14.6.

Table 14.4 Procedure for stage 2 of Experiment 1

Time (h:min:s)	Comment(s)
0:00:00	Started to inject 30 ml BA, followed by injection of 4.6 ml distilled water as line flush
0:05:40	Done injecting BA and line flush. $P = 12$ psig
9:38:00	Opened vapor valve to blow off unreacted BA with Nitrogen gas
10:46:00	Closed vapor valve and took 5 ml sample
18:12:00	Turned off heater and run cooling water through internal reactor coil with continued mixing to shut down reactor system

Table 14.5 Procedure for stage 2 of Experiment 1

Time (h:min:s)	Comment(s)
0:00:00	Started to inject 30 ml BA, followed by injection of 4.6 ml distilled water as line flush
0:09:00	Done injecting BA and line flush. $P = 10$ psig
11:41:00	Opened vapor valve to blow off unreacted BA with Nitrogen gas
13:09:00	Closed vapor valve and took 5 ml sample. $P = 10$ psig

Table 14.6 Procedure for stage 3 of Experiment 2

Time (h:min:s)	Comment(s)
0:00:00	Started to inject 5 ml MMA, followed by injection of 4.6 ml distilled water as line flush
0:03:00	Done injecting MMA and line flush. $P = 10$ psig
0:21:00	Turned off heater and run cooling water through internal reactor coil with continued mixing to shut down reactor system

14.2.4 Results

14.2.4.1 Experiment 1

GPC analysis of the Stage 1 product indicated a bimodal molecular weight distribution, which pertained to PMMA homopolymer contamination. This PMMA contamination was determined to be in the order of 10% of the total solid product. Still, the copolymer product MWD was broad with a polydispersity index in the order of 6.

One interesting feature of the latex Stage 2 product was the capability of being cast into an elastic solid film on a Petri dish. A Rheovibron dynamic mechanical analysis of the sample product film showed two equivalent glass transition temperatures at −40 and 135°C for PBA and PMMA, respectively.

A similar run was made for the formation of intermediate PMMA. At the start, the reactor contained 150 ml distilled water, 50 ml Pentane, 16 ml, and 1 g SLS. After the reactor heatup to 80°C, 50 ml distilled water/V-50 (0.27 g V-50 in 75 ml distilled water) was pumped into the reactor for 18 min. Again, the vapor space of the reactor was slowly bled for 7 h and 40 min until the pressure went down to 0 psig. The pressure was raised to 20 psig with Nitrogen gas for 7 h and 30 min in order to obtain the intermediate PMMA latex. GPC analysis of this PMMA intermediate product showed a unimodal peak with a number average molecular weight of 679,400 g/mol and a heterogeneity index of 2.5.

14.3 Stage 1 CSTR Experiment

An attempt was made to implement the two-stage formation of the PMMA–PBA block copolymer, through a first-stage CSTR operation. With *n*-Pentane as FRRPP solvent/precipitant in the first stage, the reactor had to be pressurized, while the second-stage operation could occur at an atmospheric reactor that was much larger than the CSTR. The product from the CSTR could be kept in reagent bottles, with *n*-Pentane partial pressure providing a protective gas blanket against oxygen contamination.

14.3.1 Recipe

The following recipe was used on the first-stage experiment.

Stream 1.
Sodium Lauryl Sulfate (SLS) Surfactant, 29% active in Water – 43.1 g
Distilled Water – 669.4 ml
Methyl Methacrylate (MMA) Monomer – 500 ml
t-Butyl Hydroperoxide (TBHP) Initiator, 70% active – 7.72 ml

Stream 2.
n-Pentane Solvent/Precipitant – 300 ml
Stream 3.
Distilled water – 1,314 ml
Formaldehyde Sodium Bisulfite (FSB) Formula – 3.34 g
$FeSO_4$ – 78.4 mg
Sodium Lauryl Sulfate (SLS) Surfactant, 29% active in Water – 100.55 g

All monomers were passed through inhibitor removal columns, and all fluids were bubbled with Nitrogen gas for at least 15 min. Note that Stream 1 was prepared as a pre-emulsion.

14.3.2 CSTR Reactor System

Figure 14.2 shows the process flow diagram of the Stage 1 CSTR polymerization system. The CSTR was a 300-ml Parr reactor with an electric heater jacket and a water-based cooling coil that was immersed in the reactor fluid. It was important that Streams 1 and 3 were introduced into the reactor in two separate entry lines, in order to prevent premature polymerization in the lines. It was also important that the outlet line that was passed through the ice-water cooler had a relatively small thermally conductive tube material (such as 1/8″ stainless steel tube), in order to drop the reactor fluid temperature close enough to room temperature as it entered the latex product holding tank.

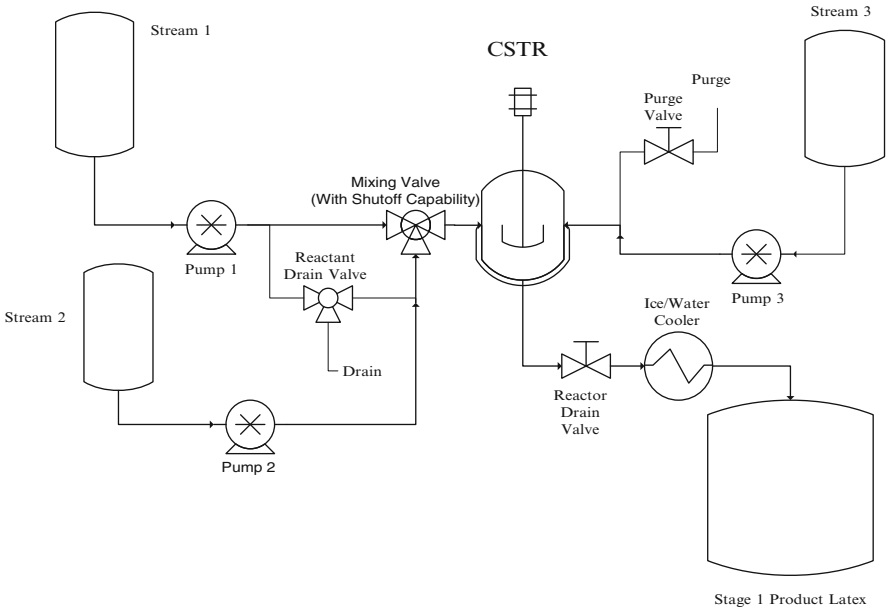

Fig. 14.2 Process flow diagram of the Stage 1 CSTR polymerization system

14.3.3 Polymerization Procedures

The first-stage reactor was operated first, and the product was loaded into 1-gallon reagent bottles that were purged with Nitrogen gas. Batches of Streams 1–3 of the first stage polymerization were prepared, in order to produce multiple gallons of the product for semibatch Stage 2 operation.

14.3.3.1 First Stage

During start-up, the reactor was purged with Nitrogen gas, through a utility line system not shown in the diagram. Then, it was loaded with 150–200 ml distilled water that was bubbled with Nitrogen gas for at least 15 min. The reactor was heated to the setpoint temperature of 60°C and operated at 50–55 psig, initially with Nitrogen gas blanket. The pump lines from Streams 1–3 were primed by allowing fluids into the drain/purge lines without letting them enter the reactor.

Table 14.7 shows the procedure on the first-stage CSTR polymerization reaction run.

Product fluids from the Stage 1 process were stored in 1-gallon reagent glass containers. Since they contained *n*-Pentane, its partial pressure was sufficient to keep ambient oxygen from deactivating the polymer radicals within the latex particles for at least a week.

14.3.3.2 Second Stage

Stage 2 polymerization was done using the same reactor system shown in Fig. 1.3. The 2-l glass semibatch reactor was typically operated at 60°C. At the start, 10 ml of Rhodapex® CO-436 was loaded into the reactor. Then, air from the reactor was purged with Nitrogen gas for 18 min. A 1-l quantity of intermediate latex from the

Table 14.7 Procedure for the first-stage CSTR polymerization reaction run (10/6/93–10/10/93 Experiments)

Time (h:min)	Comment(s)
	Start pumping Streams 1–3 into the reactor at the following flow rates:
	Stream 1: ~6 ml/min
	Stream 2: ~3 ml/min
0:0	Stream 3: ~3.7 ml/min
0:50	Product was discarded up to this point
	Product collected, and reactor outlet line plugged. Stopped pumping to clear the plug in outlet line. It took 80 minutes for reactor to attain
6:00–8:00	steady state again
12:00–16:00	Product collected
4 Days after start of experiment	Collected a total of 7 gallons of Stage 1 product

first-stage CSTR was loaded into the reactor, making sure that a Nitrogen gas blanket was present all the time.

The reactor run started with 2 h of heat-up to 60°C with a small Nitrogen gas sweep on the reactor fluid surface, in order to also remove dissolved *n*-Pentane. Subsequently, BA (equivalent to 150% of MMA added in the first stage) was gradually loaded into the reactor for 2 h, followed by a 2–3 h hold temperature. Finally, the heater was turned off, yielding a latex that formed a transparent film.

14.3.4 Results

14.3.4.1 First Stage

Results of the Stage 1 CSTR operation include:

1. Solids content: 22.2% including *n*-Pentane and 26.5% excluding *n*-Pentane
2. Coagulant level: 2 wt%
3. Residual monomer: 0–2 wt%
4. Particle size distribution: unimodal with volume-average at 0.04 μm
5. Polymer glass transition temperature: 100°C (approx.)

These are reasonable numbers, which confirmed the formation of relatively small PMMA latex particles as well as the presence of *n*-Pentane in the intermediate product latex.

14.3.4.2 Second Stage

The Stage 2 latex product contained the following properties:

1. Solids content: 46.4 wt%
2. Coagulant level: 2 wt%
3. Residual monomer: 1 wt%
4. Particle size: volume-average at 0.06 μm (unimodal)
5. Polymer glass transition temperatures: −45.4 and 97.5°C

These results indicate the likely formation of the PMMA–PBA block copolymer in latex form.

Reference

Caneba GT (2010) Free-radical retrograde-precipitation polymerization (FRRPP): novel concept, processes, materials, and energy aspects. Springer, Heidelberg

Chapter 15
Low VOC Paints and Coatings

15.1 Background and Motivation

This section pertains to the implementation of emulsion polymerization of MMA in *n*-Heptane under conventional precipitation environment (as low as 60°C reactor operating temperature), although there is the likelihood that emulsion particles react at temperature above the lower critical solution temperature (LCST). Even though phase separation below the upper critical solution temperature (UCST) is believed to occur at the start of reaction within emulsion particles, the hour-glass phase envelope of the PMMA–MMA–*n*-Heptane system has been shown to provide a pathway system temperature to attain higher levels where they could well go above the LCST. The polymerization system is based on a redox initiation formulation, and the formation of block copolymer in emulsion particles is implemented in a two-stage polymerization procedure. Solvent/precipitant is removed through a stripping operation. In order to minimize residual monomer in the system at the end of the two-stage reaction run and solvent/precipitant removal step, a chase initiator solution is admixed into the reactor. Product emulsion is used as a binder for a latex paint formulation, which is applied as a film and tested for various coating properties.

The motivation for the development of low-VOC and No-VOC paints and coatings is the fact that VOCs (volatile organic compounds) are both health and environmental hazards. The elevated quantities of indoor VOC have been linked to various life-threatening ailments, such as leukemia and lymphoma (Irigaray et al. 2007). One of the things that happen is that VOC can react with nitrogen oxide from vehicle exhausts and produce ozone, which in turn is a health hazard. Also, high levels of VOCs in the ecosystem eventually result in their photogradation to CO_2 (http://ecm.ncms.org/ERI/new/IRRpaintcoating.html). VOCs commonly found in paints and coatings include aliphatic hydrocarbons, acetone, ether, and ethyl acetate (Stoye 2006). It should be noted that low VOC products contain less than 50 g/l VOCs, while No-VOC contain less than 5 g/l (http://paintgurus.typepad.com/blog/2010/01/the-real-green-story.html).

G. Caneba and Y. Dar, *Emulsion-based Free-Radical Retrograde-Precipitation Polymerization*, DOI 10.1007/978-3-642-19872-4_15,

Table 15.1 Data for VOC emissions from users of surface coatings in the U.S. (taken from the National Emission Inventory for 1999, http://www.epa.gov/ttn/chief/trends/trends99/tier3_1999emis.pdf)

VOC source	VOC, in thousand short tons (%)
Architectural	483 (22.6)
Industrial adhesives	148 (6.9)
Wood furniture	130 (6.1)
Metal cans	113 (5.3)
Auto and light trucks	106 (5.0)
Auto refinishing	104 (4.9)
Traffic markings	93 (4.4)
Maintenance coatings	85 (4.0)
Electronic, electrical	82 (3.8)
Metal furniture	58 (2.7)
Thinning solvents	54 (2.5)
Paper	51 (2.4)
Metal coil	49 (2.3)
All other	580 (27.1)
Total	2,136 (100.0)

The magnitude of VOC generation can be gleaned through production figures for paints and coatings, as shown in Table 15.1.

It should be noted that paint products contain pigment, binder, carrier, and other additives. Pigments are normally inorganic solids that impart color and hiding power (allows concealment of the substrate), which do not contain VOCs. The binder is the polymer material that forms the solid film containing the pigment and other solid materials in the formulation; thus, it normally does not contain VOCs as well. It is in the carrier material where VOCs are found, because it keeps the formulation a liquid during storage and film application, and it allows the coverage of the binder around particulates in the formulation and over rough surfaces of the substrate. Other additives can include polymerization aids, fungicides, film formation aids, rheology modifiers, etc., which contain VOCs but are used at relatively low levels.

15.2 Formation of Latex Binder

15.2.1 Polymerization Recipes

Two similar recipes are presented in this subsection for the formation of the latex binder, and both are based on MMA–BA monomers as well as minor amounts of comonomers.

15.2.1.1 Experiment 1

A typical redox initiation emulsion polymerization recipe was subdivided into four streams.

Stream 1.
Rhodapex® CO-436 Surfactant – 13.5 g
Distilled water – 360 ml
Methyl Methacrylate (MMA) Monomer – 264 ml
T-Butyl Hydroperoxide (TBHP) Initiator – 1.163 g
Stream 2.
n-Heptane Solvent/Precipitant – 300 ml
Stream 3.
Distilled water – 150 ml
Formaldehyde Sodium Bisulfite (FSB) Formula – 1.43 g
$FeSO_4$ – 30 mg
Concentrated H_2SO_4 – three drops
Stream 4.
Butyl Acrylate (BA) Monomer – 396 ml
Glycidyl Methacrylate (GMA) Monomer – 15.84 ml
Distilled water – 99 ml
Rhodapex® CO-436 Surfactant – 1.65 g

All monomers were passed through inhibitor removal columns, and all fluids were bubbled with Nitrogen gas for at least 15 min. Note that Streams 1 and 4 were prepared as pre-emulsions.

15.2.1.2 Experiment 2

In this experiment, the following recipe was used.

Stream 1.
Rhodapex® CO-436 Surfactant – 13.5 g
Distilled water – 360 ml
Methyl Methacrylate (MMA) Monomer – 264 ml
T-Butyl Hydroperoxide (TBHP) Initiator – 1.22 g
Stream 2.
n-Heptane Solvent/Precipitant – 300 ml
Stream 3.
Distilled water – 450 ml
Formaldehyde Sodium Bisulfite (FSB) Formula – 1.428 g
$FeSO_4$ – 32 mg
Versenol – 0.112 g
Stream 4.
Butyl Acrylate (BA) Monomer – 386 ml
Methacrylic Acid (MAA) – 8.14 ml
Sipomer® WAM II – 12.45 g
Distilled water – 99 ml
Rhodapex® CO-436 Surfactant – 1.65 g

All monomers were passed through inhibitor removal columns, and all fluids were bubbled with Nitrogen gas for at least 15 min. Note that Streams 1 and 4 were prepared as pre-emulsions.

15.2.2 Experimental Setup

The experimental batch reactor system used in this work was the 2-l glass reactor system with steam/water jacket shown in Fig. 1.3. The temperature controller system has an accuracy of $\pm 1^{\circ}C$ from the setpoint temperature. Note that there is a slow continuous stream of Nitrogen gas passing through the reactor and through the water bubbler. The Nitrogen flow rate was set to see individual bubbles forming in the bubbler.

15.2.3 Polymerization Procedure

15.2.3.1 Experiment 1

At the beginning, the reactor was purged with Nitrogen gas, in order to minimize presence of oxygen that will terminate radicals that were to be generated. From this point on, the reactor chamber was maintained under Nitrogen gas atmosphere. Then, Streams 2 and 3 were admixed into the reactor, and the reactor fluid was heated to 75°C in 30 min. Table 15.2 shows the subsequent procedure used in the generation of the PMMA–PBA binder that was subsequently formulated into a latex paint.

The product latex was then analyzed for particle size distribution using a Microtrac Ultrafine Particle Size Analyzer.

Table 15.2 Experiment 1 procedure for the formation of 7/28/94 latex product

Time (h:m)	Comment(s)
0:0	630 ml of Stream 1 was continuously added into the reactor at this start of Stage I polymerization
0:44	All of Stream 1 was loaded into the reactor, which was at 73°C
1:44	Started heating the reactor linearly with time to 80°C
3:44	$T = 80^{\circ}C$, and the reactor fluid showed some bubble formation due to action of the stirrer
4:46	Reactor fluid was still bubbling, and foam was observed
5:24	Reactor fluid was still bubbling due to stirrer action, because when stirrer was stopped momentarily, gas evolution was not observed
5:26	Started Stage II by adding Stream 4 drop-by-drop. Foam formation stopped.
5:52	$T = 81^{\circ}C$
6:08	Fluid became a little viscous at 79°C; increased stirrer speed
6:19	Fluid became very viscous at 80°C
6:21	Added 400 ml Stream 4, and stopped Stream 4 addition. Admixed 200 ml distilled water instead, and T went down to 70°C
7:04	$T = 79^{\circ}C$, and started adding 100 ml of Stream 4 continuously again
7:32	All 100 ml remaining Stream 4 was loaded into the reactor
9:58	$T = 78^{\circ}C$, after quick cleanup of thermocouple due to scale formation
10:00	Reactor fluid very viscous at $T = 78^{\circ}C$
10:40	Took a sample, which has almost no BA smell
10:51	Chased reactor with five drops of TBHP; reactor fluid pH = 6–7
11:51	Turn off heating of reactor and shutdown

15.2.3.2 Experiment 2

The same start was used in Experiment 2 as that used in Experiment 1. The procedure from the start of Stage I is shown in Table 15.3.

15.2.4 Polymerization Results

Figure 15.1 shows the particle size distribution of the product latex from Experiment 1, which indicates a bimodal pattern with peaks at 0.05 and 0.29 μm. The likely reason for the bimodal particle size distribution is the breaking off of particulates into smaller pieces during formation of the BA blocks.

Stage II of the polymerization procedure. The implication of the bimodal particle size distribution is the capability of the latex particles to form tighter packed films during sedimentation and drying. Also, it should be noted that the relatively low particle sizes is consistent with a relatively large increase in viscosity of the reactor fluid.

The proposed of formation of environmentally responsible coatings from block copolymers, such as a PMMA–PBA-based latex material is depicted in Fig. 15.2. MMA is first polymerized into latex particulates containing live PMMA radicals in

Table 15.3 Experiment 2 procedure for the formation of the 1/26/95 latex product

Time (h:m)	Comment(s)
0:0	630 ml of Stream 1 was continuously added into the reactor at this start of Stage I polymerization
0:20	$T = 76°C$
0:30	$T = 76°C$
1:08	$T = 76°C$
1:30	$T = 76°C$, and all of Stream 1 was loaded into the reactor
2:01	$T = 76°C$. Started raising reactor temperature to 80°C linearly with time
2:18	$T = 79°C$. Removed condenser to facilitate vaporization of volatiles, while started adding 100 ml distilled water continuously into the reactor
2:54	$T = 82°C$. All 100 ml distilled water was admixed into the reactor
3:20	$T = 81°C$. Restore condenser into reactor system, and then started reducing reactor temperature to 60°C linearly with time
4:04	$T = 66°C$. Started loading 510 ml Stream 4
4:25	$T = 61°C$
4:50	$T = 61°C$
5:15	$T = 60°C$
5:19	$T = 60°C$. Stream 4 all loaded in
5:36	$T = 60°C$
7:37	$T = 60°C$
9:42	$T = 61°C$
11:42	$T = 61°C$
13:19	$T = 61°C$. Turned heater off while continued running stirrer to slowly cool reactor

When the cooled-off reactor was opened, there was no BA smell

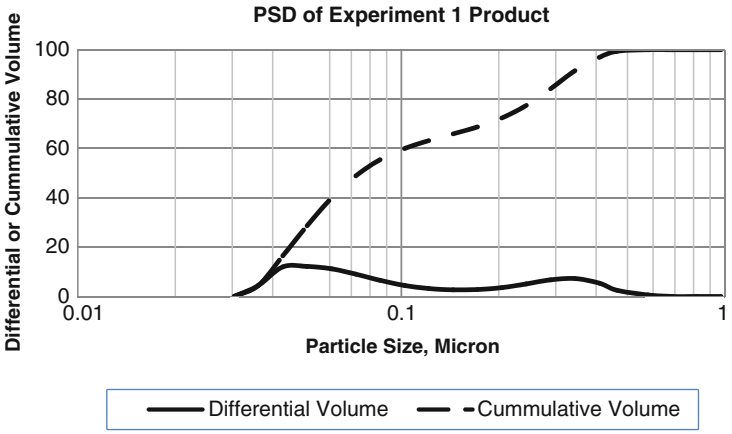

Fig. 15.1 Particle size distribution data for Experiment 1, showing a bimodal peak pattern

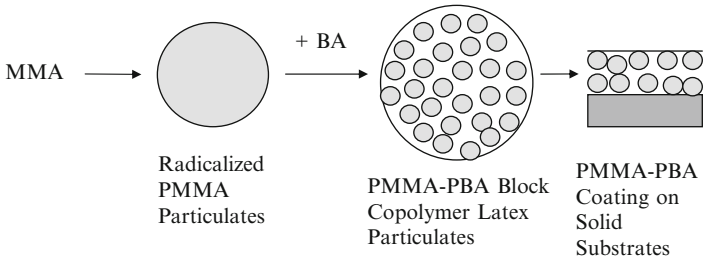

Fig. 15.2 Proposed mechanism for the formation of low VOC paints and coatings from PMMA–PBA block copolymer latex particulates. The soft BA block imparts film-forming properties, while the hard PMMA block imparts strength to the resulting film

a Stage I reactor. Then, BA is added to form PMMA–PBA block copolymer domains within the latex particles in a Stage II reactor operation. It should be noted that Fig. 15.2 is an oversimplification, because a core–shell effect is likely to occur forming bigger PMA domains in the interior of the latex particles. Comonomers can be incorporated in Stage II for various functions, such as adhesion promoters, crosslinkers, etc. Finally, coatings are produced from the PMMA–PBA block copolymer latex particulates. Alternately, the last step could also involve the formation of the PMMA–PBA binder between pigment particles.

15.3 Paint Formulation

The product from Experiment 2 was sent to Specialty Coatings Services (Louiville, KY) for formulation into an interior semigloss latex paint and subsequent testing. The formulation process started out with the preparation of the (white) pigment

dispersion, which contained the following components and proportions (Table 15.4). These components were dispersed in a high-speed mixer for 20 minutes to a Hegman grind of 4–4½. The so-called thindown used for the Experiment 2 product is shown in Table 15.5 below. The final latex fluid was then prepared using the components and their proportion in Table 15.6 below, and mixed with the thindown from Table 15.5.

Based on the above paint formulation procedure, the product had a viscosity of 110 KU, which was adjusted to 100 KU with the distilled water. The viscosity of 100 KU is a more typical brush and roll film application. The final result was a latex paint containing 31.6 vol% solids, 47.2 wt% solids, and pigment volume content (PVC) of 31.2%.

Table 15.4 Components and their weight- and volume-based proportion used in the preparation of the (white) pigment dispersion

Component	Grams	Milliliters
Distilled water	218.66	218.6
Tamol® 731	28.75	26.1
Triton® CF-10	8.25	7.7
Witco Bubblebreaker® BB625	2.5	2.5
Proxel® GXL	2.5	2.1
KTPP	5.0	2.1
Ti-Pure® R-900	562.5	140.6
Minex® 7	175.0	67.1

Table 15.5 Thindown components and quantities used with Experiment 2 product

	Quantity	
Component	Grams	Milliliters
Pigment dispersion from Table 15.4	438.2	194.6
Distilled water	54.5	54.3
Natrosol® Plus	0.9	0.7

The distilled water and Natrosol® Plus were premixed by hand for 2 minutes, and then added to the pigment dispersion slurry under high speed agitation for 30 min

Table 15.6 Components and their quantities that were mixed with the thindown (Table 15.5 dispersions), in order to produce the final paint latex material

	Quantity	
Component	Grams	Milliliters
Binder Emulsion (Experiment 2 Product), adjusted to pH = 6–7 with 45% KOH Solution	559.0	537.4
Triton® X-100	1.5	1.4
Witco Bubblebreaker® BB625	1.0	1.0
Acrysol® RM2020	8.7	8.3
Acrysol® QR-1374	4.35	4.2

15.4 Film Formation and Paint Testing

A commercial Porter International semigloss, interior latex paint was used as control, which was among the best available material for comparison. Even though this control produced a light gray coating compared to the white paint produced from the Experiment 2 binder, resulting coating properties comparison was deemed credible.

15.4.1 Brushout Results

Paint brushouts were obtained by brushing the fluid dispersions onto black Laneta paper. Details are shown below.

15.4.1.1 Gloss/Sheen

Gloss/sheen measurements were made based on the intensity of reflected light from the dried paint materials at angles relative to the vertical. Gloss data were obtained from measurements at 20° and 60° angles, while sheen data were obtained from reflected light at 85° angle. Results are shown in Table 15.7.

The above data indicates good gloss/sheen results considering that the control is the best available semigloss paint material in the market.

15.4.1.2 Flow/Leveling

As shown in the resulting Laneta charts, flow/leveling properties of both Test Coating and Control were comparable. This means that the resulting paint material from the Experiment 2 binder did not show application problems onto solid surfaces.

15.4.1.3 Wet Edge/Open Time

Both Test Coating and Control showed very good wet edge/open time performance. Open time for the Test coating was found to be 10 min, which indicates the time within which a dried coating can be touched up or painted on without showing the edge of the previously applied coating.

Table 15.7 Gloss/sheen data for the test coating relative to control

Paint material	20°	60°	85°
Test coating	2	10	40
Control	4	36	60

15.4.1.4 Brushability

This property pertains to how much of the paint from the brush is transferred to the substrate during a dynamic brushing operation. Thus, it depends on how the viscosity changes with shear rate. The Test Coating was formulated to have a relatively low viscosity relative to the Control during the brushing operation. For example, at 0.3 RPM in the Brookefield viscometer, the Test Coating had a viscosity of 8,500 cPs while the Control had a viscosity of approximately 80,000 cPs. The result is that the test coating had poor hiding power per brush stroke compared to the Control. What compensates for this deficiency is the observation that the Test Coating dries much faster than the Control, which allowed repeated application onto the substrate until the desired hiding power was reached. Higher dynamic viscosities can also be achieved with optimal rheology modifiers during paint formulation.

15.4.2 Block Resistance

Block resistance pertains to the situation when a block of material (wood, masonry, or a flower pot) is set on top of a dried coating, and whether the block could be removed from the painted surface after a certain period of time. A coating that has good block resistance will not bond with the block material. One of the anecdotal stories occurs when the paint material ended up on the surface of the block rather than the substrate it was originally applied onto. Another situation involved the creation of an imprint of a flowerpot on the painted surface.

Block resistances of both Test Coating and Control were measured using the Rohm and Haas Resistance Test Method No. 606–91. Test and Control coatings were applied onto a Laneta chart using a 3.0 mil Bird film applicator and aged for 24 h. The coatings were placed face-to-face on which a #8 rubber stopper with 1,000-g weight was placed for 18 h at room temperature. The charts were separated and evaluated according to the test procedure. Another set of coatings on Laneta charts were similarly pressed face-to-face at 120°C for 30 min. Then, the weights were removed and allowed to set at room temperature for 30 min before separating. Evaluation of block resistance results were done using the numerical description shown in Table 15.8.

Results of this block resistance test are shown in Table 15.9. Note that precision of the ratings is ± 1 upon repeated trials by the same operator. They indicate much better block resistance for the Test Coating compared to the control, which is probably due to the nanocomposite-type of domain structure within the Test Coating films, as indicated in Fig. 15.2.

Table 15.8 Numerical description of block resistance results

Numerical rating	Tackiness	Performance result
10	No tack	Perfect
9	Trace tack	Excellent
8	Slight tack	Very good
7	Slight tack	Good
6	Moderate tack	Good
5	Moderate tack	Fair
4	Severe tack, no seal	Fair
3	5–25% seal	Poor
2	25–50% seal	Poor
1	50–75% seal	Poor
0	Complete seal	Very poor

Table 15.9 Block resistance results for the test coating and control at two temperatures

Sample coating	Room temperature	120°F
Test coating	10	10
Control	4	2

15.4.3 Scrub Resistance

Scrub resistance of interior paints is an important property when the coating is used near doors, windows, and frequently used areas that normally get soiled or stained. Scrubbing with a detergent–water solution is normally done to restore these surfaces; thus, it is important that coatings have to be able to resist repeated scrubbing. In the test procedure, a standard detergent was used on the coatings applied onto black Laneta paper and scrubbed with nylon brittles. Scrubbing action was done usually with a motorized system that applied cyclic forward and reverse linear motion of the brush material. The coating was fixed at the bottom of a flat boat container with the detergent solution always present on the surface being scrubbed. During the scrubbing operation, the coating was being removed from the surface in contact with the brush material until only the Laneta paper substrate is visible. The operation was topped when a continuous line of the substrate became visible and the number of brush cycles was counted at that point in time. Normally, it would take at least 1,000 scrub cycles for a commercial interior coating to show failure.

For the Test Coating, scrub failure occurred after 189 and 200 cycles; the Control took 2,200 cycles before scrub failure. This means that the absence of coalescing solvent in the Test Coatings resulted in reduced particle cohesion, which manifested in relatively low scrub resistance. The recommendation for the Test Coating was that it should not be used in areas that will be heavily soiled if more frequent repainting had to be avoided. Still, the fact that it is a low VOC type, surface reapplication would not result in adverse levels of VOC exposure even at relatively low level ventilations.

15.4.4 Stain Resistance

Stain resistance tests were done to determine the capability of coatings to resist ordinary household stains. It involves applying representative household stains, and then attempting to scrub them off using a standard nonabrasive detergent solution. Formally, the test is based on using the Rohm and Haas Resistance Test Method No. 610–91. Various stains were applied onto films over black Laneta paper substrate. The films were applied onto the substrate using a Bird 3.0 mil applicator, and dried for a week at 77°F and 50% relative humidity. Stains used for the test include crayon, HB lead pencil, lipstick, black ballpoint pen, mustard, ketchup, and coffee. After the stains are applied to the coatings, 200 scrub cycles with a 1% Tide® solution was consistently applied to remove the stains. With this procedure, it was found that both Test Coating and Control exhibited good stain resistance properties.

15.4.5 Adhesion Over Aged Alkyd

The idea behind this test method is that old paint and coating materials have been produced using alkyd formulations, and new coatings should exhibit the capability of being painted onto alkyd surfaces. For this test, smooth and lightly sanded alkyd surfaces were used. The Test Coating was applied onto both surfaces, and air-dried for 7 days. Then, adhesion was tested using a crosshatch adhesion tester based on ASTM D3359. The results were very good at 5B over the sanded surface and 4B over the gloss surface.

15.5 Discussion of Results

Relatively small latex particle sizes as shown from Experiment 1 data indicate the feasibility of film formation from latex binder systems without the need for coalescing solvents. Small latex particle sizes pack very well into films, leaving very little interparticle spacings.

As a whole, the dry paint material obtained from the Experiment 2 binder exhibited adequate properties for interior coatings application. For most part, its performance characteristics are comparable to that of the Control, except in its brushability and scrub resistance properties. What makes the test paint attractive is that it has a low VOC content, which mainly comes from the various paint formulation additives.

The new generation PMMA–PBA latex coating that was developed had a similar procedure and recipe to that of Experiment 2. The difference is that diacetone acrylamide, a reactive comonomer, was used in Stage II along with BA. Then, in the

paint formulation stage, adipic dihydrazide was used to provide a water-soluble crosslinker.

With this coating, good semigloss enamels were formed and scrub resistances were found to be in the order of 600–1,000 scrub cycles. If the same formulation modification was used with Experiment 2, it is believed that better film performance could further be obtained.

Therefore, the various methods and formulation presented in the section shows that the emulsion-based FRRPP method can indeed be applied toward the formation of low VOC emulsion paints and coatings.

Reference

Irigaray P, Newby JA, Clapp R, Hardell L, Howard V, Montagnier L, Epstein S, Belpomme D (2007) Biomed Pharmacother 61(10):640

Stoye D (2006) "Paints and Coatings", in: Ullmann's Encyclopedia of Industrial Chemistry, Wiley-VCH, Weinheim

Chapter 16
Oil Spill Control from Emulsion-Based FRRPP Foaming Surfactant Systems

The 2010 rig disaster from the Deepwater Horizon/Macondo well off the Gulf of Mexico and its aftermath has rekindled the debate on deepwater drilling and offshore oil exploration in the United States. The heavy use of dispersants from the ill-fated well has been known, and it has been documented that underwater oil plumes are lurking beneath the water surface (Thibodeaux et al. 2011). There is a need to understand the processes involved in the formation of these plumes, and how to address their lingering presence.

16.1 Envisioned Mode of Application

In Sect. 5.2 of Caneba (2010), a particular type of vinyl acetate–acrylic (VA–AA) salt tapered block copolymer (called B6-1) was shown to exhibit excellent performance as a foaming surfactant for enhanced oil recovery. The underlying reason was cited as the capability of the polymeric surfactant to form a relatively stable displacement front between the aqueous phase and oil phase, while the aqueous phase is being pushed against the oil phase by a foaming gas. It should therefore be no surprise that the same mechanism could be used in the displacement of oil from the water surface laterally toward areas where it can be efficiently collected or disposed of. The same foam front can be used to raise an underwater oil plume to the surface of the water, where it can be collected. Finally, the foam can be used to separate and raise the oil that is stuck on the seafloor, where it can be further raised to the surface with the same foam system. All this is shown in Figs. 16.1 and 16.2.

Variations of the B6-1 VA–AA tapered block copolymer involved higher AA content and the incorporation of ethylene grafts from the AA segments. The latter case allows for more interaction with the oil and lower temperature applications.

G. Caneba and Y. Dar, *Emulsion-based Free-Radical Retrograde-Precipitation Polymerization*, DOI 10.1007/978-3-642-19872-4_16,

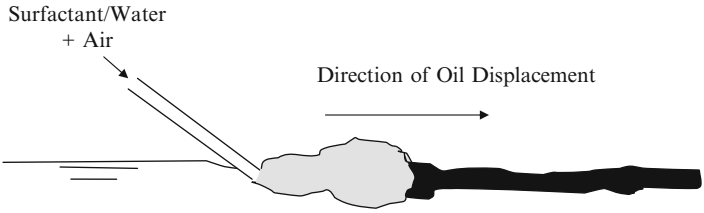

Fig. 16.1 Lateral oil displacement from surface of open water using the foam that was generated from a surfactant–water mixture

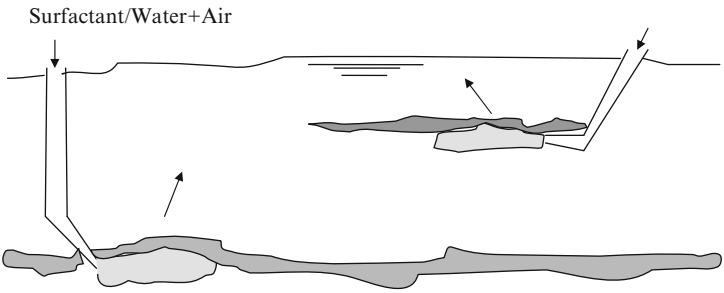

Fig. 16.2 Near-vertical displacement of oil from the seabed and from underwater plumes using foam that was generated from a surfactant–water mixture

16.2 Investigation of Foaming Properties of Surfactants

Foaming properties are being investigated using a variation of the Miles-Ross method (ASTM D1173). Essentially, the system consists of an annular column (called the column receiver), wherein surfactant solution is dropped from the top reservoir. The resulting kinetic energy of the falling fluid from the top reservoir creates the foam in the receiver. In the annular section, constant temperature water is passing through, which comes from a constant temperature bath. The height of the foam in the inner cylindrical cavity of the receiver is measured as a function of time. A schematic diagram of the entire Miles-Ross system is shown in Fig. 16.3. Figure 16.4 shows the picture of the actual system. Finally, Fig. 16.5 shows the schematic diagram of the column receiver.

The procedure for the use of the Miles-Ross system (Fig. 16.3) includes the following steps:

1. Condition the surfactant solution at the operating temperature. This is usually done by immersing the solution in the circulating bath of the Miles-Ross system.
2. Adjust the receiver (B) so that it is plumb.
3. Adjust the reservoir (A) so that a stream of water emerging from the orifice will strike the bottom center of the receiver (B).

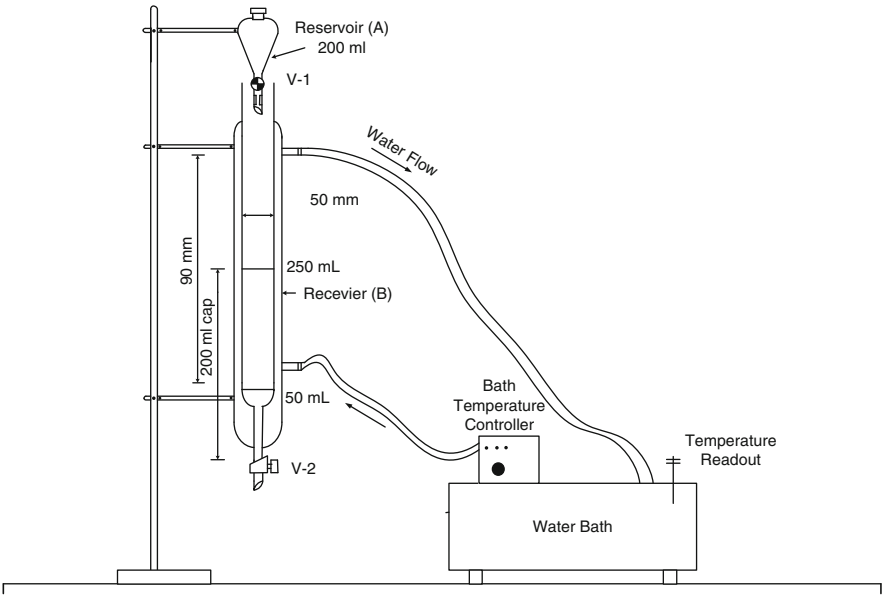

Fig. 16.3 Schematic diagram of the modified Miles-Ross test system

4. Be sure that the receiver (B) and reservoir (A) are clean. The final step in the cleansing shall be a thorough rinsing with distilled water. If the glass surfaces are clean, the distilled water should flow over the side walls in an unbroken film, finally draining without the appearance of droplets on the glass.
5. Close the stopcock (V-2) of the receiver (B). By means of a 50 ml. volumetric pipette, introduce 50 ml of test solution in to the receiver (B). The solution should run down the side walls of the receiver (B) to avoid foam formation and wet the entire interior of the receiver (B). Hold the tip of the pipette against the side wall of the receiver (B) and slowly move the tip around the circumference of the tube so that the solution will flow down on all sides.
6. Fill the reservoir (A) with 200 ml of the surfactant solution.
7. Place the reservoir (A) in position at the head of the receiver and open the reservoir stopcock (V-1).
8. When all the liquid has run out of the reservoir (A), start the stopwatch and take foam height readings immediately, and every 5 min. The first reading is an accepted standard; however, additional indications of the relative stability of various foams may be obtained in those cases where breakdown does occur in 5 min.
9. The readings should be taken as follows: A millimeter scale is placed behind the receiver (B) so that the zero mark is opposite the point in the receiver (B) which would be reached by total volume of liquid introduced into the receiver (B). The foam production is measured at the top of the foam column at the highest average height to which the rim of the foam has reached. This height is

Fig. 16.4 Picture of the modified Miles-Ross system

proportional to the volume of air remaining in the foam. Additional measurements of the foam heights may be taken at suitable intervals.

10. Empty receiver (B) of solution and while the stopcock is open flush down side walls with distilled water until all foam has been swept out of the bottom.

For safety awareness, the following equivalent materials safety data sheet (MSDS) is employed when handling the surfactant solutions.

RESEARCH SAMPLE SAFETY DATA SHEET
(Compiled on October 22, 2010)

SECTION 1: CHEMICAL IDENTIFICATION

NAME : Poly(vinyl acetate-*co*-acrylate salt), Self-Emulsion in Water

SYNONYMS : 2-Propenoic acid with ethenyl acetate, hydrolyzed; Partially hydrolyzed vinyl acetate-ammonium acrylate copolymer

(continued)

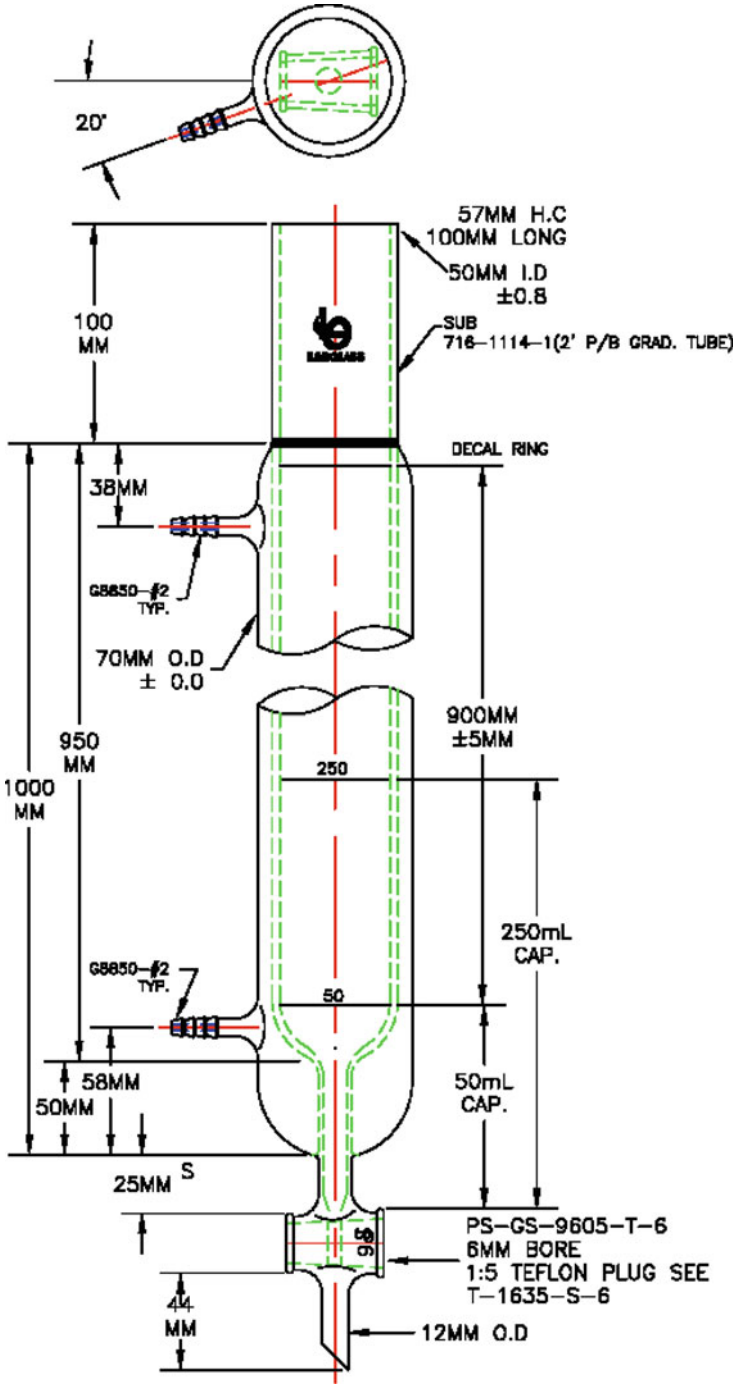

Fig. 16.5 Schematic diagram of the Miles-Ross column receiver

RESEARCH SAMPLE SAFETY DATA SHEET
(Compiled on October 22, 2010)

CATALOG # : Not available
CAS # : [903900-50-5]

RTEC # : Not available

SECTION 2: COMPOSITION AND INFORMATION ON INGREDIENTS

Block copolymer of vinyl acetate and acrylic acid (Neutralized) with about 4-15 wt % acrylic acid before neutralization

The emulsion contains 0.1-5 wt % solids in water.

SECTION 3: HAZARDS IDENTIFICATION

The effects of the polymer sample are not known. All precautions should be taken until the properties of the material are fully determined.

SECTION 4: FIRST AID MEASURES

EYES : Flush with copious amounts of water for at least 15 minutes. Assure adequate flushing by separating the eyelids with fingers.
SKIN : Wash with soap and copious amounts of water for at least 15 min.
INHALATION : Remove to fresh air. Monitor breathing. If problems exist consult a physician.
INGESTION : Wash out mouth with water provided person is conscious. Call a physician.

SECTION 5: FIRE FIGHTING MEASURES

EXTINGUISHING MEDIA
Water spray, carbon dioxide, dry chemical powder, or appropriate foam.

SPECIAL FIREFIGHTING PROCEDURES
Wear self-contained breathing apparatus.

UNUSUAL FIRE AND EXPLOSION HAZARDS
The material may decompose under fire conditions to form flammable mixtures in air.

SECTION 6: ACCIDENTAL RELEASE MEASURES

Wear shoes and working gloves.

Sweep up, place in a bag, and hold for waste disposal. Liquid can be wiped with paper towel and dried before disposal.

(continued)

RESEARCH SAMPLE SAFETY DATA SHEET
(Compiled on October 22, 2010)

SECTION 7: HANDLING AND STORAGE

Store in a tightly closed, sealed container. Avoid contact with or exposure to material.

SECTION 8: EXPOSURE CONTROLS- PERSONAL PROTECTION

Wear chemical safety glasses.
Use protective clothing, and working gloves.
Do not get into eyes.
Wash thoroughly after handling.
Keep sample tightly closed.
Store in a cool dry place.

SECTION 9: PHYSICAL AND CHEMICAL PROPERTIES

APPEARANCE : White fluid; plastic material when dried

PHYSICAL PROPERTIES : Sticks to wood, glass, concrete, metal after heated and then cooled.

SECTION 10: STABILITY AND REACTIVITY

STABILITY:
Stable under dry conditions and under neutral pH.

INCOMPATIBILITIES:
None.

HAZARDOUS COMBUSTION OR DECOMPOSITION PRODUCTS:
Not completely established.

HAZARDOUS POLYMERIZATION:
Will not occur

SECTION 11: TOXICOLOGICAL INFORMATION

May be harmful by ingestion.

May cause eye irritation.

May cause skin irritation.

To the best of our knowledge, the chemical, physical, and toxicological properties of this material have not been investigated.

(continued)

RESEARCH SAMPLE SAFETY DATA SHEET
(Compiled on October 22, 2010)

SECTION 12: ECOLOGICAL INFORMATION

Data not available.

SECTION 13: DISPOSAL CONSIDERATIONS

Dissolve or mix the material with a combustible solvent and burn in a chemical incinerator equipped with an afterburner and scrubber. Observe all federal, state, and local environmental regulations.

SECTION 14: TRANSPORT INFORMATION

The properties of this material have not been fully determined, so all precautions should be observed during transport. Transport in a sealed container.

SECTION 15: REGULATORY INFORMATION

Not available.

SECTION 16: OTHER INFORMATION

This is a new type of material. Its properties have not yet been determined, but solid in emulsion should not be too different from a dry glue material

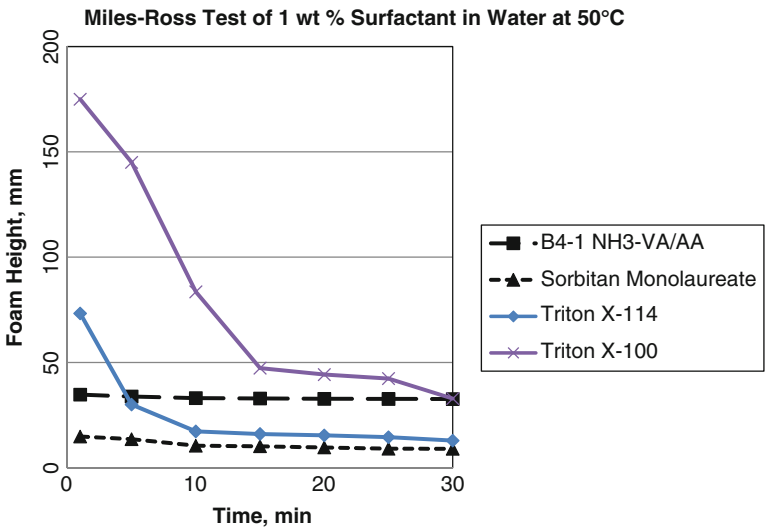

Fig. 16.6 Foam height vs. time for 1 wt% surfactant in various surfactant–water solutions using the Miles-Ross system at 50°C

Foam height measurements were first taken 1 min after the 200 ml surfactant solution was poured from the reservoir. In Fig. 16.6, foam heights vs. time are plotted for 1 wt% of various surfactant–water solutions using the Miles-Ross system at 50°C. It can be seen that the B4-1 VA/AA-based solution had a stable foam height vs. time at relatively high values. It is also important to consider that for petroleum foam displacement, surfactants with oxygenated hydrophobic groups are needed (Caneba and Axland 2002). Based on Fig. 16.6, the B4-1 NH_3-VA/AA polymer surfactant performed very well especially under longer time foam stability test. It should be noted that foam height measurements were averages based on foam volume, and the foam column of Triton X-100 was not stable. It had relatively large air gaps in the foam column, which quickly developed after 10 min. This means that such a surfactant will not be able to sustain a blown foam in a certain location when applied to displace petroleum.

References

Caneba GT (2010) Free-radical retrograde-precipitation polymerization (FRRPP): novel concept, processes, materials, and energy aspects. Springer, Heidelberg. ISBN 978-3-642-03024-6

Caneba GT, Axland JE (2002) J Miner Mater Character Eng 1(2):97

Thibodeaux LJ, Valsaraj KT, John VT, Papadopoulos KD, Pratt LR, Pesika NS (2011) Environ Eng Sci 28:87

Chapter 17
Polymer Modification of VA–AA-Based Copolymer Emulsions

Even in neutralized form, VA–AA-copolymers and their emulsions in water can undergo various modification reactions, either catalyzed by acids or bases. These modification reactions have been carried out either to probe the reaction mechanism, to generate a desired product, and/or as a condition for an application that could use the VA–AA-based emulsion copolymers.

An obvious result of reaction of VA–AA-based copolymers and their emulsions in water is the hydrolysis of the vinyl acetate segments (Bristol 1961). In aqueous or even humid environments, this is accompanied by the release of acetic acid and the conversion of the vinyl acetate segments to those of vinyl alcohol, as depicted in Fig. 17.1 below.

There are other possible reaction mechanisms associated with some of the un-neutralized AA segments. The manner of neutralization of the AA segments would also result in modification reactions. For example, if ammonia is used to neutralize the AA segments, secondary and tertiary amine reactions still occur with acids especially at elevated temperatures.

The easiest method of analyzing the reaction fluid is through a combination of solubility and precipitation methods. At a certain point in reaction time space, some precipitate can be formed, and the precipitate and supernatant fluid can be separated. The precipitate can be tested for its solubility in various solvents; if it does not dissolve in anything, then it is safe to say that it is a crosslinked material. The supernatant fluid can be exposed to various possible solvents and nonsolvents, in order to obtain other precipitates which can be separated through a centrifuge. Also, precipitate and supernatant fluid can be dried and further analyzed.

17.1 Acid-Catalyzed Polymer Modifications

To implement this type of polymer modification, reactant acid which also functions as a catalyst is simply added into the VA–AA-based emulsion copolymer in water. Then, the mixture is heated up until a change in color and/or fluid consistency is

G. Caneba and Y. Dar, *Emulsion-based Free-Radical Retrograde-Precipitation Polymerization*, DOI 10.1007/978-3-642-19872-4_17,

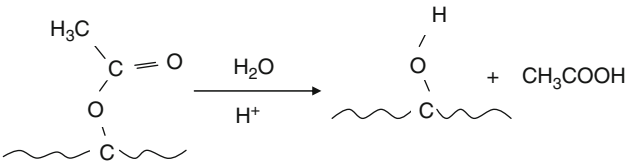

Fig. 17.1 Hydrolysis of vinyl acetate segments of VA–AA-based copolymers and their emulsions, wherein acetic acid is produced in the presence of water and catalyzed by acids

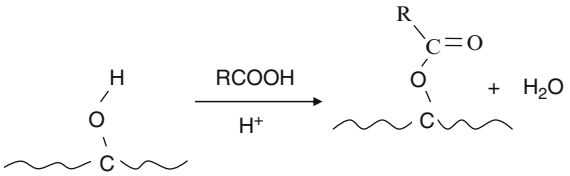

Fig. 17.2 Polymer graft formation through the esterification of vinyl alcohol segments that are formed from acid-catalyzed hydrolysis of vinyl acetate segments (as shown in Fig. 17.1)

observed. If vinyl acetate segments are catalyzed by the acid to form vinyl alcohol segments, then the added acid can attack the hydroxyl group to undergo an esterification reaction. This would result in the formation of various grafts along the hydrophobic portion of the VA–AA-based copolymer chain (See Fig. 17.2).

17.1.1 Reaction with Acetic Acid

Acetic acid concentrations of 0.1 and 1 M in water were prepared and bubbled with Nitrogen gas for at least 15 min. Also, VA–AA-based copolymer emulsions were prepared to approximately 1 wt% solids, and also bubbled with Nitrogen gas for at least 15 min. The two mixtures were then mixed at various proportions in preweighed 25-ml sealed bottles under a Nitrogen gas atmosphere.

Reactions of the sealed bottles containing the VA–AA-based copolymers and acetic acid were carried out in high throughput experimentation (HTE) heater blocks at a temperature of 110°C (See Fig. 17.3 below) (Tiwari R Unpublished results). Samples were ran for a total reaction time of 4 h relative to the point when the temperature of the block system reached 110°C.

The first set of modification with acetic acid was done on a KOH-neutralized VA/AA tapered block copolymer with 8 wt% AA content. The KOH used for neutralization assures that modification would occur from the hydrophobic segments of the polymer. The starting surfactant–water solution had 0.5 wt% solid, and 10 g of it was used. Amounts of acetic acid added resulted in concentrations of 0, 0.1, and 1 M acetic acid in the mixture. After 4 h of reaction,

a precipitate was formed, and was dried into a yellow solid product. The amounts of reactants and products are shown in Table 17.1 below.

It is evident from Table 17.1 that some of the acetate groups were incorporated into the hydrophobic portions of the copolymer chain, probably into vinyl alcohol segments that are adjacent to the K-Acrylate segments.

In another set of experiments, ammonia-neutralized VA/AA surfactant in water (1 wt% in water) was used. A total of ten samples were exposed to acetic acid. Table 17.2 shows the formulations and results of the experiment. Again,

Fig. 17.3 High throughput experimental block system used in polymer modification experiments

Table 17.1 Hydrolysis formulations and results of 0.5 wt% KOH-neutralized VA/AA tapered block copolymer (8 wt% AA) with Acetic acid. Reaction was done at 110°C for 4 h

Acetic acid concentration	Wt surfactant–water, g	Wt yellow solid precipitate, g	Wt surfactant solid, g	Wt precipitate/Wt surfactant solid
0	10	0	0.05	0
0.1 M	10	0.0451	0.05	0.90
1 M	10	0.0657	0.05	1.30

Table 17.2 Hydrolysis formulations and results of 1 wt% ammonia-neutralized VA/AA tapered block copolymer with acetic acid. Reaction was done at 110°C for 4 h

Sample#	Acetic acid concentration, M	Wt surfactant–water, g	Wt yellow solid precipitate, g	Wt surfactant solid, g	Wt precipitate/Wt surfactant solid
1	1	10	0.3525	0.1	3.525
2	1	10	0.3525	0.1	3.525
3	1	10	0.3525	0.1	3.525
4	1	10	0.3521	0.1	3.521
5	1	10	0.3527	0.1	3.527
6	0.1	10	0. 2990	0.1	2.990
7	0.1	10	0.2990	0.1	2.990
8	0.1	10	0.2995	0.1	2.995
9	0.1	10	0.2995	0.1	2.995
10	0.1	10	0.2995	0.1	2.995

precipitates were formed and the supernatant solutions were colorless. This implies that all the surfactant material was incorporated in the precipitate.

It is evident from Table 17.2 that the amine groups from the hydrophilic portions of the surfactants reacted with the acetic acid to form the precipitate. In order to obtain a more controlled polymer modification with a hydrocarbon group, a lower temperature is needed and a larger hydrocarbon group should be used. This led to the work involving the use of stearic acid that is reacted with the VA/AA-based surfactants at 70°C only. Such effort is presented in Chap. 18.

17.2 Base-Catalyzed Polymer Modifications

Base-catalyzed modifications of VA–AA-based copolymer are proposed to occur due to the base-catalyzed hydrolysis of the vinyl acetate segments, as depicted in Fig. 17.4.

Some of the applications of this mechanism are outlined in the foregoing subsections.

17.2.1 Reactions with Caustic-Alumina Solutions

In order to simulate the remediation of the red sludge material from a broken dike wall of a repository in Hungary, a caustic-alumina mixture was treated with VA–AA-based copolymer surfactant solutions. The sludge material was a waste that was generated from the Bayer process, which was employed to extract aluminum from bauxite ore (Habashi 2005), as shown in the chemical equation below (http://en.wikipedia.org/wiki/Bayer_process).

$$Al_2O_3 + 2OH^- + 3H_2O \rightarrow 2\left[Al(OH)_4\right]^-$$

Hot NaOH at 175°C is used as the OH^- source in the above chemical equation. The waste red mud material contained unextracted alumina and unrecovered NaOH, rendering it with a pH of 9. It has been expected that the sludge material would be gathered into two 400-ha fields contaminated to a depth of 5 cm in one of them and 10 cm deep on the other.

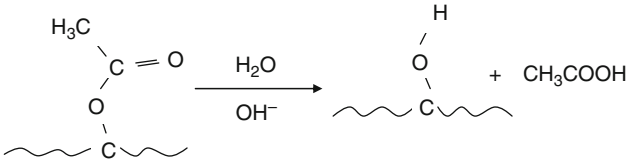

Fig. 17.4 Mechanism for the base catalysis of vinyl acetate segments from the VA–AA-based copolymer surfactants, wherein acetic acid is produced

Table 17.3 Simulated treatment of the red mud sludge with KOH-neutralized 9/11/02 VA/AA solution in water

Ratio (v/v) of $NaOH/Al(OH)_3$-to-KOH Neutralized 9/11/02 VA–AA (1.0 Wt%) in water	Resulting pH (±0.25)
1:1	6.8
2:1	7.0
5:1	7.3
10:1	7.5

In order to determine the feasibility of using VA–AA surfactants to treat the red sludge contamination, mixtures of α-Alumina and NaOH in water were prepared in distilled water as a model-active caustic material within the actual system. Then, various amounts of a VA–AA surfactant material (KOH-neutralized 9/11/02 VA/AA Product) were added and the resulting pH values of the treated mixtures were measured. Within a minute of the preparation of the treated mixtures, pH values changed from 9 to constant lower values, depending on the amount of surfactant that was added into the system (Table 17.3).

In order to obtain the amount of solid VA–AA-based surfactant that would be needed to treat the red sludge fields in Hungary to result in a pH of 7, Table 17.3 shows that a target of 2:1 v/v ratio of $NaOH/Al(OH)_3$-to-KOH Neutralized 9/11/02 VA–AA (1.0 wt %, polymer described as thickened B6-1 in Section 5.1 of Caneba, 2010) surfactant in water. The calculation of the required amount of surfactant follows.

The capability of the multifunctional surfactant for fast neutralization of the simulated red mud depends on its concentration in water. For a resulting pH of 7 from the pH of 9, there is a need for 0.36 wt% equivalent VA/AA copolymer surfactant in water (Table 17.3). If one assumes a porosity of 50% for the red mud and the requirement to cover one pore volume of the red mud with the multifunctional surfactant solution to attain a pH of 7, the areas and contamination depths (5 cm depth of 400 ha and 10 cm depth of 400 ha) will require 7,334,000 kg of equivalent VA/AA copolymer solid surfactant. If this were produced in bulk scale as a commodity polymer ($1.5–2 per lb), it will cost in the order of 24–32 million $ to manufacture the copolymer. Other minor material costs include: neutralizing KOH (to neutralize 6 wt% of surfactant solid made up of acrylic acid segments), water, initiator, and polymerization solvent (first batch and subsequent make-up amounts). As for the speed of manufacture, if there are no major scale-up problems, it will take around 50 days to produce the entire amount using a 20,000 gallon reactor (three batches per day). If a 5,000 gallon reactor is to be used, it will take around 200 days to produce the entire amount. It should be noted that the reaction can be done in an atmospheric reactor; thus, it is possible to find large-scale atmospheric autoclave units from a chemical or polymer manufacturer company.

Based on these results and prior knowledge of the behavior of VA–AA-based surfactants, the mechanism of the treatment of the red caustic alumina is through the base-catalyzed hydrolysis of the VA segments (Fig. 17.4), wherein the acetic acid product neutralizes the NaOH from the caustic alumina solution. This is an unusual base neutralization mechanism from a surfactant material that also functions as a cleaning agent.

It would be straightforward to say that treating the sludge with acetic acid would be quite suitable. However, the following reasons can be stated as advantages of using the VA–AA-based surfactant material.

1. Workers' safety during the preparation of the formulation
2. Workers' safety during the spraying operation; the use of VA/AA-copolymer-based detergent–neutralizer copolymer will produce little mist and will not pose a danger from oversprays
3. Equipment corrosion considerations
4. Less water use compared to direct acid treatment
5. Better treatment of exposed surfaces; VA/AA-copolymer-based detergent–neutralizer copolymer facilitates detachment/removal of red sludge particulates and will involve reduced final rinse operation due to its mild and effective neutralization capabilities
6. Reduction of dust formation when the treated red mud sludge dries up in the summer
7. The capability to use the detergent–neutralizer for other related detergent-based operations

There are more than two dozen similar repositories of Soviet-era caustic red sludge sites in Hungary, and their containing walls are in danger of breaking down in the near future. There will always be the possibility of using VA–AA-based surfactants for fast neutralization and remediation of contaminated sites.

17.2.2 Reactions with Calcium-Alkaline Solution

One of the features of VA–AA-based copolymer surfactants for applications at high alkaline solution (pH = 12). In this case, foaming behavior was observed after exposure to high pH, compared to behavior of a standard surfactant, such as SDS or SLS. $Ca(OH)_2$ was used as the alkaline source. Preliminary experiments indicate short-term foaming behavior of both SDS- and VA/AA-based surfactant solutions in water at pH = 12 from $Ca(OH)_2$. It seems that the VA/AA-based surfactant solution at pH = 12 foamed by as much as 50–100% better that the solution based on SDS. On the longer time scale of a week or more at room temperature, the SDS-based solution precipitated, while the VA/AA-based surfactant solution at pH = 12 has not precipitated at all.

References

Bristol JE (1961) Hydrolysis of polyvinyl acetate. U.S. Patent No. 2,995,548, 8 Aug 1961

Caneba GT (2010) Free-radical retrograde-precipitation polymerization (FRRPP): novel concept, processes, materials, and energy aspects. Springer, Heidelberg, pp 281–282. ISBN 978-3-642-03024-6

Habashi F (2005) Hydrometallurgy 79:15

Chapter 18
Oil Dispersants from FRRPP-Based Surfactants

18.1 Background

The use of Corexit® to disperse oil that was spilled from the BP Deepwater Horizon drilling platform off the Gulf of Mexico just a few months ago has been quite controversial, due to the presence of more aggressive *t*-butanol and/or hydrocarbon carrier fluids in the formulations. There is a continuing search for more environmentally responsible oil dispersant formulations, since oil spills from offshore platforms are expected to continue to occur in the future. A tabulation of various dispersants registered in the USEPA website (http://www.epa.gov), their effectiveness and toxicities is shown in Table 18.1.

We are developing crude oil dispersants based on VA/AA surfactants. Preliminary scaled-down Swirling-Flask test (Fingas et al. 2000) involving these surfactants and Louisiana light crude indicate that Oil Dispersion Effectiveness values are only in the 25% range without the use of volatile organic compounds (VOCs) in the formulation (Tiwari R Unpublished results). To increase this value, VA/AA surfactants have been modified by reaction with stearic acid, in order to increase its affinity with hydrocarbon components in crude oil.

18.2 Reaction of VA/AA-Based Surfactants with Stearic Acid

Stearic acid, $(CH_2)_{17}COOH$, is a material that is insoluble in water, but is soluble in acetone (Heryan et al. 2007). Thus, it can be admixed into neutralized VA–AA acetone solution and allowed to react upon heating in a high throughput experimentation block system (Fig. 17.3). A typical operating temperature is 70°C, and reaction occurs from a few hours to almost a day. A desired product from this operation is a polymer surfactant with olefin-grafted hydrophobic blocks. Such a product would have more affinity to heavier hydrocarbon material, such as crude oil, tar, shale oil, and other bitumen materials.

G. Caneba and Y. Dar, *Emulsion-based Free-Radical Retrograde-Precipitation Polymerization*, DOI 10.1007/978-3-642-19872-4_18,

Table 18.1 Registered dispersants, their effectiveness and toxicities to aquatic life at the USEPA website that have been considered for application in the BP oil spill at the Gulf of Mexico in the summer and fall of 2010

	Toxicity (LC50 values in ppm)		Effectiveness (%)		
Product (1:10 Product-to-No. 2 Fuel oil ratio)	Menidia (96-h)	Mysidopsis (48-h)	Prudhoe Bay crude oil	South Louisiana crude oil	Average of crude oils
BIODISPERS	5.95	2.66	51.00	63.00	57.00
COREXIT® EC9500A	2.61	3.40	45.30	54.70	50.00
COREXIT® EC9527A	4.49	6.60	37.40	63.40	50.40
DISPERSIT SPC 1000™	7.90	8.20	40.00	100.00	73.00
FINASOL OSR 52	5.40	2.37	32.50	71.60	52.10
JD-109	3.84	3.51	26.00	91.00	58.50
JD-2000™	3.59	2.19	60.40	77.80	69.10
MARE CLEAN 200	42.00	9.84	63.97	84.14	74.06
NEOS AB3000	57.00	25.00	19.70	89.80	54.80
NOKOMIS 3-AA	7.03	5.56	63.20	65.70	64.50
NOKOMIS 3-F4	100	58.40	62.20	64.90	63.55
SAF-RON GOLD	9.25	3.04	84.80	53.80	69.30
SEA BRAT #4	23.00	18.00	53.55	60.65	57.10
SEACARE ECOSPERSE 52 (see FINASOL® OSR 52)	5.40	2.37	32.50	71.60	52.10
SEACARE E.P.A. (see DISPERSIT SPC 1000™)	7.90	8.20	40.00	100.00	73.00
SF-GOLD DISPERSANT (see SAF-RON GOLD)	9.25	3.04	84.80	53.80	69.30
ZI-400	8.35	1.77	50.10	89.80	69.90
ZI-400 OIL SPILL DISPERSANT (see ZI-400)	8.35	1.77	50.10	89.80	69.90

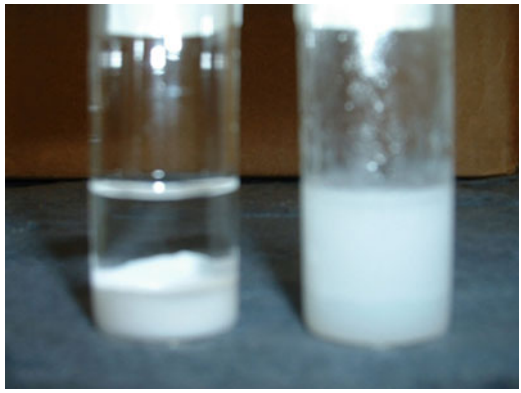

Fig. 18.1 Picture of container bottles that indicate clear top layer for a mixture of *n*-Heptane with VA–AA-based surfactant solution where no polymer modification reaction did (*Right*) and did not (*Left*) occur

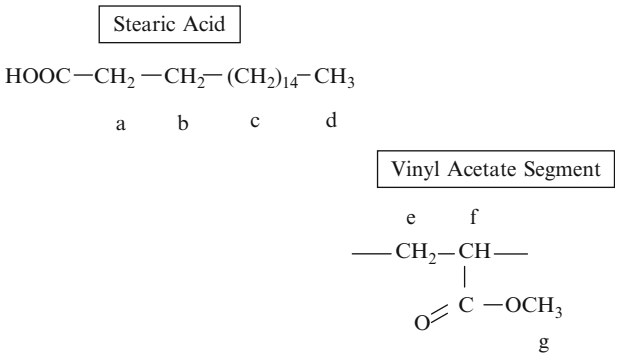

Fig. 18.2 Chemical shift identifications for proton NMR peaks of stearic acid and vinyl acetate segments. Chemical shifts are (**a**) ~2.4 ppm, (**b**) ~1.7 ppm, (**c**) ~1.3 ppm, (**d**) ~0.8 ppm, (**e**) ~2.1 ppm, (**f**) ~5.2 ppm, (**g**) ~2.3 ppm

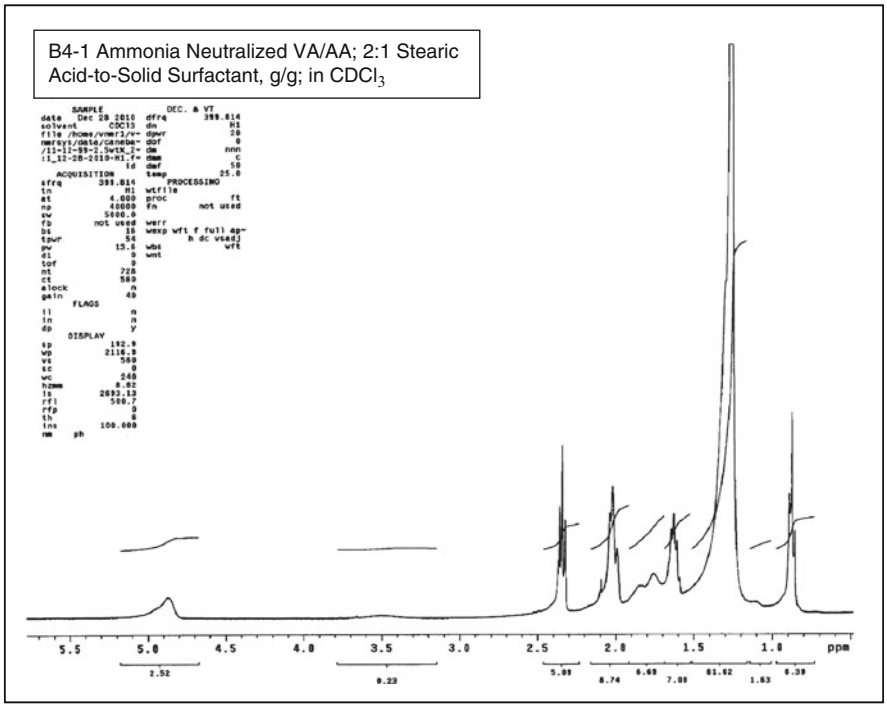

Fig. 18.3 Proton NMR spectrum of B4-1 ammonia neutralized VA/AA; 2:1 stearic acid-to-solid surfactant, g/g; in $CDCl_3$. The surfactant contains 4 wt.% acrylic acid before these segments were neutralized with ammonia

Various proportions of stearic acid-to-surfactant solid were formulated. Usually, a precipitate is formed when modification reaction was noted to occur. An equal volume of the reaction fluid material was mixed with an equal volume of *n*-Heptane, in order try to obtain a stable dispersion. Polymer modification reaction was noted when two cloudy layers of fluid were obtained. When the top *n*-Heptane-rich layer was noted to be a clear fluid, no modification reaction would have occurred. The cloudy top layer indicates that the *n*-Heptane was dispersed with the aid of the stearic acid-modified VA–AA-based polymer surfactant. These two possibilities are shown in Fig. 18.1.

Top *n*-Heptane layers were obtained from samples and dried, first through airdrying and then vacuum-drying at 50°C under full vacuum for 1 h. Then, the dried solid products were analyzed through proton nuclear magnetic resonance (^{1}H-NMR) spectroscopy, using $CDCl_3$ or Pyridine-d_5 as solvents. A literature search provided chemical shift identifications for proton peaks of stearic acid (http://lipidlibrary.aocs.org/nmr/1NMRsat/index.htm) and vinyl acetate segments (Brandolini and Hills 2000), as shown in Fig. 18.2.

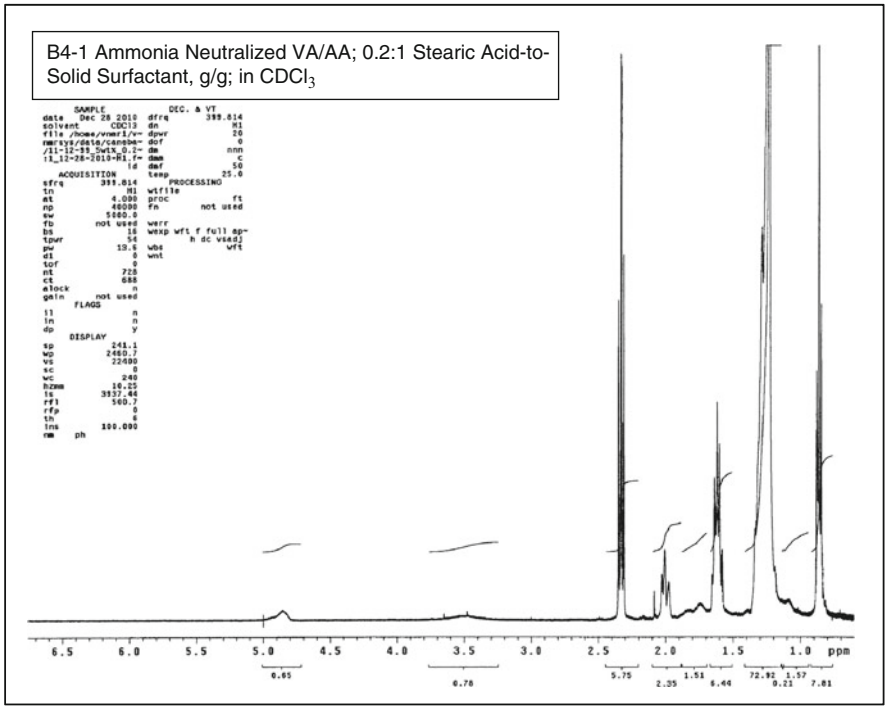

Fig. 18.4 Proton NMR spectrum of B4-1 ammonia neutralized VA/AA; 0.2:1 stearic acid-to-solid surfactant, g/g; in $CDCl_3$. The surfactant contains 4 wt.% acrylic acid before these segments were neutralized with ammonia

It is evident from Fig. 18.3 that the material contains stearic acid, as evidenced by peaks a, b, c, and d, based on peak identifications shown in Fig. 18.2. In addition, peaks e, f, and g of vinyl acetate segments are shown, except that peak g seemed to overlap with peak e. This indicates that some of the ester group has been transesterified with the stearic acid forming hydrocarbon grafts. A similar story is seen in Fig. 18.4, which indicates that less stearic acid used in the modification reaction did not drastically affect modified multipolymer compositions.

In Fig. 18.5, the same multipolymer sample was analyzed as that in Fig. 18.3, except that Pyridine-d_5 was used as solvent. Results of the transesterification are confirmed, and the amine as well as some hydroxyl groups around 3.5 ppm have been enhanced.

In Fig. 18.6, a VA/AA-based copolymer surfactant with 20 wt.% AA content was used, and a small amount of carboxylic acid proton at around 10 ppm is seen. An expanded view of the spectrum (Fig. 18.7) of the same multipolymer results in an analysis similar to those of Figs. 18.3–18.5.

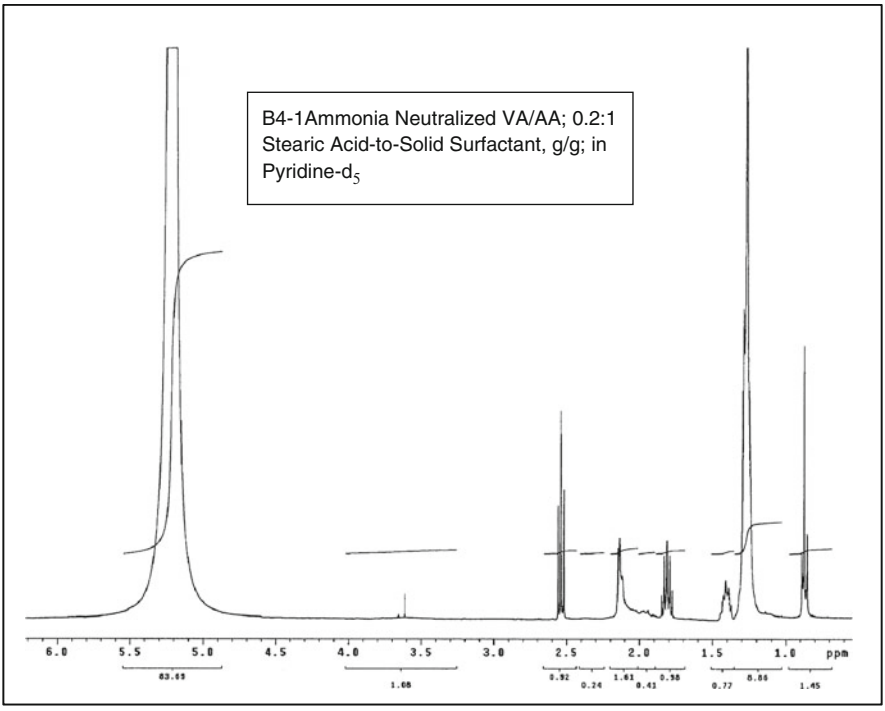

Fig. 18.5 Proton NMR spectrum of B4-1 ammonia neutralized VA/AA; 0.2:1 stearic acid-to-solid surfactant, g/g; in Pyridine-d_5. The surfactant contains 4 wt.% acrylic acid before these segments were neutralized with ammonia

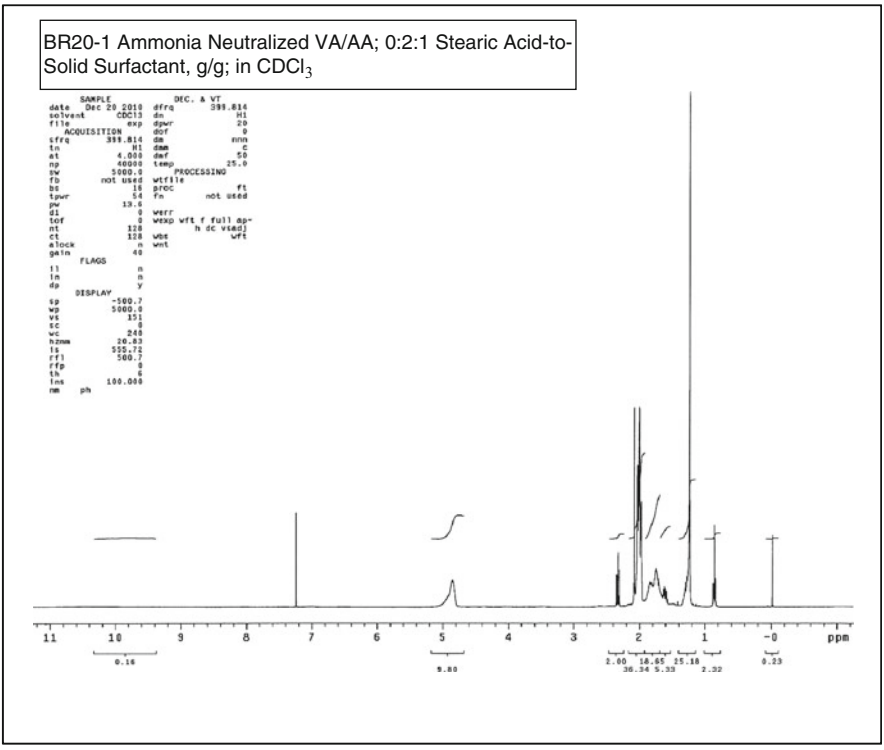

Fig. 18.6 Proton NMR spectrum of BR20-1 ammonia neutralized VA/AA; 0.2:1 stearic acid-to-solid surfactant, g/g; in $CDCl_3$. The surfactant contains 20 wt.% acrylic acid before these segments were neutralized with ammonia

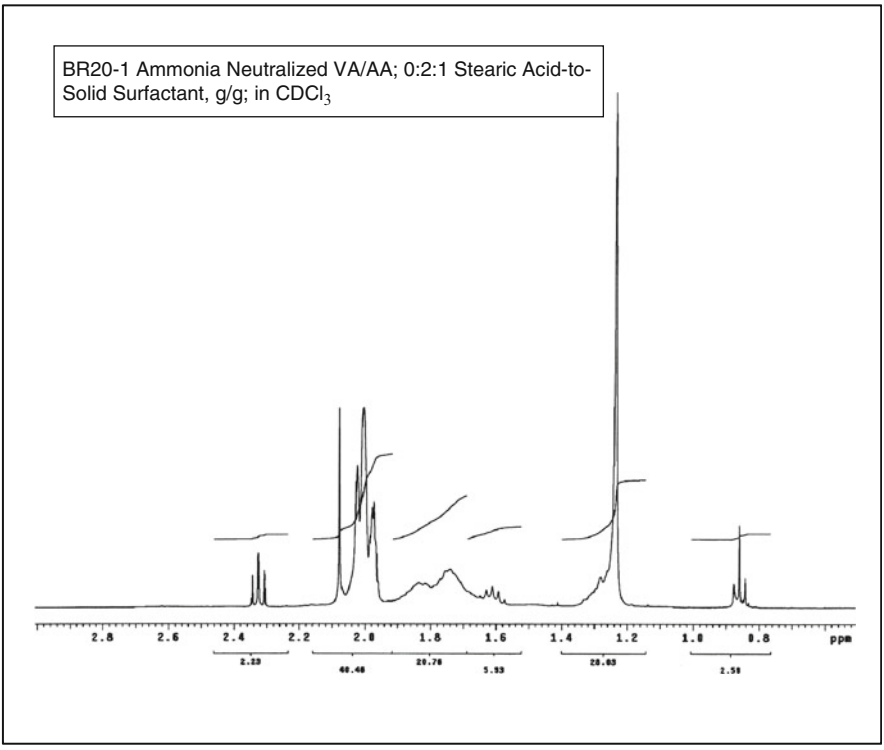

Fig. 18.7 Expanded Proton NMR spectrum of BR20-1 ammonia neutralized VA/AA; 0.2:1 stearic acid-to-solid surfactant, g/g; in $CDCl_3$. The surfactant contains 20 wt.% acrylic acid before these segments were neutralized with ammonia

It is therefore evident from apparent dispersibility properties as well as from proton NMR results that the stearic acid was incorporated as grafts onto the segments of the ammonia-neutralized VA/AA-based copolymer surfactants.

References

Brandolini AJ, Hills DD (2000) NMR spectra of polymers and additives. Marcel-Dekker, New York, p 180

Fingas MF, Fieldhouse B, Wang Z, Sigouin L, Landriault M, Mullin JV (2000) Recent results from dispersant testing. In: Proceedings of the 23rd annual arctic and marine oilspill program technical seminar, 14–16 June 2000, Vancouver, Environmental Canada, pp. 681–695

Heryan R, Hasan M, Abdullah E, Kumoro AC (2007) Sci Asia 33:469

Index

G. Caneba and Y. Dar, *Emulsion-based Free-Radical Retrograde-Precipitation Polymerization*, DOI 10.1007/978-3-642-19872-4,